Virginia Tech Report
EE SATCOM 86-5

Satellite Communications Group
Electrical Engineering Department
Virginia Polytechnic Institute and State University
Blacksburg, Virginia 24061

FADE DURATIONS IN SATELLITE-PATH MOBILE RADIO PROPAGATION

Robert G. Schmier
Charles W. Bostian

This work was performed for
Jet Propulsion Laboratory
California Institute of Technology
and was sponsored by
National Aeronautics and Space Administration
under Contract 956512

Report 86-5

December 1986

Virginia Tech Report
EE SATCOM 86-5

Satellite Communications Group
Electrical Engineering Department
Virginia Polytechnic Institute and State University
Blacksburg, Virginia 24061

FADE DURATIONS IN SATELLITE-PATH MOBILE RADIO PROPAGATION

Robert G. Schmier
Charles W. Bostian

This work was performed for
Jet Propulsion Laboratory
California Institute of Technology
and was sponsored by
National Aeronautics and Space Administration
under Contract 956512

Report 86-5

December 1986

Fade Durations in Satellite-Path Mobile Radio Propagation

by

Robert Gordon Schmier

C.W. Bostian, Chairman

(ABSTRACT)

Fades on satellite to land mobile radio links are caused by several factors, the most important of which are multipath propagation and vegetative shadowing. Designers of vehicular satellite communications systems require information about the statistics of fade durations in order to overcome or compensate for the fades. Except for a few limiting cases, only the mean fade duration can be determined analytically, and all other statistics must be obtained experimentally or via simulation.

This report describes and presents results from a computer program developed at Virginia Tech to simulate satellite path propagation of a mobile station in a rural area. The simulator was developed using 869 MHz balloon data provided by Wolfhard Vogel of the University of Texas at Austin and was tested using helocopter data provided by Wolfhard Vogel and Julius Goldhirsh of the Johns Hopkins University Applied Physics Laboratory. It generates rapidly-fading and slowly-fading signals by separate processes that yield correct cumulative signal distributions and then combines these to simulate the overall signal. This is then analyzed to yield the statistics of fade durations.

Table of Contents

I. INTRODUCTION

Mobile telecommunication services are usually available only in metropolitan centers; at present, there is no cost-effective way to accomodate rural and remote users. For the past decade NASA has studied geostationary satellites as a solution to this problem. NASA expects a satellite based communication system to extend the range of existing terrestrial based cellular systems. In addition, it will provide voice and data communications to mobile users over a wide geographical area for such applications as dispatch, emergency rescue, position location, drug enforcement, and mobile telephone. A target of 1.2 million subscribers over 7 years is considered realistic, requiring around 350 channels, with operating costs somewhat lower than charges for equivalent services using the public-switched telephone network [17].

The first phase of NASA's technology development program for a Land Mobile Satellite System (LMSS) is called the Mobile Satellite Experiment (MSAT-X). This program is managed by the Jet Propulsion Laboratory (JPL) and is aimed at developing and testing the ground segment technologies required for a more advanced second generation system. These technologies include vehicle antennas, voice processing

schemes, spectrally efficient modulation, and fade resistant coding. NASA's goals are to use 2.4 kbps digital voice or data in a 5 kHz channel with Gaussian minimum shift keying modulation. The experimental part of the program will consist of two years of testing using the first generation MSAT satellite. The proposed operational frequencies are in the UHF and L-bands, with the FCC presently allocating space in the L-band and setting aside additional space in the UHF band for future use.

Proper selection of modulation and coding schemes requires knowledge of the LMSS radio channel, and the channel characteristics are a function of the propagation effects. So is the link margin required to provide adequate signal power. Consequently, the success or failure of LMSS depends heavily upon knowledge of propagation impairments and upon steps taken to defeat them. Measurements of channel performance in phase 1 of the PROSAT mobile satellite program (initiated by the European Space Agency) revealed that even in open countryside, shadowing effects from trees and other obstacles produce fades of 15 dB or so for significant amounts of time; hence, allowing a 15 dB fade margin in the system will only produce 80 percent circuit continuity [17]. The designer of a mobile communication system must attempt to overcome the fading caused by propagation impairments by proper system design. The design requires knowledge of both primary and secondary fading statistics. In particular, the statistics of fade durations must be known in order to design a reliable system. Hence, there is considerable interest in the statistical distribution of fade durations. However, measurement results are usually given because, with the exception of a few limiting cases, only the mean fade duration can be determined analytically. Even the mean fade duration can only be determined for fades with no line of sight blockage. Any other fade duration statistics must be obtained experimentally or via simulation.

This report describes a software modeling approach to the simulation of the dynamic characteristics of fade durations in rural land mobile communications. The model rests on the assumption that a fading mobile signal magnitude can be separated into basic component parts. These consist of a slowly varying lognormally distributed component and a rapidly varying Rayleigh component. We will show this assumption to be valid for the data analyzed. The model is expressed in a software simulator that regenerates the signal envelope received by a mobile. Its input is a cumulative distribution plot of the signal received by the mobile; this can be either derived from measured data or estimated. The model output is analyzed for fade duration statistics.

Chapter 2 provides background material for LMSS communications. Chapter 3 reviews previous simulators designed for LMSS use. Chapter 4 follows the development of the initial Virginia Tech (VT) software simulator designed for LMSS use. Chapter 5 introduces improvements to the VT simulator and verifies its operation by comparing its output to measured data. Chapter 6 finishes with conclusions and recommendations for future use and study of the simulator.

II. PROPAGATION MECHANISMS AND SIGNAL CHARACTERISTICS

2.1 Introduction

Phenomena that effect propagation on land-mobile satellite systems are different both from those in fixed satellite systems and those on terrestrial mobile radio systems. Fixed service satellite systems use highly directive antennas that are relatively free from multipath and shadowing effects, such as due to trees, that are found in a land-mobile system with smaller, less directive antennas. The signal in terrestrial mobile radio systems is typically dominated by multipath fading and blockage effects by terrain obstacles because of the extremely low elevation angles. Land mobile satellite systems, on the

other hand, encounter less severe impairments and unblocked line of sight conditions often prevail.

The received signal arriving at the land-mobile antenna has three components: a direct wave, a specularly reflected wave, and diffusely reflected waves. The direct wave is the line-of-sight (LOS) signal from the satellite and is affected by the troposphere, the ionosphere, and obstacles in the propagation path. The specular component is reflected from the surface near the vehicle and combines coherently with the direct component. The diffuse component is composed of all the scattered energy from the rough terrain in the vicinity of the vehicle less any specular component. These three components are shown in Figure 2.1-1; all these components are affected by vegetation and man made shadowing obstacles which attenuate the direct and specular components and which may increase or decrease the diffuse component.

The first part of this chapter will highlight current theory for describing propagation mechanisms affecting LMSS operation. A summary of the basic physics involved follows in Section 2.2, drawn from [7] and more complete reports of Smith et al. [24], Flock [16], and preliminary CCIR Study Group 5 documents [11]. Section 2.3 discusses construction of the total received mobile signal for both unshadowed and vegetatively shadowed conditions. Section 2.4 digresses from propagation issues and summarizes some probability concepts and methods of describing fading signals. It serves as a background for discussion in later chapters.

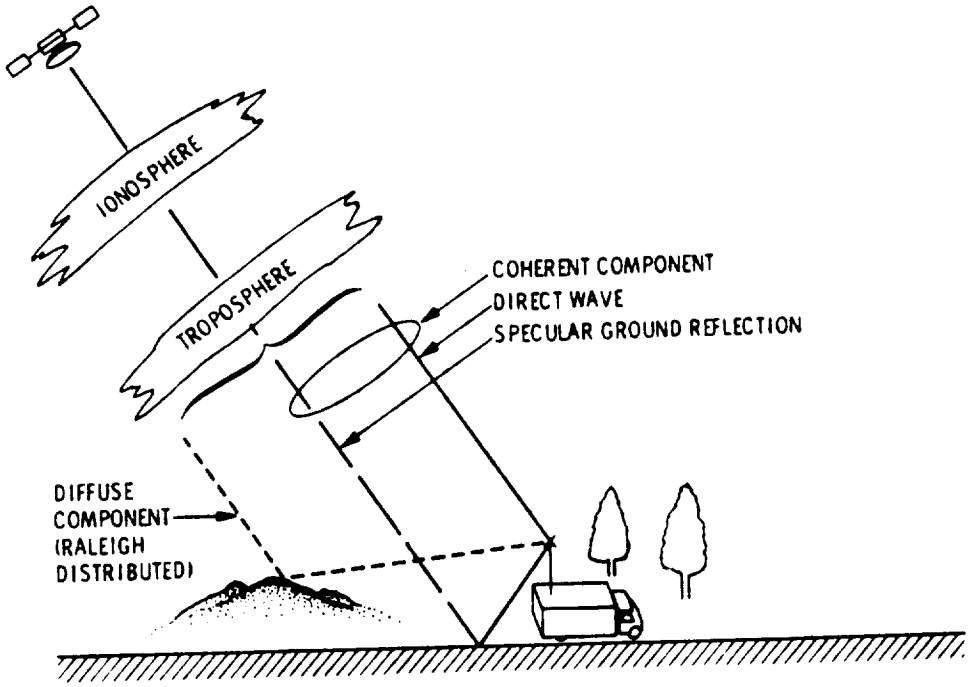

Figure 2.1-1. A physical representation of the LMSS channel showing the direct, specular, and diffuse components for unshadowed propagation. From Vogel and Smith [28]

2.2 Mobile Signal Components

2.2.1 Direct Component

The direct component is principally affected by shadowing obstacles on the earth's surface such as trees and overpasses, but it may also be degraded by ionospheric and tropospheric effects. These include Faraday rotation, group delay, absorption, dispersion, refraction, and scintillation, all of which result from interaction with the earth's magnetic field and the ambient electron content as a wave passes through the ionosphere. Extreme values for these effects are summarized in Table 2.2-1 for two possible LMSS frequencies assuming an elevation angle of 30 degrees, a zenith electron content of 10^{18} electrons/m^3 , and one-way propagation. Faraday rotation appears to pose the most significant problem, but use of circular polarization is expected to minimize any difficulties. Scintillations can also be ignored in LMSS because they seldom are significant for elevation angles above 10 degrees (30 degrees and above are typical for the continental U.S.) and frequencies below 10 GHz [28].

Moisture in the lower atmosphere accounts for tropospheric effects on the direct component. Table 2.2-2 shows predicted one-way tropospheric losses for an elevation angle of 30 degrees and indicates that these losses are also negligible.

Shadowing by obstacles, however, causes significant attenuation. In rural areas where LMSS will be used, obstacles of greatest concern include overpasses and vegetation. Overpasses, assuming they contain enough steel mesh, cause complete loss of the direct signal [27]. Vegetation in the LOS path, on the other hand, causes significant but only

Table 2.2-1. Estimated maximum ionospheric effects for an elevation angle of 30°, one-way propagation, and a zenith electron column of 10^{18} electrons/m^3. From Smith et al. [24]

Effect	Frequency Dependence	Magnitude	
		850 MHz	1600 MHz
Faraday Rotation	$1/f^2$	150°	42°
Propagation delay	$1/f^2$	0.35s	0.1s
Variation in direction of arrival	$1/f^2$	16 sec. of arc	4.7 sec of arc
Refraction	$1/f^2$	> 50"	> 14"
Absorption (mid-lats)	$1/f^2$	>0.014 dB	>0.004 dB
Dispersion	$1/f^3$	0.65 nsec/MHz	0.1 nsec/MHz

Table 2.2-2. Estimated tropospheric attenuation for an elevation angle of 30° and one-way propagation. From [11]

Effect	Magnitude (dB)	
	850 MHz	1600 MHz
Clear air absorption		
3 g/m^3 (dry)	0.06	0.07
7.5 g/m^3 (average)	0.06	0.07
17 g/m^3 (moist)	0.06	0.07
Cloud attenuation		
0.5 g/m^3, 1 km thick	<0.01	<0.01
1 g/m^3, 2 km thick	<0.01	<0.01
Fog attenuation		
0.05 g/m^3 (average), 0 to 75m ht.	---	---
0.05 g/m^3 (heavy), 0 to 150m ht.	---	---
Rain attenuation		
5 mm/h	<0.01	<0.01
25 mm/h	<0.1	<0.1

partial shadowing of the direct component. Attenuation of the direct component by vegetation is assumed to be, and is shown to be in Section 4.2, lognormally distributed.

Since one can assume complete loss of the direct component of the signal under overpasses, and this is fairly well understood, we will not examine this aspect of shadowing. We will also ignore ionospheric and tropospheric effects on the direct component since they have been found to be negligible. Shadowing by vegetation, on the other hand, is significant and presently not well understood. This element of shadowing is important and must be considered in our analysis and modeling efforts. Analytic solutions for fades in LMSS due to vegetative shadowing are not yet mature so they will be pursued from a statistical viewpoint for development of a fading signal model.

2.2.2 Specular Component

The specular component is a phase coherent wave reflected from the ground in the vicinity of the mobile receiver. This component may cause deep fades in the total received signal if its amplitude is comparable to that of the direct component and its phase is opposite. The specular component is primarily reflected from the region of the first Fresnel zone on the scattering surface. Equations for the location and size of this elliptical region are defined in [3]. Generally, the Fresnel zone size decreases with increasing grazing angle and frequency.

Circularly polarized waves like those to be used in LMSS produce specular reflected waves that are elliptically polarized. Reflections from grazing angles below the Brewster angle, which may vary from 6 to 27 degrees, result in waves with the same sense as the

incident wave. For grazing angles above the Brewster angle, the specular reflection will be of opposite sense to the incident wave. Because the elevation angle in LMSS usually will vary from 20 to 60 degrees, most specular reflections will arrive above the Brewster angle and be polarized in the opposite sense to the incident wave.

The magnitude of the specular component is determined by the reflection coefficient for the ground surface in the area of the first Fresnel zone. The specular reflection coefficient, R_S , is derived from a simple model in [3] and is defined as

$$R_S = \rho_S D R_0 \tag{2.2-1}$$

where ρ_S is the surface roughness factor, D is the divergence coefficient caused by the curvature of the earth, and R_0 is the complex voltage reflection coefficient for a smooth planar earth.

The surface roughness factor, ρ_S , approaches unity for a smooth surface and decreases for increasing surface irregularity [3]. The curved earth divergence factor, D, is approximately unity for LMSS applications [28]. The complex voltage reflection coefficient, R_0 , depends on the surface conductivity, relative permittivity, grazing angle, and the polarization of the incident wave [18]. Figure 2.2-1, taken from Butterworth [8], gives an indication of the reflection coefficient for a right hand circularly polarized incident wave as a function of grazing angle. The reflected wave consists of a combination of right hand and left hand polarized components. For Figure 2.2-1, conditions of medium dry soil, a frequency of 870 MHz, and a surface irregularity standard deviation of 0.1 m are assumed. The Brewster angle for these conditions is 15 degrees and the figure shows domination of the left hand component above this angle.

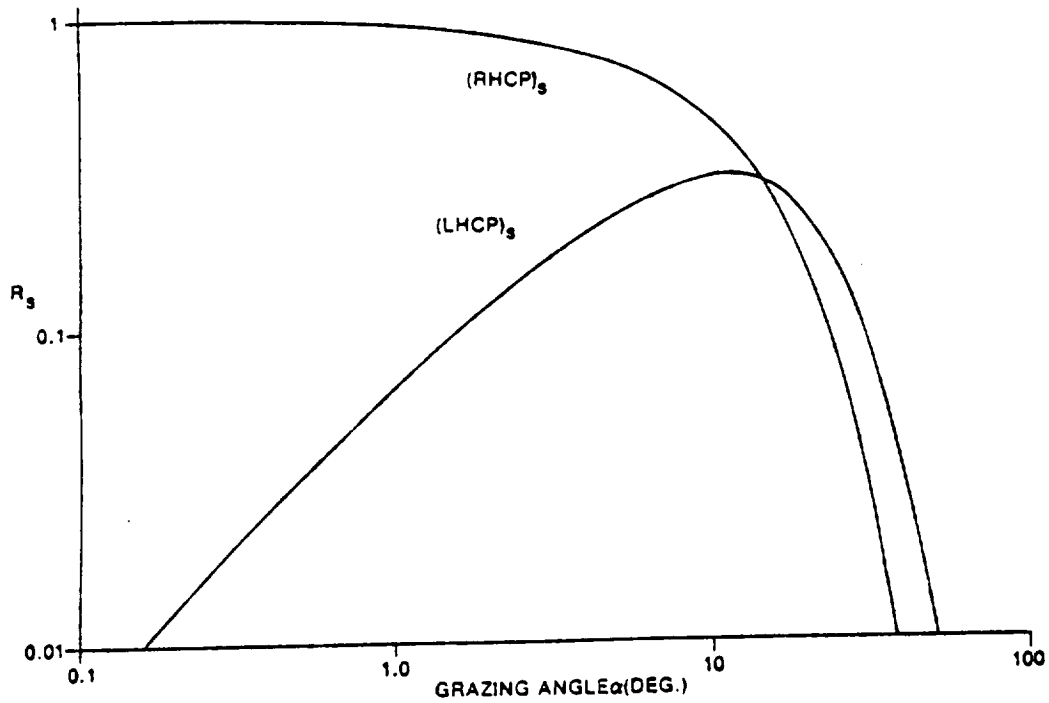

Figure 2.2-1. Components of the specular reflection coefficient as a function of the grazing angle for a RHCP incident wave at 870 MHz. From Butterworth [8]

The antenna pattern must also be included when determining the overall effect of the specular component. Antennas considered for use in LMSS are not very directive, but they do exhibit a relatively low gain for signals received below the horizon and they do discriminate against signals polarized in the opposite sense to the incident wave. The specular component in LMSS is received by the antenna from below the horizon where the antenna gain is low. In addition, the grazing angle for the specular component is usually greater than the Brewster angle leading to opposite polarization of the specular component and discrimination against the specular component by the antenna.

In an analysis made by Butterworth [8] which included antenna effects such as polarization and low angle discrimination, fade depths from specular waves were found to be a negligible 1 dB for elevation angles above 20 degrees. As a result of this analysis and others [28], we expect the specular component to be neglegible in LMSS links with elevation angles above 20 degrees, and we will ignore it in our analysis of the received signal envelope.

2.2.3 Diffuse Component

The diffuse component is the phase incoherent portion of the total received mobile signal and represents the sum of all of the waves scattered from the terrain around the mobile, but outside the first Fresnel zone. The diffuse component has little directivity and its magnitude is assumed to be Rayleigh distributed while its phase is uniformly distributed. Interference of the diffuse component with the direct component causes rapid fading in the received mobile signal.

A simple relationship to determine the average magnitude of the diffuse component is presented in [3] and is given as

$$R_D = \rho_d R_0 \tag{2.2-2}$$

where R_D is the diffuse reflection coefficient, ρ_d is the diffuse scattering coefficient, and R_0 is the reflection coefficient of a smooth planar earth. For very rough surfaces and non-directional antennas, R_D is reported to have an average value of 0.35. If the scattering surface is absorptive, such as vegetation covered ground (this includes vegetation near the ground, but not vegetation above the mobile such as trees), then R_D will be on the order of 0.1 [3].

As with the specular component, the antenna pattern affects the influence of the diffuse component on the received signal. Because the antenna gain rolls off below the horizon, most of the contribution by the diffuse component will be from angles above the horizon. Consequently, the average diffuse component is small relative to the direct component (usually over 10 dB), but it cannot be ignored because it is Rayleigh distributed and fades as large as 5 dB can be expected for small percentages of time.

2.3 Total Mobile Fading Signal

2.3.1 Unshadowed Mobile

In the case of propagation for the unshadowed mobile, shown previously in Figure 2.1-1, the received signal has two significant components. The coherent component consists of the direct wave and the negligible specular ground reflection. The incoherent component consists of the diffuse reflections. There is no fading of the direct wave due to obstacles for the case of the unshadowed mobile, and as discussed previously, atmospheric effects are negligible. For this case, the combination of the components may be represented as

$$R_1 = R_{dir} + R_{spec} + R_{dif} \tag{2.3-1}$$

Neglecting the specular component, this reduces to

$$R_1 \approx R_{dir} + R_{dif} \tag{2.3-2}$$

Since the direct component is essentially constant relative to the fast varying diffuse component and the diffuse component is Rayleigh distributed in amplitude and uniformly distributed in phase, the total received unshadowed signal has a Rician distribution [4].

2.3.2 Vegetatively Shadowed Mobile

Propagation mechanisms for vegetatively shadowed mobile communications are shown in Figure 2.3-1. The problem of modeling a vegetatively shadowed mobile signal is presently not well understood. Again the received signal has two significant components, the coherent direct and specular waves and the incoherent diffuse reflections from both the terrain and the vegetation. In the case of the shadowed mobile, the specular and atmospheric effects on the direct component are still negligible, but in this case there is fading of the direct wave due to obstacles in the propagation path.

Neglecting the specular component, the combination of the components may be represented as

$$R_1 \approx R_{dir} + R_{dif} \tag{2.3-3}$$

Here the diffuse component is still assumed to be Rayleigh distributed in magnitude and uniformly distributed in phase, and the direct component is assumed to be lognormally ditributed [25]. The distribution of the total received shadowed signal, i.e. the combination of the Rayleigh distributed diffuse component and the lognormally distributed direct component, will be referred to as the VS (vegetatively shadowed) distribution and is discussed in detail in [25].

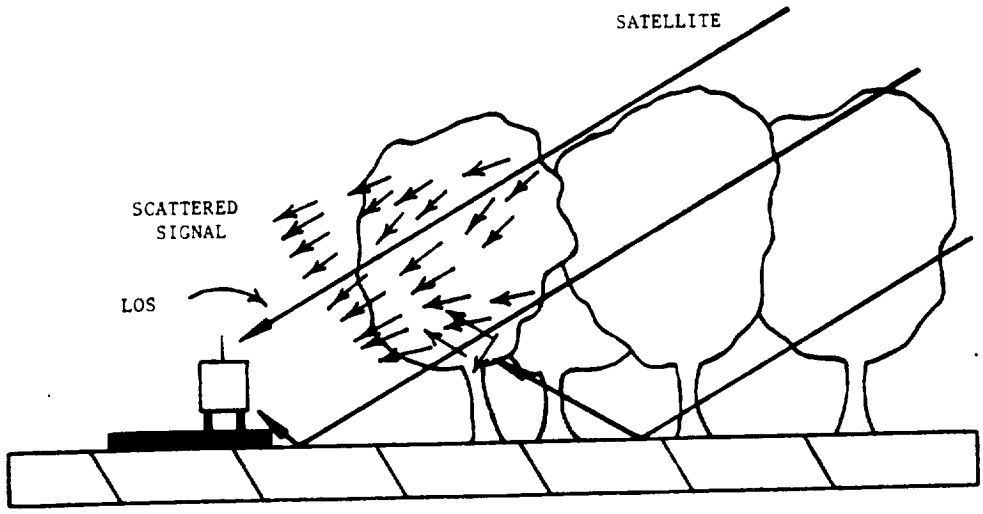

Figure 2.3-1. A physical representation of the LMSS channel showing the LOS, specular, and diffuse components for vegetatively shadowed propagation [25].

2.4 Statistical Functions For Mobile Signal Analysis

2.4.1 Primary Statistics

Primary statistics include the probability density function and the cumulative distribution function. The important distribution functions necessary for describing LMSS signals include the Rayleigh, Rician, lognormal, and the VS distributions. Each of these is discussed here for future reference.

Rayleigh Density Function

The magnitude of the diffuse component of the mobile signal is described by the Rayleigh density function. The diffuse component is the sum of many random phasors, each of which may be represented by amplitude A_i and phase φ_i. The result, in equation form, is

$$R_{dif} = r \exp[j\theta] = \sum_{i=1}^{N} A_i \exp[j\varphi_i] \tag{2.4-1}$$

where r is the amplitude of the diffuse component, θ is the phase of the diffuse component, A_i and φ_i are the amplitude and phase (phase measured with respect to the direct component), respectively, of the i th component of the scattered wave. If the magnitude of each A_i is much smaller than the magnitude of r, φ_i is uniformly distributed, and N is sufficiently large, then r can easily be proven to be Rayleigh distributed and θ uniformly distributed [4]. These conditions appear to be reasonable in LMSS for

scattering from a rough surface such as the ground, and the Rayleigh model appears justified. The density function for the Rayleigh distribution is defined as

$$p(r) = \frac{2r}{\alpha^2} \exp\left[-\frac{r^2}{\alpha^2} \right] \quad , \; r \geq 0$$
$$p(r) = 0 \quad , \; r < 0 \tag{2.4-2}$$

where r is the envelope voltage of the received signal and α^2 is the mean square value of r.

Rician Density Function

The Rician density function arises for the case of a Rayleigh distributed diffuse component in the presence of a strong, constant direct component. For unshadowed propagation, the total received mobile signal is the sum of the diffuse component (Rayleigh distributed in magnitude and uniformly distributed in phase) and the relatively constant direct component. This may be expressed as

$$R_1 = r \exp[j\theta] = A_0 \exp[j\varphi_0] + w \exp[j\varphi] \tag{2.4-3}$$

where r is the amplitude of R_1, θ is the phase of R_1 relative to the direct component, A_0 is the amplitude of the direct component, φ_0 is the phase of the direct component, w is the amplitude of the diffuse component, and φ is the phase of the diffuse component relative to the direct component. The total received signal for this case will be Rician distributed with a density function defined as [4]

$$p(r) = \frac{2r}{k^2} \exp\left[- \frac{(r^2 + A_0^2)}{k^2} \right] I_0\left(\frac{2A_0 r}{k^2}\right) \qquad r \geq 0 \tag{2.4-4}$$

$$p(r) = 0 \qquad , \; r < 0$$

where $k^2 = \alpha^2$ or the mean square value of the Rayleigh component alone, A_0 is the voltage amplitude of the direct component, and I_0 is the modified Bessel function of order zero. By normalizing the amplitude of the direct component to unity, this reduces to

$$p(r) = \frac{2r}{k^2} \exp\left[- \frac{(r^2 + 1)}{k^2} \right] I_0\left(\frac{2r}{k^2}\right) \qquad , \; r \geq 0 \tag{2.4-5}$$

$$p(r) = 0 \qquad , \; r < 0$$

where $k^2 = \alpha^2/A_0^2$ and r is now a ratio of the received signal level to A_0.

The Rician distribution can be completely specified by the parameter k or by the decibel equivalent, K, which is defined as

$$K = 20 \log_{10} k \tag{2.4-6}$$

The parameter K can be interpreted as the power in the Rayleigh component of the signal relative to the power in the constant component. There is some ambiguity in the literature for the definition of K; it is sometimes defined as $20 \log_{10}(1/k)$ which gives a value with the opposite sign as Equation 2.4-6. We will always use Equation 2.4-6 to define K.

Lognormal Density Function

The lognormal density function is used to describe slow fading of the direct component of the mobile signal when vegetative shadowing is present. The probability density of a lognormally distributed signal is defined as [19]

$$p(r) = \frac{1}{\sqrt{2\pi}\,\sigma r}\exp\left[-\frac{1}{2}\left(\frac{\ln r - \mu}{\sigma}\right)^2\right] \quad , \; r \geq 0 \tag{2.4-7}$$

$$p(r) = 0 \quad , \; r < 0$$

where r is the signal voltage amplitude, μ is the mean of ln(r), and σ is the standard deviation of ln(r). If r is converted to its decibel form, R, where R is defined as

$$R = 20\log_{10} r \tag{2.4-8}$$

then R is normally distributed. The density function of R is

$$p(R) = \frac{1}{\sqrt{2\pi}\,\sigma_R}\exp\left[-\frac{1}{2}\left(\frac{R - \mu_R}{\sigma_R}\right)^2\right] \tag{2.4-9}$$

where μ_R and σ_R are the mean and standard deviation of R. The mean and standard deviation of R can be related to those of r by [7]

$$\mu_R = (20\log_{10} e)\,\mu \tag{2.4-10}$$

and

$$\sigma_r = (20\log_{10} e)\,\sigma \tag{2.4-11}$$

where e is the base of the natural logarithm.

VS Density Function

The VS density function is used to describe the sum of a slowly fading vegetatively shadowed direct component and a Rayleigh distributed diffuse component. This density function is similar to the Rician function, but now instead of being constant, the direct component of the mobile signal is a lognormally distributed random phasor. The total received signal may be expressed as

$$R_1 = r \exp[j\theta] = z \exp[j\varphi_0] + w \exp[j\varphi] \tag{2.4-12}$$

where r is the amplitude of R_1, θ is the phase of R_1 relative to the direct component, z is the lognormally distributed direct component, φ_0 is the uniformly distributed phase of the direct component, w is the amplitude of the diffuse component, and φ is the phase of the diffuse component relative to the direct component. The density function for the received signal in this case is the VS density function and is defined as [20]

$$p(r) = \frac{r}{b_0\sqrt{2\pi d_0}} \int_0^\infty \frac{1}{z} I_0\left(\frac{rz}{b_0}\right) \exp\left[- \frac{(\ln z - \mu)^2}{2 d_0} - \frac{(r^2 + z^2)}{2 b_0} \right] dz \tag{2.4-13}$$

where r is the signal voltage, b_0 represents the average scattered power due to multipath, z is the lognormally distributed component, $\sqrt{d_0}$ and μ are the standard deviation and mean of ln z, and I_0 is the modified Bessel function of order zero. The signal voltage, r, is lognormal for large values and Rayleigh distributed for small values [20].

Distribution Functions

Signal level statistics are usually not displayed using density functions, but with a cumulative distribution function (more often shortened to distribution function) plotted

on probability paper. The cumulative distribution functions (CDF) refer either to the function for which the signal exceeds a level R, G(R), or to the function for which the signal is below a level R, F(R). These are defined as [4]

$$F(R) = P\{r \leq R\} = \int_{-\infty}^{R} p(r)\, dr \tag{2.4-14}$$

$$G(R) = P\{r \geq R\} = \int_{R}^{\infty} p(r)\, dr \tag{2.4-15}$$

where p(r) is the probability density function, F(R) is the probability that the signal is less than the threshold R, and G(R) is the probability that the signal exceeds the threshold R. G(R) and F(R) have the following properties [22]

$$0 \leq F(R) \leq 1; \quad 0 \leq G(R) \leq 1 \tag{2.4-16}$$

$$F(-\infty) = 0, \quad F(+\infty) = 1; \quad G(-\infty) = 1, \quad G(+\infty) = 0 \tag{2.4-17}$$

$$F(M) = G(M) = 0.5, \quad M \equiv \text{median value} \tag{2.4-18}$$

$$F(R_2) \geq F(R_1), \quad G(R_2) \leq G(R_1); \quad R_1 \leq R_2 \tag{2.4-19}$$

$$G(R) = 1 - F(R) \tag{2.4-20}$$

The primary statistic most often found in the literature, and in this work, is G(R). To display G(R) graphically, probability paper is used. Both logarithmic and Rayleigh probability paper will appear here. Both forms of probability paper use an ordinate axis labeled in decibels and an abscissa labeled in percent. On logarithmic probability paper, a lognormal distribution plots as a straight line. On Rayleigh probability paper, a Rayleigh distribution plots as a straight line. The mean of G(R) can be read directly from either probability paper as the ordinate value at the 50% point on the abscissas. For lognormal distributions, the standard deviation, σ_R , may be calculated from [1]

$$\sigma_R = R_{84\%} - R_{50\%} = R_{50\%} - R_{16\%} \tag{2.4-21}$$

where the R values are in decibels and correspond to the points at the percents noted in the subscripts.

In general, G(R) is most commonly plotted on logarithmic probability paper. Rayleigh probability paper is only used in our work as a check to determine if a signal is Rayleigh distributed (i.e., if the CDF of a signal plots as a straight line on Rayleigh probability paper, then the signal is Rayleigh distributed). Example plots of lognormal distributions on logarithmic probability paper are shown in Figure 2.4-1. Plots for Rician distributions, again on logarithmic probability paper, are shown in Figure 2.4-2. An example Rayleigh distribution is plotted in Figure 2.4-3 on Rayleigh probability paper and in Figure 2.4-4 on logarithmic probability paper. An example of a VS distribution on logarithmic probability paper is shown in Figure 2.4-5.

2.4.2 Secondary Statistics

The secondary statistics of interest in our work include fade duration and interfade interval. Fade duration is defined as the amount of time attenuation exceeds a given threshold. Interfade duration is defined as the amount of time between fades of a given duration. A graphical illustration of fade and interfade durations is given in Figure 2.4-6.

These secondary statistics describe the dynamic, time-varying characteristics of the signal received by the mobile. The dynamics of the mobile signal depend on conditions such as shadowing, mobile speed, signal source direction, and antenna pattern [7]. We

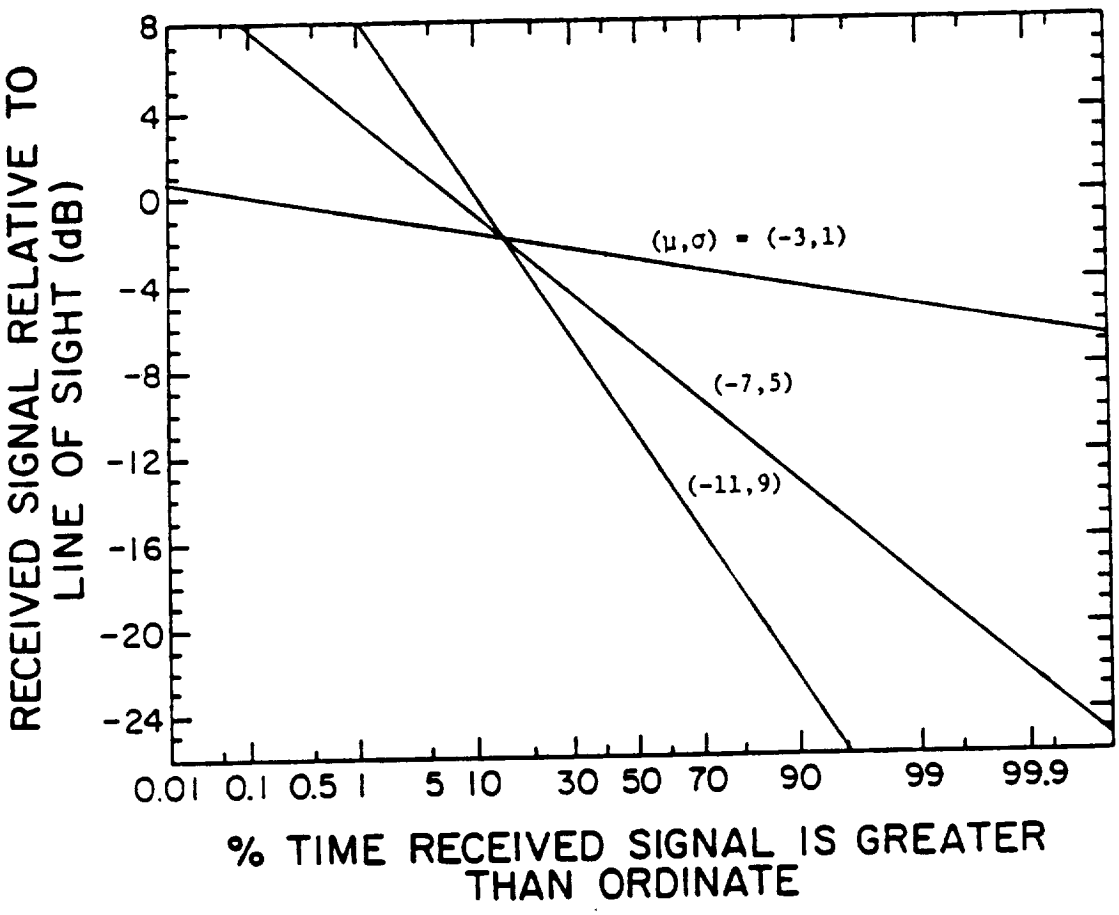

Figure 2.4-1. Cumulative distribution functions for lognormally distributed signals. The values of the mean (μ) and the standard deviation (σ) are in dB [7].

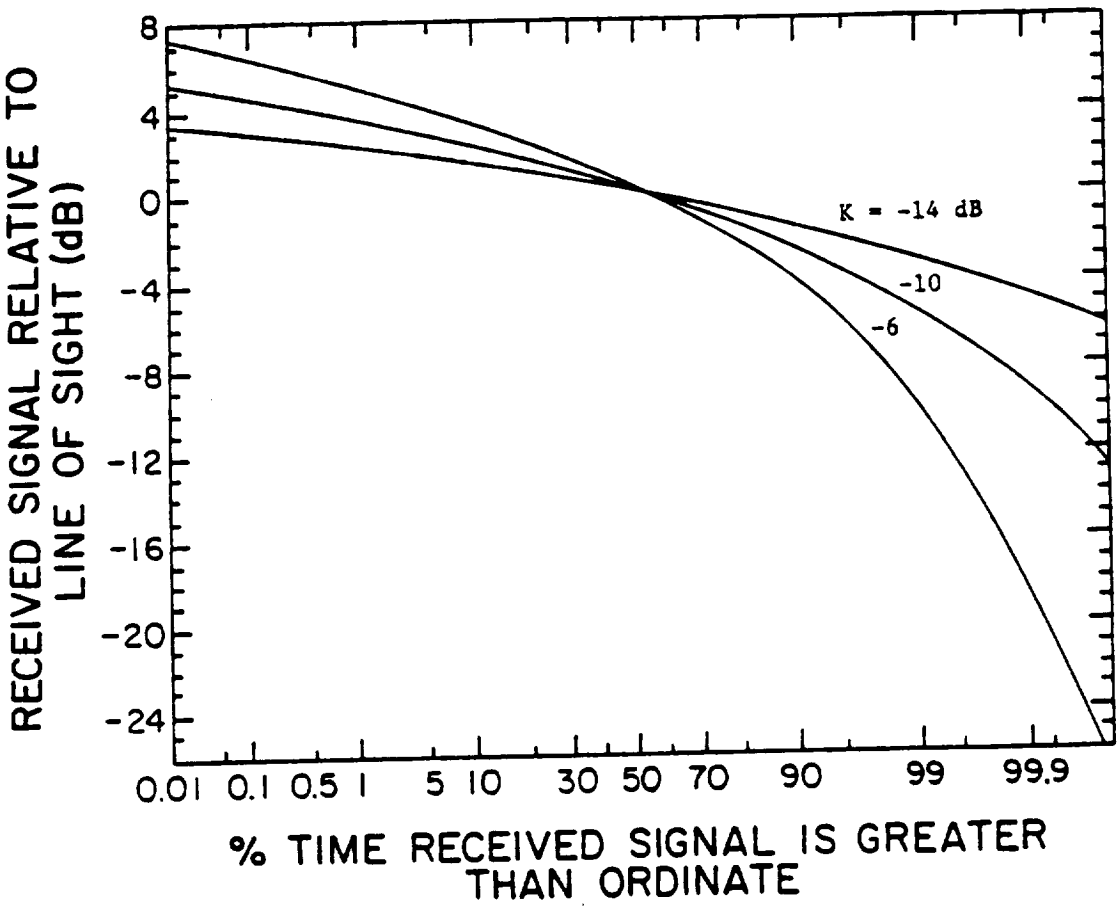

Figure 2.4-2. Cumulative distribution functions for Rician distributed signals [7].

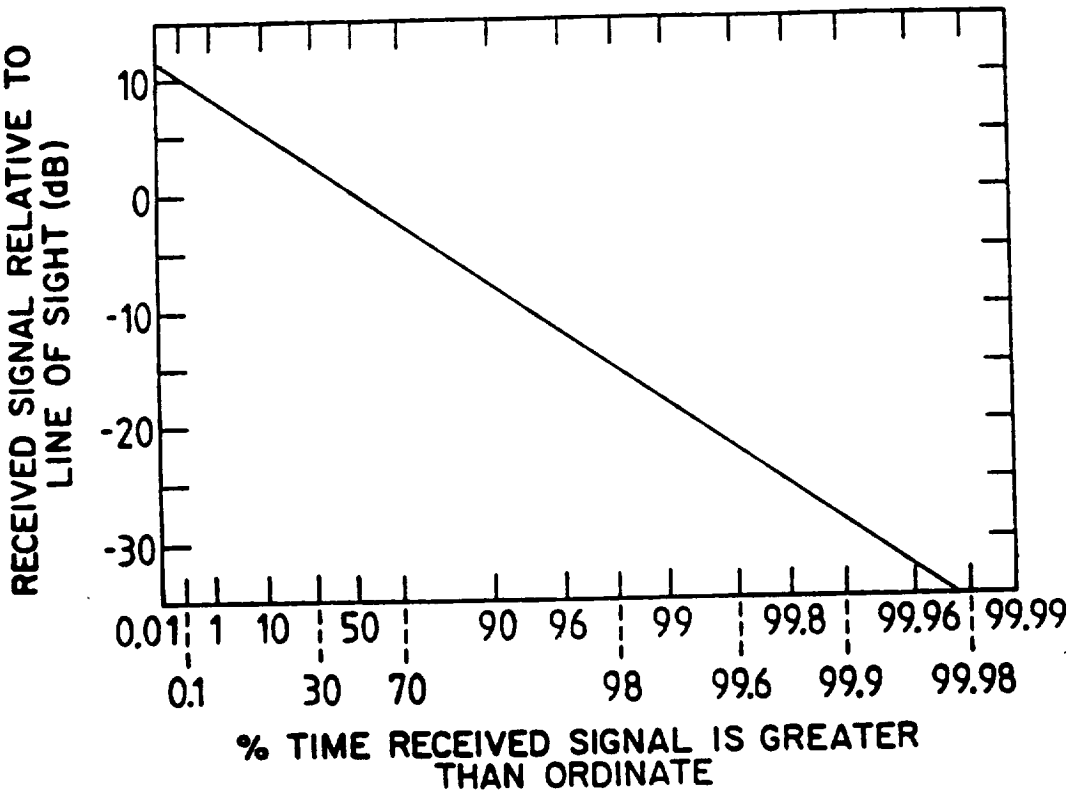

Figure 2.4-3. Cumulative distribution function for a Rayleigh distributed signal plotted on Rayleigh probability paper.

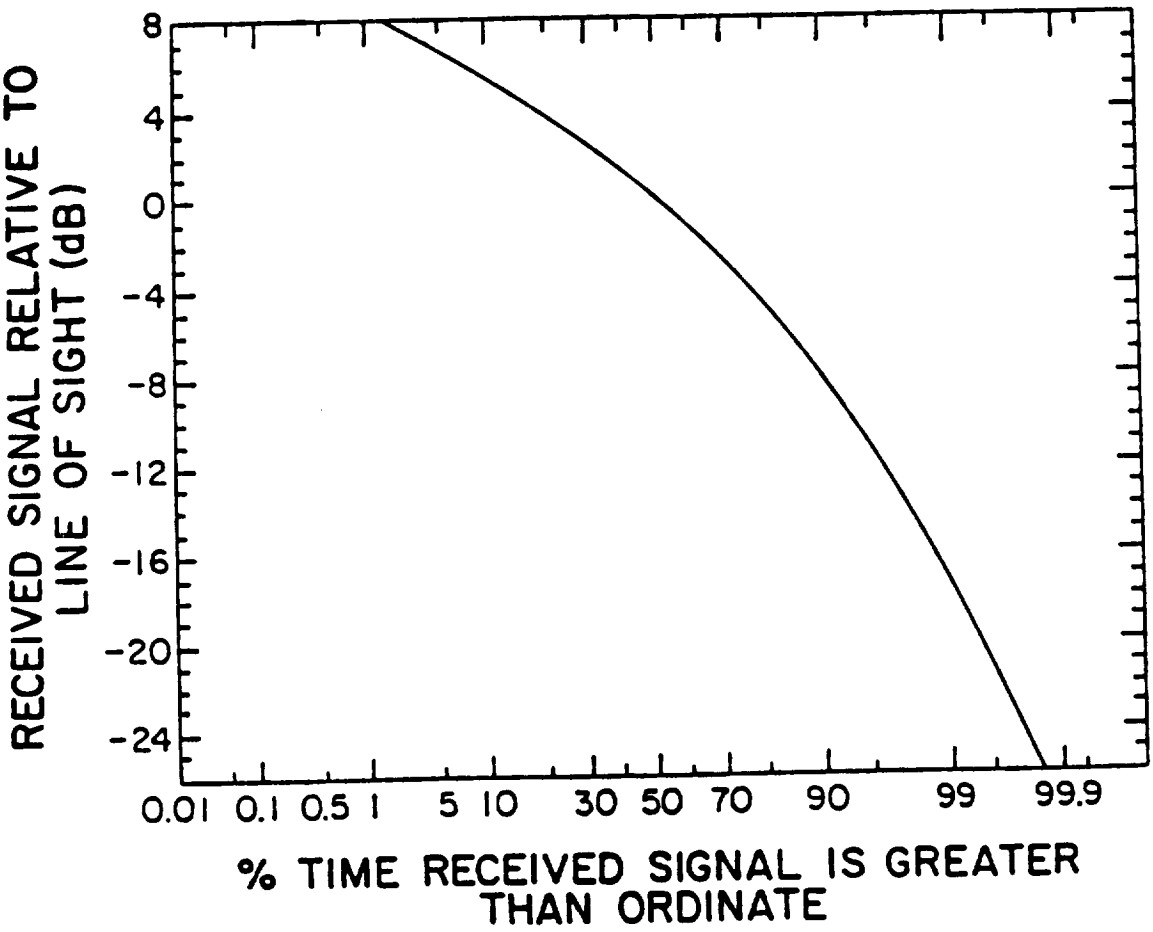

Figure 2.4-4. Cumulative distribution function for a Rayleigh distributed signal plotted on logarithmic probability paper.

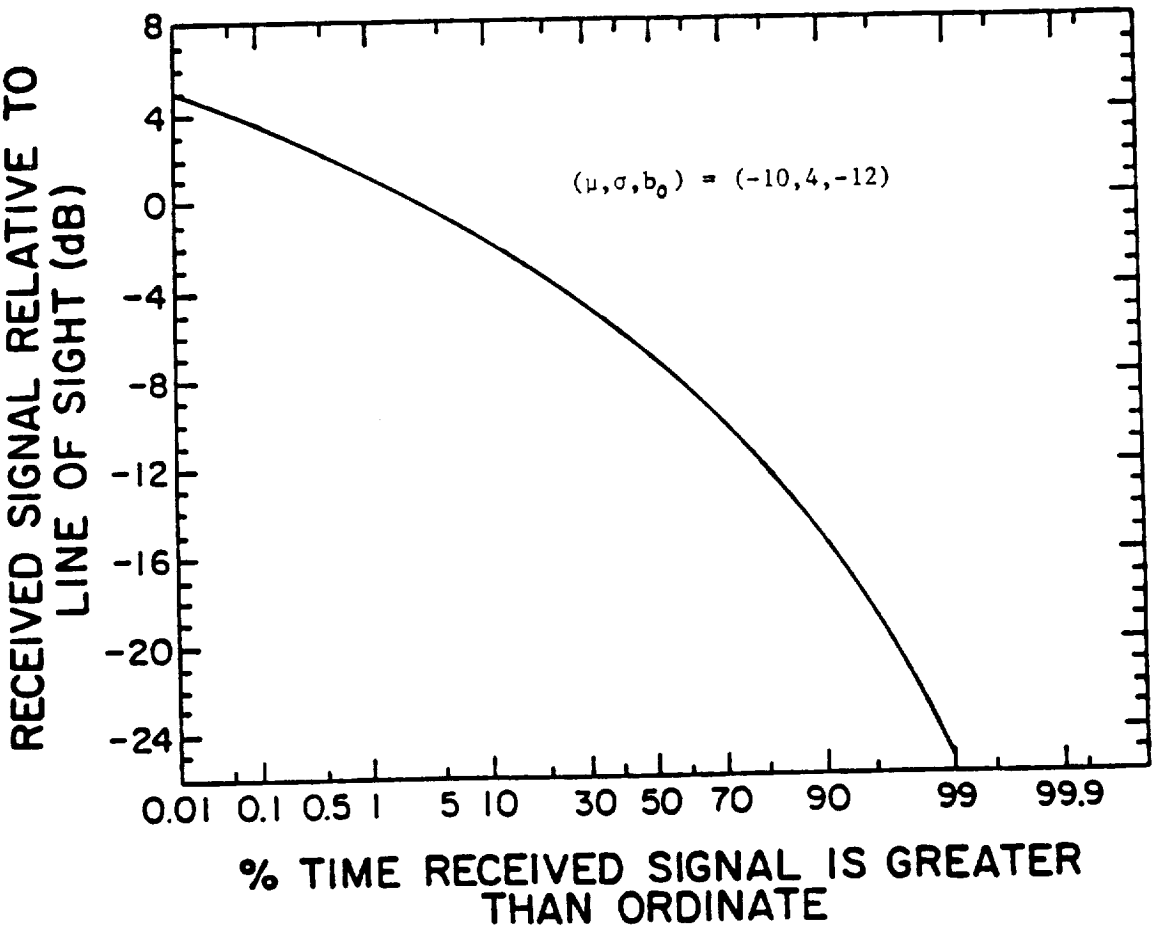

Figure 2.4-5. Cumulative distribution function for a VS distributed signal [25].

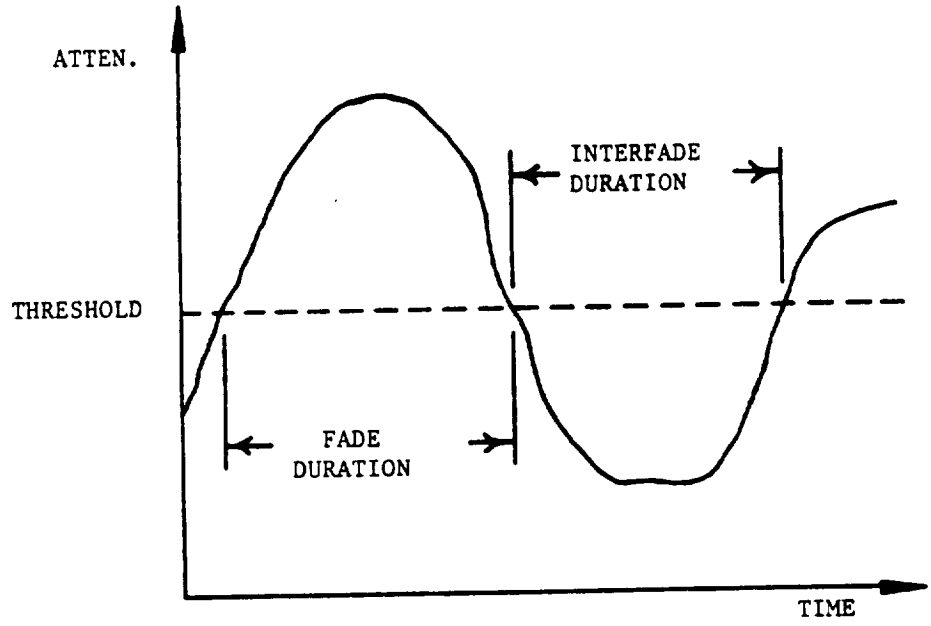

Figure 2.4-6. Definition of fade and interfade duration [6].

are primarily concerned with fade durations of the mobile signal in this work and will only treat this secondary statistic.

Little has been done in LMSS for fade duration studies, hence the methods for displaying fade durations in this work have been drawn from rain attenuation studies. There are three common ways to display rain fade and interfade duration results for a specified period. One way is a fade duration table such as that shown in Table 2.4-1,which shows the number of fades or events which fall in each threshold and duration bin. A second way is with a histogram showing the number of events for each threshold. A histogram is shown in Figure 2.4-7. Finally, fade and interfade duration results can be displayed as cumulative distributions, one for each threshold. In this case, the ordinate indicates the number of events with a duration greater than or equal to the abscissa. An example is given in Figure 2.4-8.

These methods for displaying fade durations must be modified slightly for LMSS applications. In our LMSS work, vehicle speed is normalized by time so that duration of a fade is given in wavelengths traveled by the mobile instead of time. Other than this minor modification, the three methods for displaying rain fade durations are directly applicable to LMSS.

In this work we are interested in finding a way to predict fade duration results for a location where a cumulative distribution plot has either been estimated or measured. Few analytical results are available for this problem. Consequently, we are interested in a model which will generate a time sequence of attenuation points given a distribution plot for input. From this sequence of attenuation points, we will generate fade duration statistics.

Table 2.4-1. Fade duration table for Vogel's 1978, CTS data at 11.7 GHz, 50.0° elevation angle, circular polarization [26].

Duration	Threshold (dB)				
(min.)	3	6	10	20	25
0 - 1	32	31	11	16	2
1 - 2	9	7	4	1	0
2 - 4	11	12	6	0	1
4 - 8	13	9	5	1	
8 - 16	11	7	2		
16 - 32	9	1			
32+	2				

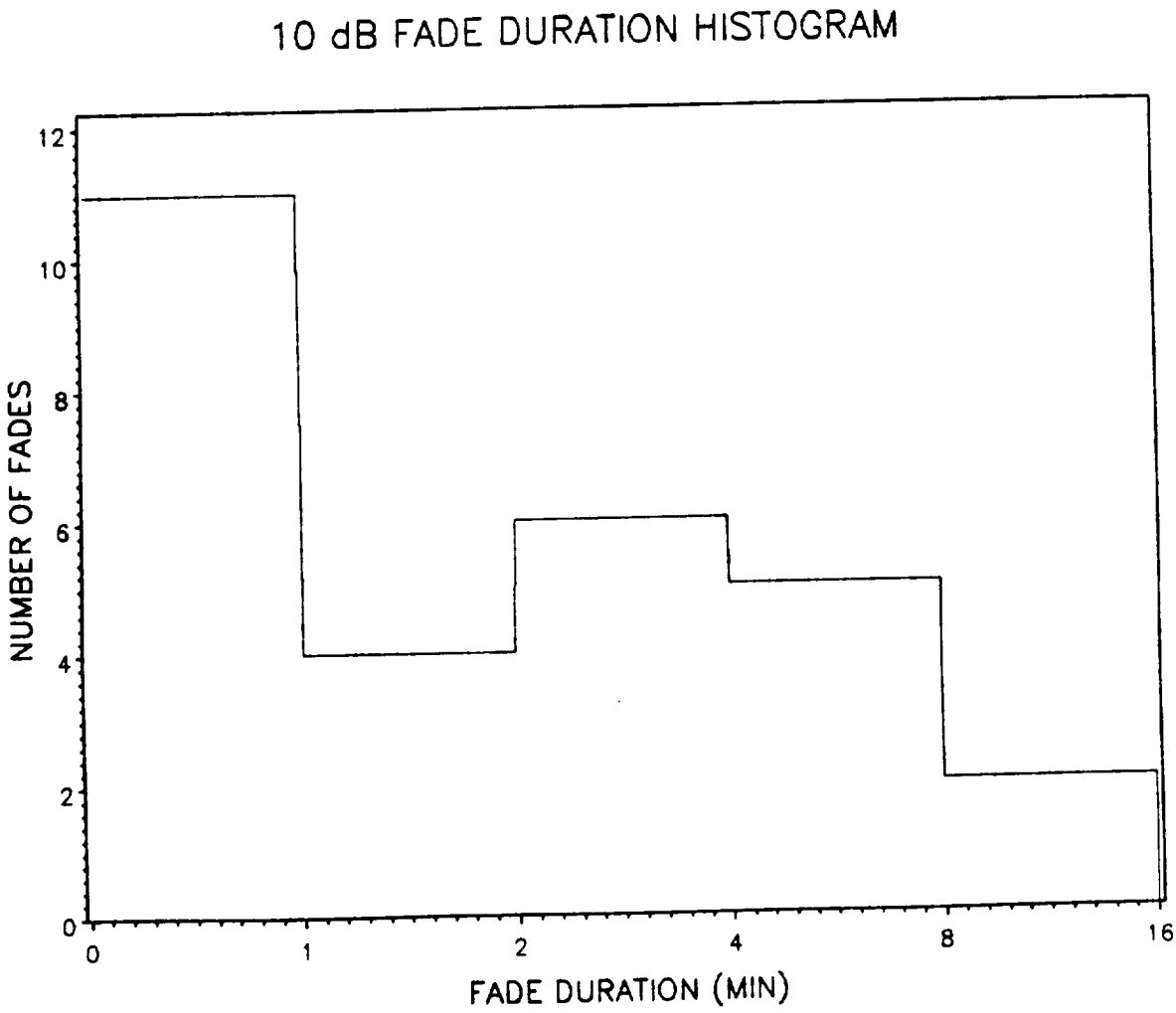

Figure 2.4-7. Fade duration histogram for 10 dB fades from Vogel's February 1978 - January 1979 CTS data at 11.7 GHz, 50.0° elevation angle, circular polarization from [26]

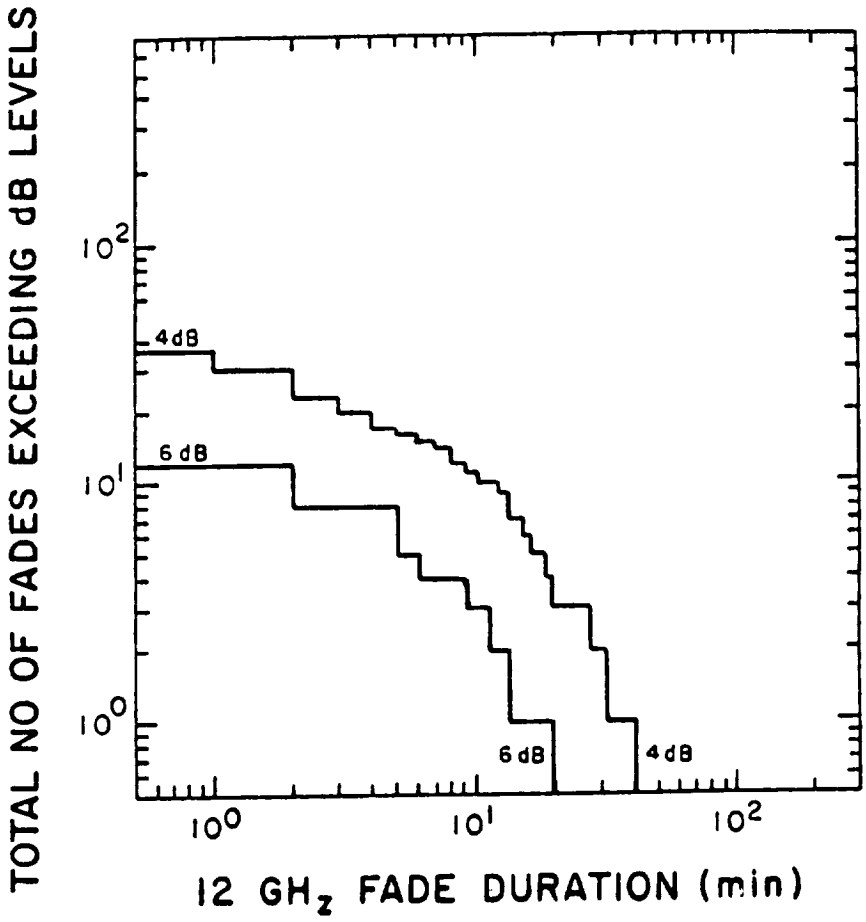

Figure 2.4-8. Cumulative fade duration distributions at two thresholds for satellite-path propagation through rain.

III. REVIEW OF THE LITERATURE

There have been only limited efforts and a few experimental studies aimed at characterizing earth-space propagation related to LMSS. A good summary of LMSS propagation experiments and modeling efforts is presented in [7] with additional modeling efforts given in [25]. There is a total lack of analytic results for fade durations in LMSS. Because of this lack of analytic results, simulators have been developed to obtain the dynamics of a LMSS signal. This chapter summarizes these simulators after first providing some needed background on the time behavior of LMSS signals and signal distributions.

3.1 Summary of Experimental LMSS Study Results

From the experimental studies reviewed in [7], a comparison of different data sets shows that the signal fading statistics behave in a fairly predictable manner. This predictable behavior is seen in Figure 3.1-1 which shows a cumulative distribution plot comparing

three different data sets. These curves appear to have Rician distribution characteristics at high signal levels and lognormal characteristics at low signal levels. The Rician portion of the curves appears to be insensitive to elevation angle and shadowing [9].

One set of experiments was conducted by the Canadian Communications Research Center (CRC) at 870 and 1542 MHz. Measurements made by a mobile following a balloon-borne transmitter in wide open regions recorded multipath signal statistics that followed a Rician distribution with a mean value for the diffuse to line-of-sight component ratio of -11 dB. Figure 3.1-2 shows an example of a distribution plot of the unshadowed CRC data, but K for this case is -14 dB. Measurements made by a mobile following a helocopter-borne transmitter in vegetatively shadowed areas showed that signal statistics depended strongly on the vegetation present. Figure 3.1-3 shows the effect of shadowing on a distribution plot. In these measurements the Rician portion of the curves changed little with the amount of shadowing.

Other experiments were conducted by Wolfhard Vogel, Garry Hess, and Roy Anderson. These experiments had findings similar to the CRC experiments; hence, they will not be covered in detail here. Figure 3.1-4 shows a typical time plot of a received mobile signal. It is drawn from one of Vogel's experiments where he used a balloon-borne transmitter to simulate a satellite signal.

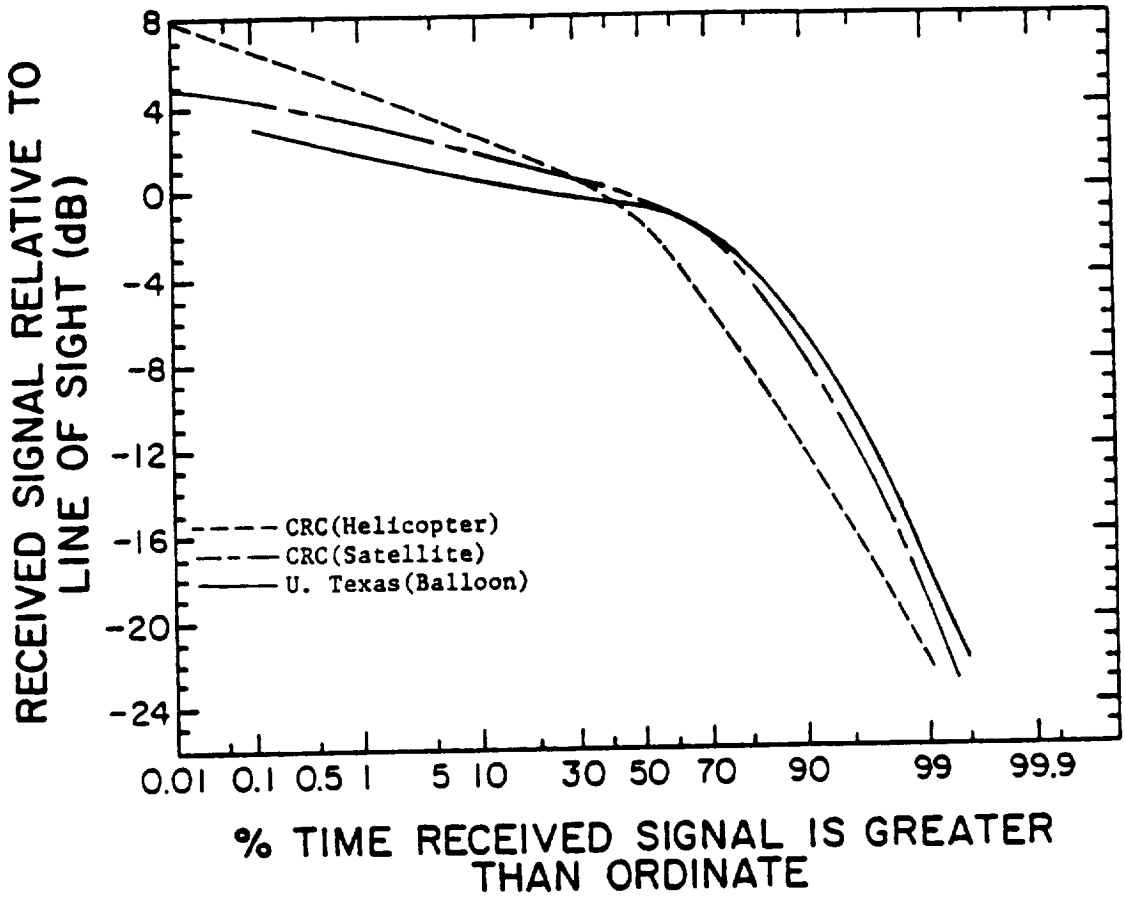

Figure 3.1-1. A comparison of the distribution functions for two CRC experiments and Vogel's first balloon experiment [7].

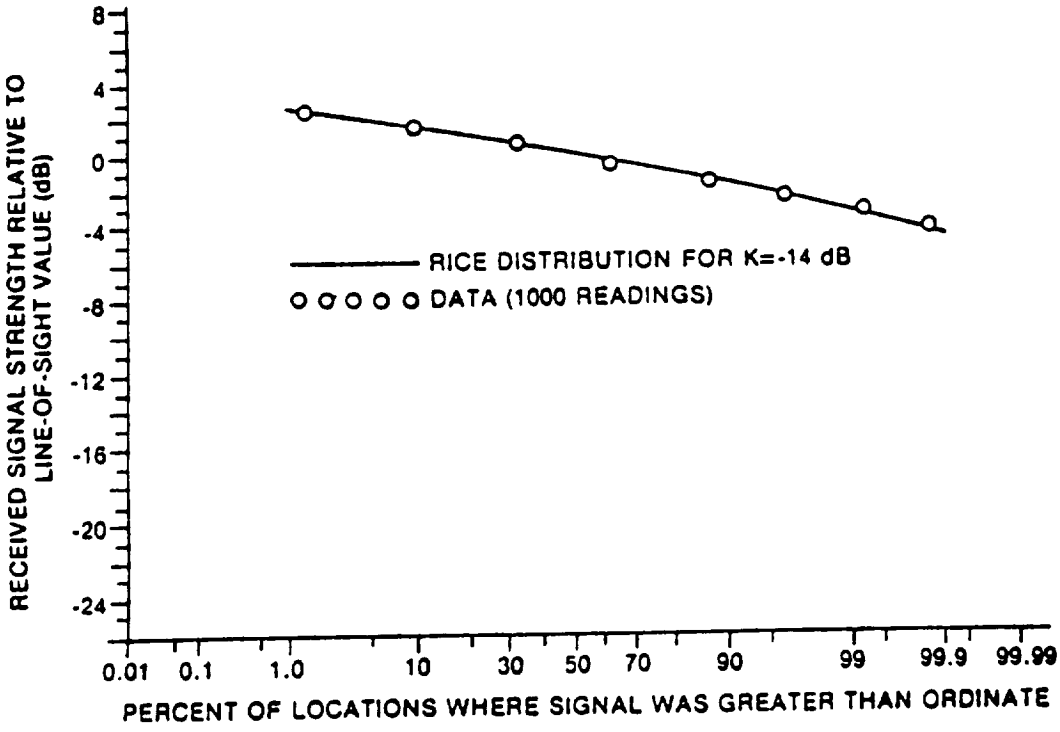

Figure 3.1-2. Comparison of the cumulative distribution function of an unshadowed data set with a Rician distribution. From Butterworth [8]

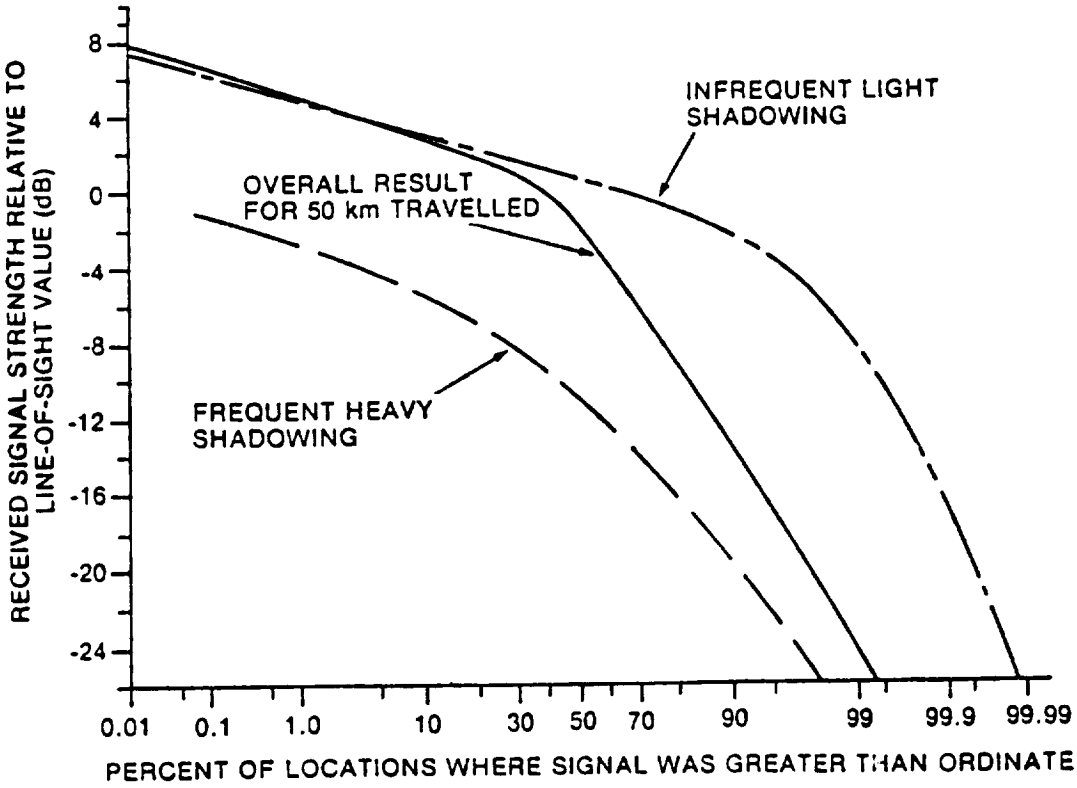

Figure 3.1-3. Distribution functions for September, 1982, helicopter measurements. From Butterworth [8]

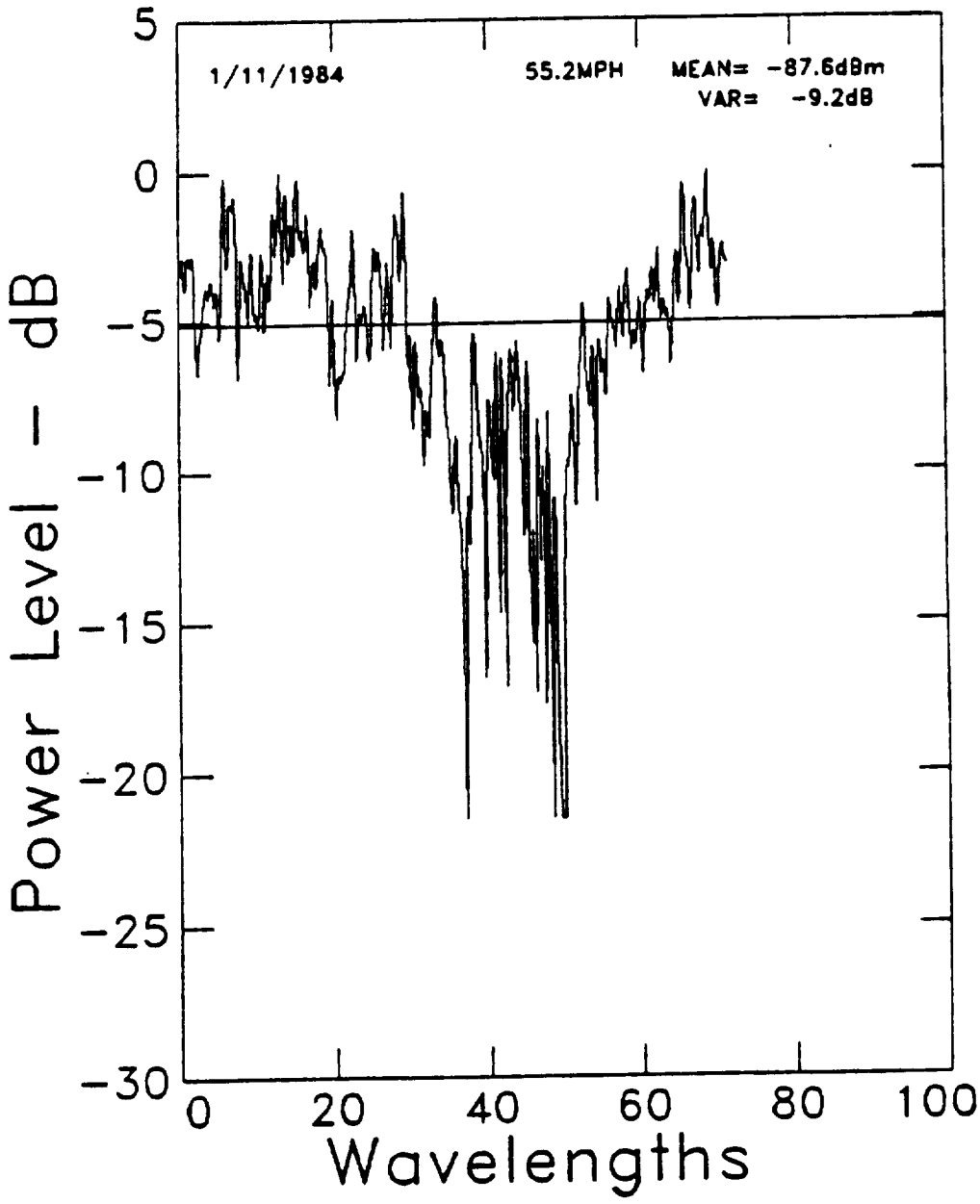

Figure 3.1-4. A one-second time plot of received signal power measured in a pine forest. From Vogel [27]

3.2 Signal Simulators for LMSS

Because of the lack of analytic results for LMSS signal dynamics, several simulators have been developed to synthesize an LMSS signal whose dynamics can be analyzed. These include a hardware simulator at CRC and two simulators at The Jet Propulsion Laboratory (JPL), one implemented in hardware and the other in software.

3.2.1 CRC Hardware Simulator

The hardware simulator developed at CRC is reported by Butterworth in [9] and [10]. It is designed to reproduce the fading effects for land, sea, and air mobile applications. Only the land mobile application will be discussed here. The hardware simulator was built and tested using two different configurations. We will discuss only configuration 2 as described in [10]; Figure 3.2-1 shows a block diagram of this configuration.

In the CRC simulator, the input signal is split into two paths: a direct path where the signal is attenuated according to a lognormal distribution by a voltage controlled attenuator (VCA) and a path where the signal is modulated in amplitude and phase by a Rayleigh fading generator (RFG). The RFG is a quadrature modulator controlled by two independent pseudo-random sequences (I and Q). The spectrum of these sequences is shaped by special filters so that the resulting RFG output signal has a spectrum similar to the multipath signal received by an omnidirectional land-mobile antenna. By

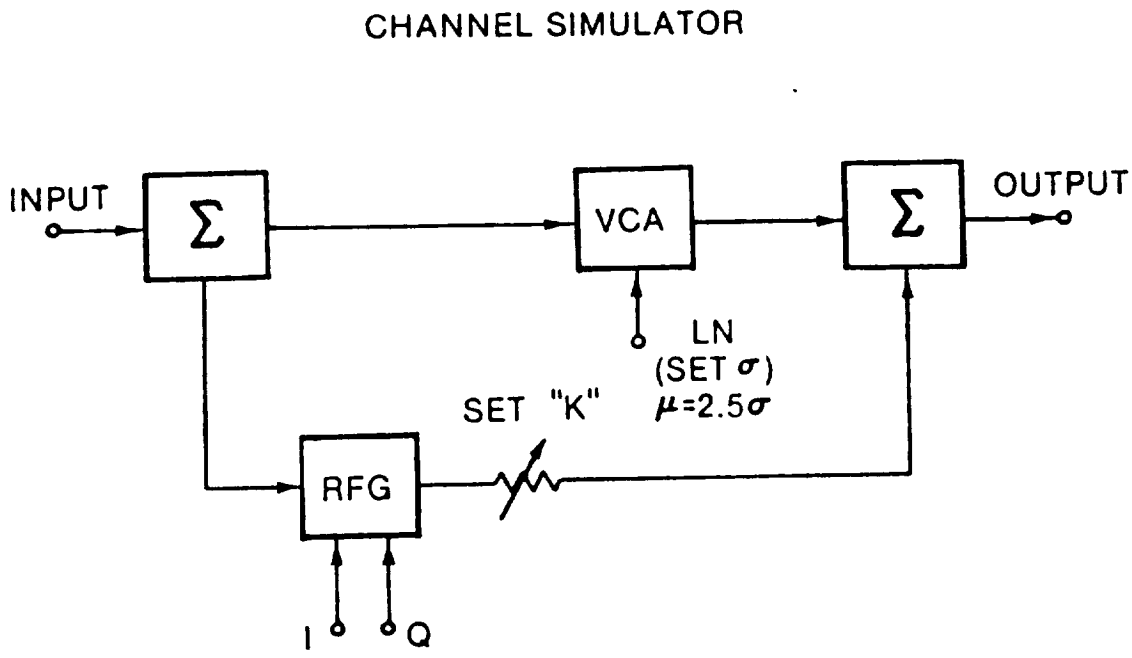

Figure 3.2-1. Configuration 2 of the CRC hardware simulator. From Butterworth [10]

varying the cut-off frequency of the lowpass shaping filters, the simulated vehicle speed can be controlled [10].

The VCA emulates the shadowing effects of such roadside obstacles as trees and buildings. The VCA applies a lognormally distributed attenuation to the direct component of the signal. It is controlled by a third pseudo-random sequence (LN) which varies at a rate of one-hundredth of that of the I and Q sequences. The fading rate was determined by looking at an experimentally obtained chart-recording of a received satellite signal such as that shown in Figure 3.2-2. The thick black line in this figure approximates the long-term mean value of the signal which varies due to shadowing effects. This figure shows that shadowing variations in the signal are much slower than the rapid variations due to diffuse multipath effects. After the shadowing fade rate has been set, the mean value of the VCA attenuation is automatically set to 2.5 times the standard deviation produced by the control sequence LN. The standard deviation can be set from 0 to 6 dB in 1 dB steps.

The simulator is usually controlled by the pseudo-random sequences I,Q, and LN, but this has the drawback of being unable to simulate accurately non-stationary statistics. Shadowing is one of the non-stationary statistics resulting because some routes are shadowed while others are not. If the simulator is controlled by recorded LMSS data instead of the pseudo-random sequences, then the non-stationary phenomena can be better approximated. External control signal input ports on the CRC simulator are provided for this purpose, but no information is presently available on this mode of operation.

To evaluate the simulator, the output signal was processed and analyzed with the same equipment as that used for the CRC field tests mentioned in Section 3.1. Figure 3.2-3

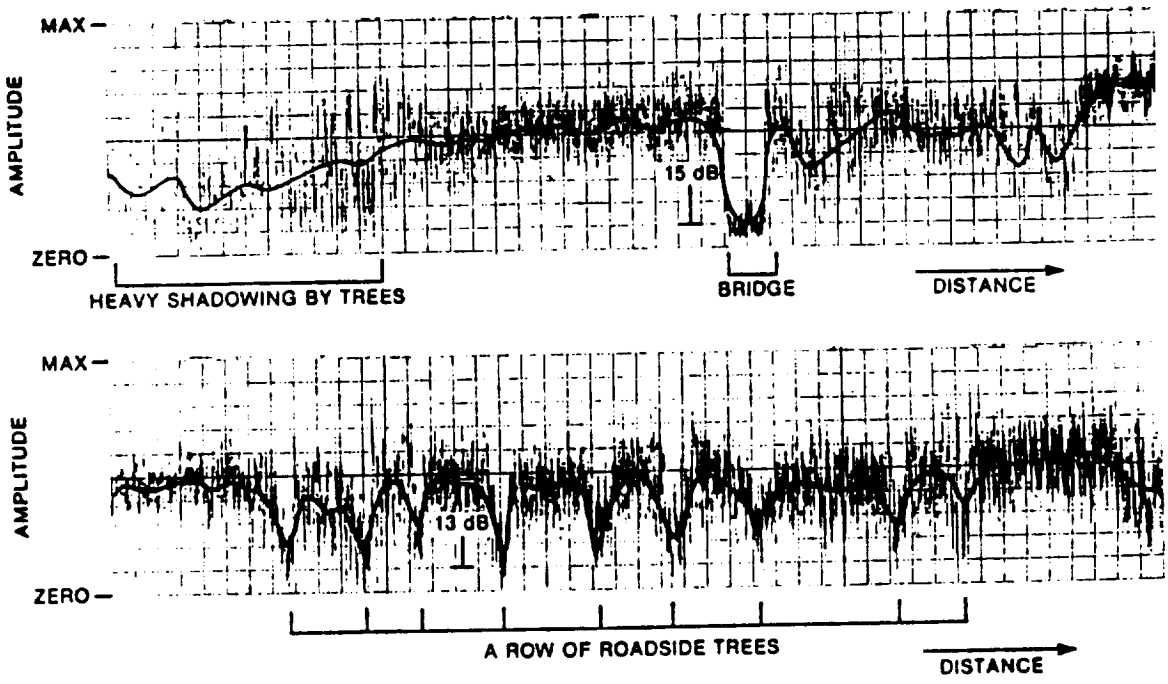

Figure 3.2-2. Time plots of the signal level showing the effects of shadowing obstacles. From Butterworth [10]

shows distribution functions for empirical LMSS data collected using INMARSAT MARECS-A satellite and an omnidirectional antenna. The goal was to match the output of the simulator to the suburban data curve in this figure. Trial and error procedures showed the data were most accurately modeled for unshadowed conditions by a Rician distribution with a constant K of -10 dB, and a mean and standard deviation chosen for the shadowing of -7.5 dB and 3 dB respectively. The total empirical data set was constructed by concatenating samples of shadowed and unshadowed data sets in the proper proportions. Figure 3.2-4 shows the results from this mixing procedure on the signal statistics using 33% shadowed data points. Butterworth noted this curve matches the suburban data curve of Figure 3.2-3 very closely. Butterworth also compared level-crossing rates (number of times that the signal envelope crosses a threshold level with positive slope in a given period of time) and average fade durations (average amount of time that the signal envelope spends below a threshold level) for the simulator output and the suburban data curve and found them to match satisfactorily, but he did not discuss fade duration statistics.

Distribution functions for other proportions of data are shown in Figure 3.2-5. The curve for 5% shadowing was noted to be a reasonable match to the rural farmland data of Figure 3.2-3 [9]. Thus by varying the percentage of shadowed data points which are included in the overall simulated data set, other data sets may be simulated.

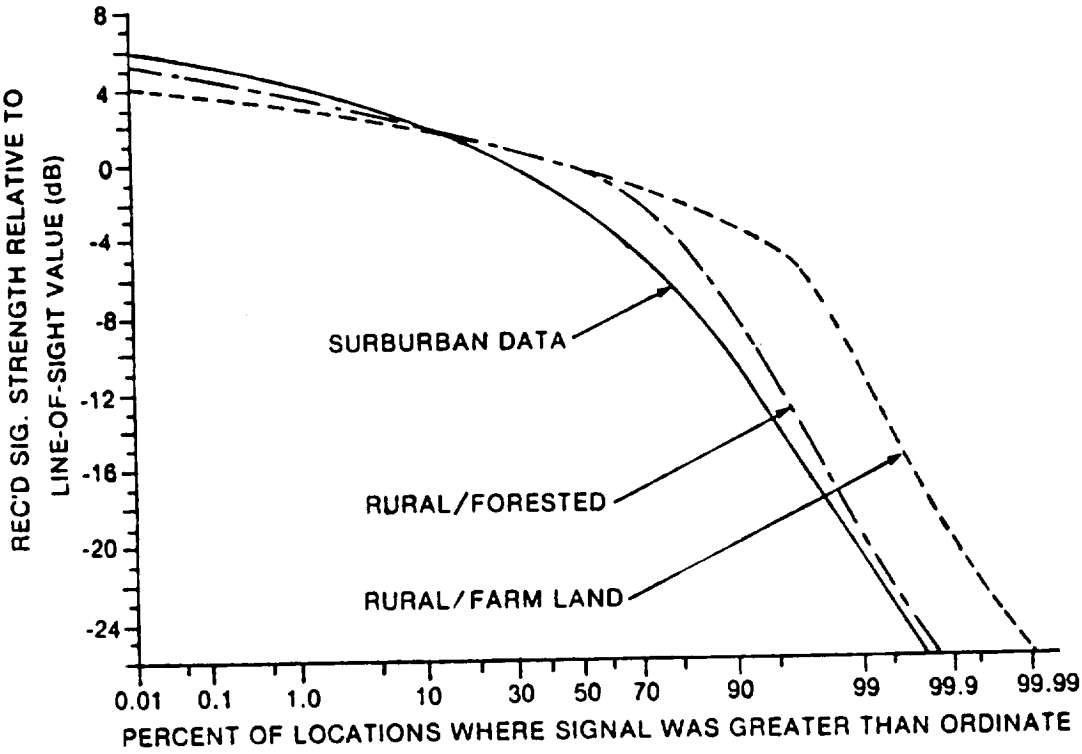

Figure 3.2-3. Distribution functions for November, 1982, MARECS-A measurements. From Butterworth [9]

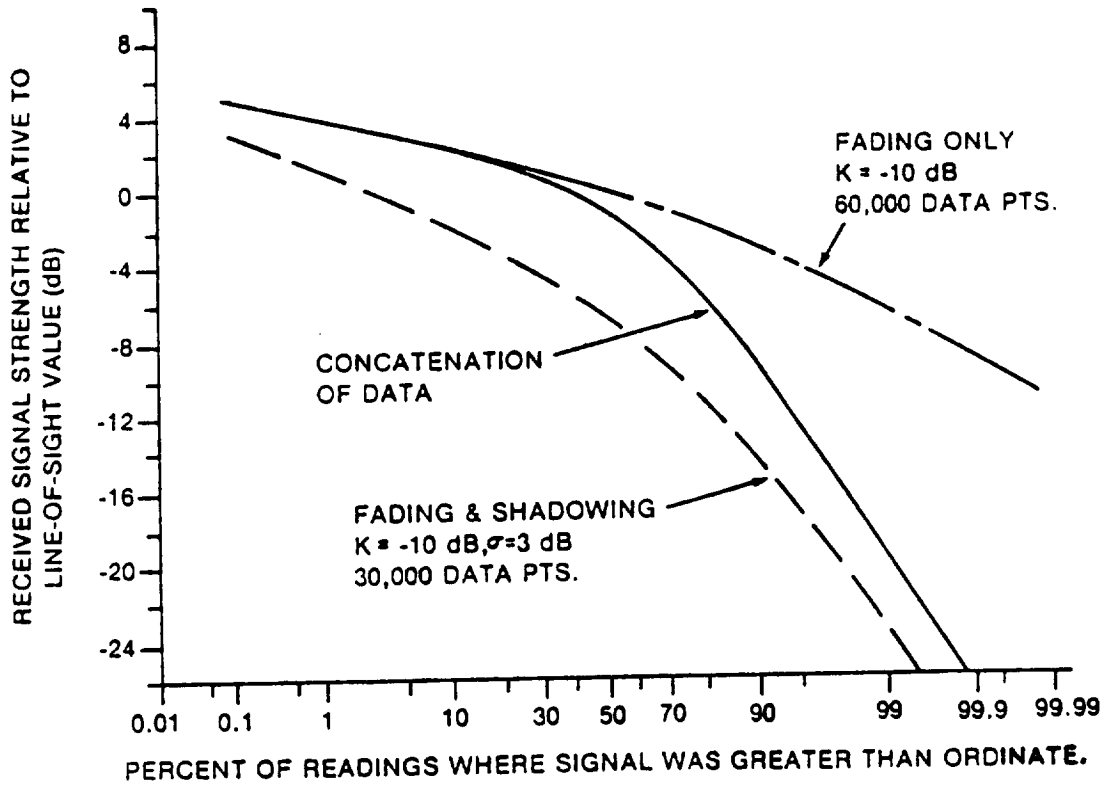

Figure 3.2-4. Distribution functions of simulator data with 33% shadowed data in the concatenated result. From Butterworth [9]

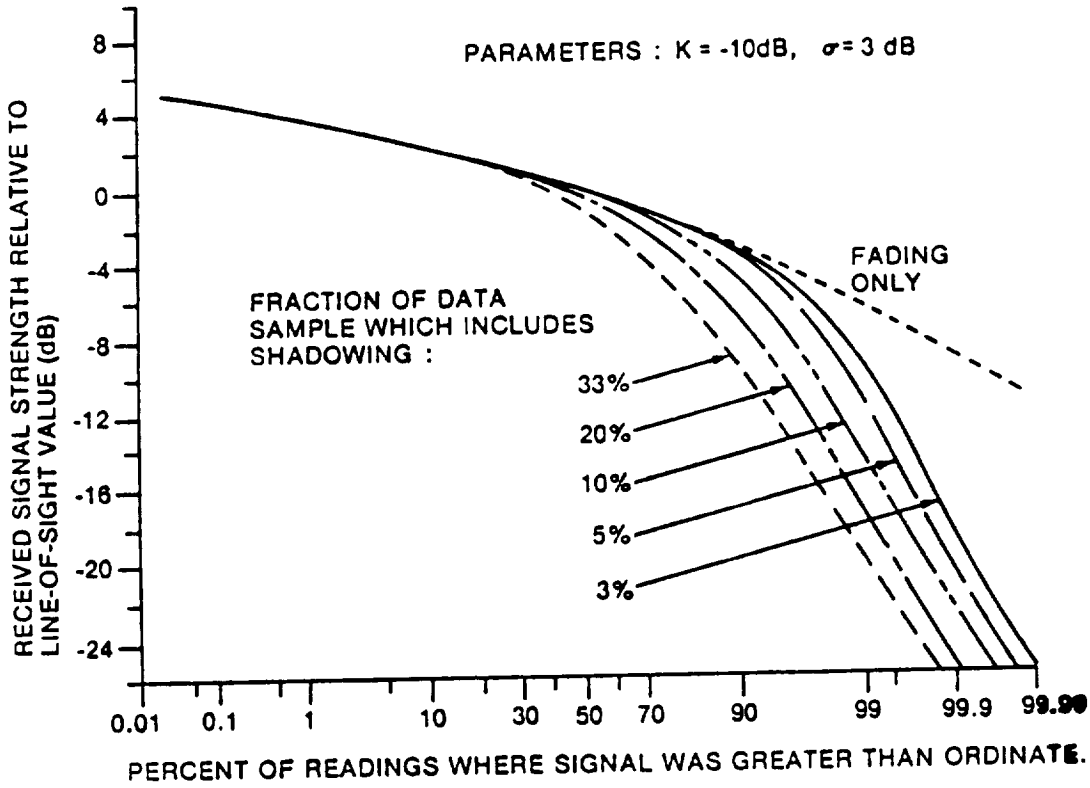

Figure 3.2-5. Distribution functions of the CRC simulator data for various percentages of shadowing. From Butterworth [9]

3.2.2 JPL Hardware Simulator

The hardware simulator developed at JPL was designed to perform end-to-end evaluation of LMSS communication links. The simulator can mimic such multiple channel impairments as multipath fading, Doppler shift, thermal noise, adjacent and cochannel interference, bandlimiting, and nonlinearities.

The process of synthesizing propagation impairments in the JPL simulator is very similar to that for the CRC simulator. To represent multipath fading, the input signal is split into two paths: a direct path and a path where the input signal is modulated by a Rayleigh multipath generator. The resulting signal envelope has a Rician distribution. This approach for generating multipath propagation effects is identical to that of the CRC simulator, but the direct path in the JPL simulator cannot be dynamically attenuated to simulate vegetative shadowing.

The JPL simulator has been used to evaluate bit error rates of GMSK and 2-bit MSK modulation under various fading conditions [13,14] and to test NBFM modulation on voice systems [23]. There has been no further verification of the signal fading statistics beyond confirming that the output signal spectrum approximated theoretical predictions for a Rician fading signal.

3.2.3 JPL Software Simulator

The JPL software simulator has different capabilities than the JPL hardware simulator and is designed more for analyzing the dynamic statistics of a fading mobile signal. The software simulator generates multipath fading in the same manner as both hardware simulators. The spectrum of the fading multipath signal can be adjusted for the speed of the mobile, and Doppler shifts can be put into the direct component. In addition, the software simulator can include effects of a specular component and of an antenna pattern. These features make the software simulator more flexible than the hardware simulators, but the software simulator presently does not incorporate shadowing effects [15].

A sample of the amplitude time plot produced by the JPL software simulator, which produces 2400 samples per second, is shown in Figure 3.2-6. Analysis of the amplitude level statistics showed close agreement between the simulator output and those of a Rician distribution. Histograms of fade duration and interfade interval were also made for two different Rician K parameters at a threshold of -5 dB. These are shown in Figures 3.2-7 and 3.2-8. Note that the fade durations were not normalized to wavelengths traveled as we plan. No further analyses were reported to correlate software simulator output with fading statistics observed from empirical measurements.

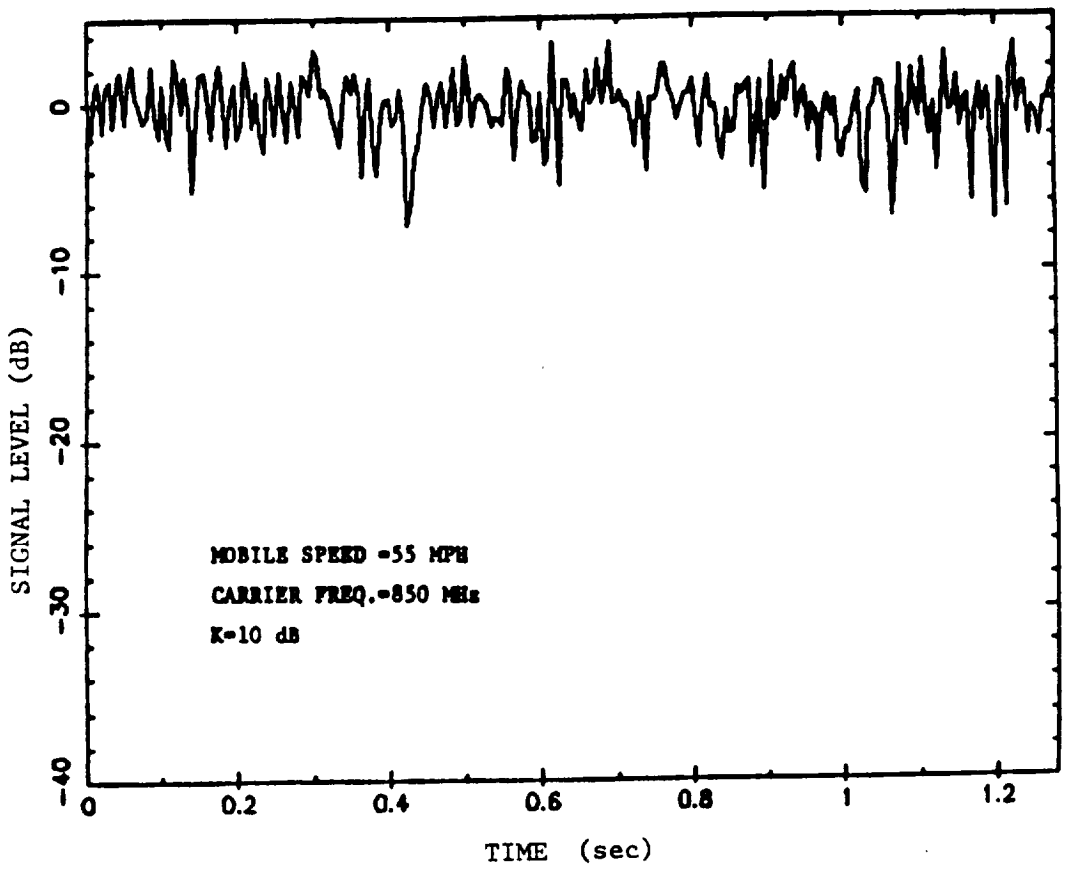

Figure 3.2-6. Sample time plot of the signal level from JPL's software channel simulator. From Divsalar [15]

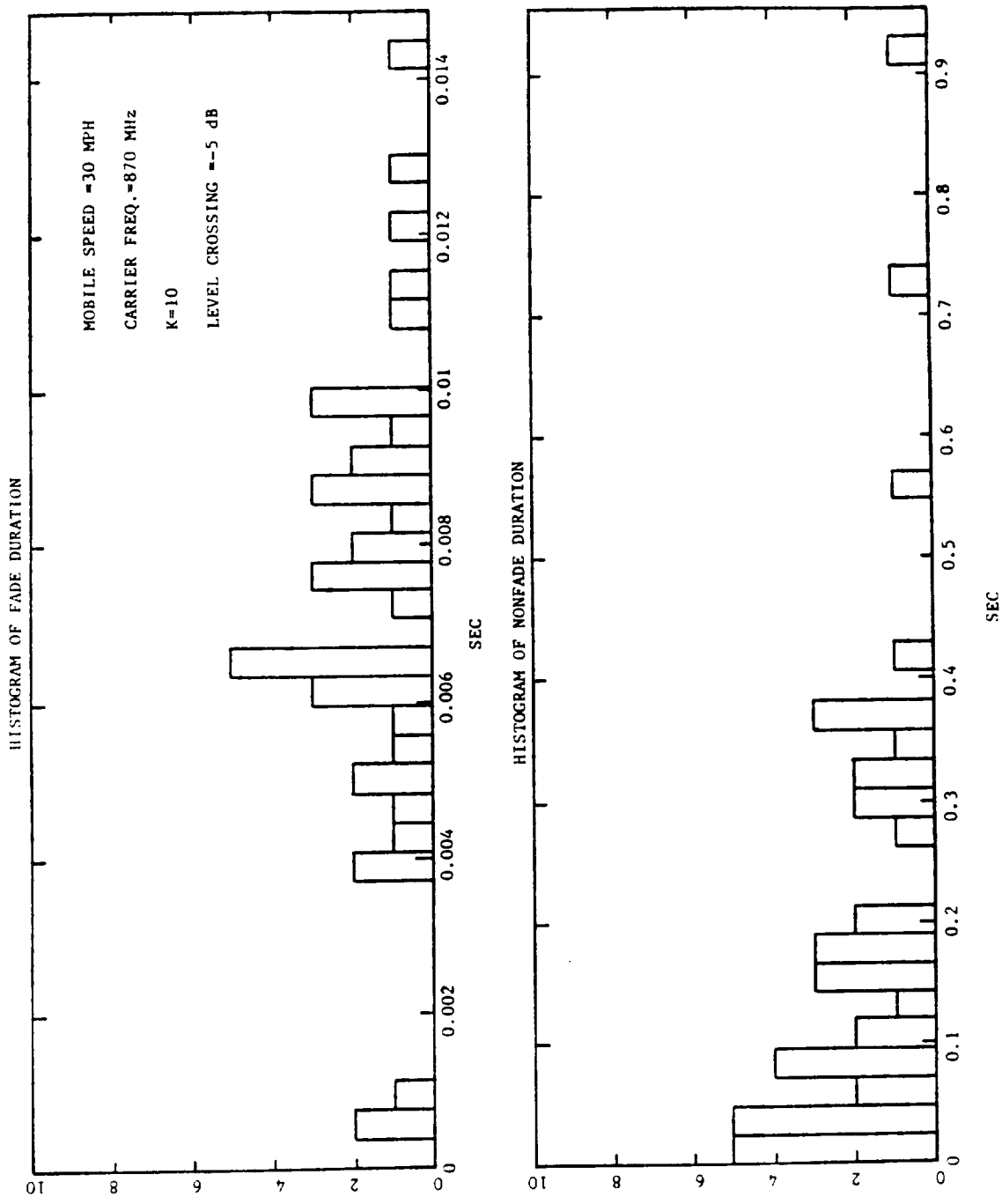

Figure 3.2-7. Histogram of fade durations for data output by the JPL software simulator with K = 10. From Divsalar [15]

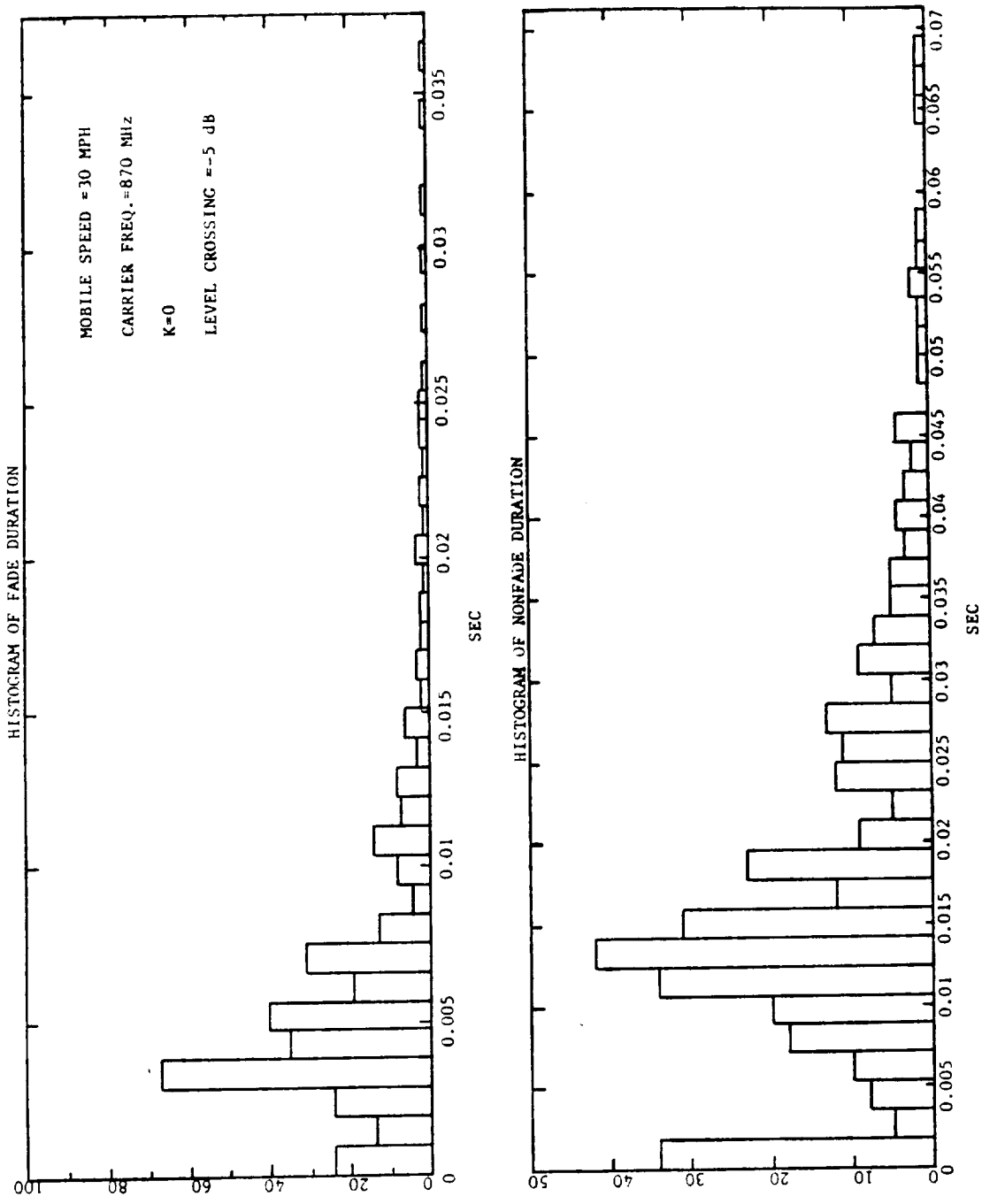

Figure 3.2-8. Histogram of fade durations for data output by the JPL software simulator with K = 0. From Divsalar [15]

3.2.4 Summary and Comparison of Simulators

The three LMSS simulators discussed all have the same basic configuration which was shown for the CRC hardware simulator in Figure 3.2-1. Each generates the diffuse process for the multipath fades in exactly the same manner. Beyond its basic configuration and multipath fade generators, each of the simulators has some unique features, but only the CRC simulator can dynamically model vegetative shadowing. This feature in the CRC simulator is extremely important and necessary in a LMSS simulator because vegetative shadowing plays a large role and is responsible for much of the deep fading in the received mobile signal.

Our simulator was developed using all the previous simulators as a guide. Our primary concerns in the simulator are multipath and vegetative fading. The basic configuration of our simulator, the Virginia Tech (VT) simulator, is the same as the JPL and CRC simulators. Initially, the diffuse process in the VT simulator is generated exactly as in the other simulators. The vegetative shadowing, however, is generated differently than in the previous simulators. To account for vegetative shadowing, the VT simulator uses a scaled version of a lognormal, universal data set that is based on an empirical data set. This scaling procedure is discussed in detail in Section 4.4. Because the scaling procedure is most easily implemented in software (in addition to flexibilities offered by software) we opted to build our simulator using software instead of hardware.

IV. SIMULATOR DEVELOPMENT

4.1 Introduction

In rural areas, LMSS fades are primarily due to shadowing by vegetation and interference between line-of-sight and diffusely reflected waves. The fades due to vegetation account for observed slow fades while fast fades result from the diffusely reflected component. The unshadowed fast fades appear to have a Rician distribution due to a phasor addition of the line-of-sight signal from the satellite and the Rayleigh distributed multipath signal. The slow fades of the direct component of the signal due to vegetation appear to be lognormally distributed. The overall shadowed fading signal appears to have a VS distribution due to a phasor addition of the lognormally fading line-of-sight signal and the Rayleigh distributed multipath signal. The overall

cumulative distribution of the signal received by a partially shadowed mobile can be well approximated as a combination of a Rician and a VS distribution [25].

Using a total probability approach, the overall cumulative distribution can be separated into a Rician portion for the unshadowed mobile and a VS portion for the shadowed mobile. The Rician portion of the distribution is completely defined by K, the ratio of the power in the diffuse Rayleigh component of the signal to the power in the line-of-sight component. The VS portion of the distribution is defined by the mean and standard deviation of the lognormal component (μ_R, σ_R) and $\overline{K}$, the ratio of the power in the diffuse Rayleigh component to the power in the unshadowed line-of-sight component. The parameter $\overline{K}$ is related to the parameter b_0 in Equation 2.4-13 by $\overline{K} = b_0 + 3\text{dB}$. All of these parameters (K, $\overline{K}$, μ_R, and σ_R) are needed to describe a received LMSS signal and are necessary inputs to a simulator.

In the VT simulator, the K parameter of the Rician portion of the distribution is used to determine the inputs to a software Rayleigh generator. The output of the Rayleigh generator is then added to a constant to produce a Rician distribution with the proper K value. The result is a software-generated Rician signal that represents the unshadowed portion of the data received by the mobile.

Generation of the shadowed mobile signal is more complicated because three parameters are needed to specify the VS distribution. Here, the $\overline{K}$ parameter of the Rayleigh portion of the VS distribution is used to determine the inputs to a software Rayleigh generator that produces the rapidly varying component of the vegetatively shadowed signal. The mean and standard deviation of the lognormal portion of the VS distribution are used to generate the slow fades. The mean and standard deviation are supplied to a software generator that scales an existing universal data set to produce a slowly varying signal.

This slowly varying lognormally distributed signal represents the slowly varying component of the vegetatively shadowed signal. The slow and fast fading components of the shadowed signal are added as complex voltages to finally generate the total shadowed signal.

The total data set for the signal received by the mobile is created by concatenating shadowed and unshadowed data sets. The percentage of shadowed data used to construct the total data set corresponds exactly to the percentage of shadowing of the line-of-sight signal encountered by the mobile. The data set represents received signal level as a function of wavelengths traveled by the mobile. It may be analyzed for any dynamic fade statistics after construction.

In Section 4.2, we show that a LMSS signal can indeed be separated into its component parts. Section 4.3 discusses development of the initial Rayleigh generator used to generate the fast varying component of both shadowed and unshadowed mobile signals. Section 4.4 discusses development and background work for the lognormal signal generator used to generate the slowly varying component of the vegetatively shadowed mobile signal. Section 4.5 combines the Rayleigh generator and the lognormal signal generator to create the overall simulator.

4.2 Separation of the Data into Component Parts

Development of the VT simulator relies on the assumptions that an unshadowed mobile signal can be broken into Rayleigh and constant components and that a shadowed mobile signal can be broken into Rayleigh and lognormally distributed components. In this section, we show this is true by separating measured signals into a fast varying component which is Rayleigh distributed in magnitude (for both shadowed and unshadowed conditions) and uniformly distributed in phase (for unshadowed only) and a slowly varying component which is lognormally distributed (for shadowed conditions).

4.2.1 Data Base for Simulator Development

To verify that an LMSS signal can be separated into component parts, a data base was required. (The data are also required later to create a universal data set for generating slowly varying fades.) The data set which we used for these purposes was generously supplied by Wolfhard Vogel of the University of Texas at Austin. He provided 37 minutes of data from his November 1984, balloon measurements. This data set contains both shadowed and unshadowed measurements and is ideal for simulator development. The data were processed so that it provides records of signal level as a function of wavelengths traveled. Appendix A discusses the processing in detail.

4.2.2 Slowly Varying, Lognormal Component

The slowly varying component of the fading signal was extracted by representing the total received mobile signal as a complex voltage and taking a running average. Essentially this corresponds to low-pass filtering the data to obtain the slowly varying signal component. The running average is performed by sliding an averaging window across the data. The average of all the points within the window determine the value for the point at the center of the window. As the window slides across the data, the fast varying diffuse component of the data is removed by the averaging process. The result is a slowly varying signal that corresponds to the direct component of the signal and the mean of the original signal. Figure 4.2-1 shows 100 wavelengths of Vogel's data with vegetative shadowing present and the running average (with a 20 wavelength long window) of the data superimposed.

The size of the window chosen for the running average for all of Vogel's data is 20 wavelengths. This value was selected by trial and error, but an illustration should show the validity of the choice. Figure 4.2-2 presents the same 100 wavelengths of data as Figure 4.2-1, but now running averages with windows of 10, 20, 40, and 80 wavelengths are superimposed. The 10 wavelength long running average has not yet removed the fast varying component of the signal; running averages with less than 10 wavelength windows contain even more of the fast varying component. The 40 and 80 wavelength (and anything longer) running averages have lost the integrity of the fade. The 20 wavelength running average is the only one which adequately removes the fast varying component of the signal and retains the integrity of the fade. Windows from approximately 15 wavelengths to 30 wavelengths appear adequate and the overall data separation process was found to be relatively insensitive to window lengths between

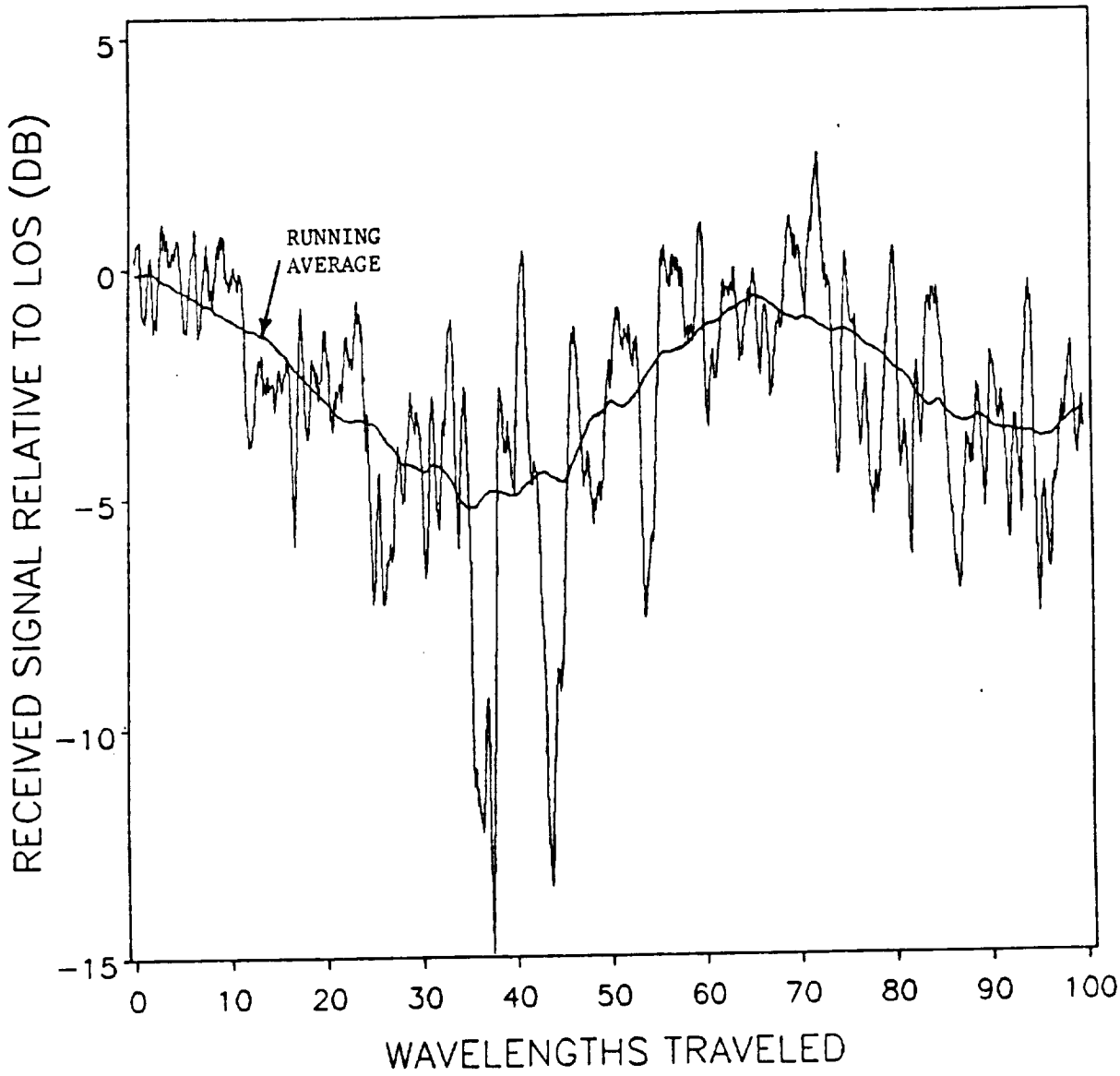

Figure 4.2-1. 100 wavelengths of data set TD090954 and superimposed running average for a 20 wavelength long averaging window.

these. Examination of a number of fades like those in Figure 4.2-1 and the insensitivity of the separation process to windows between 15 and 30 wavelengths led to a choice of a 20 wavelength window for removing the slow fades from Vogel's data.

After the window size was determined for the running average, portions of the data were processed to remove the slowly fading component. The output of the running average, which corresponds to the direct component of the LMSS signal (i.e. the averaging process removes the diffuse component) was then processed to determine the cumulative distribution. In order to determine the distribution of the output of the running average during vegetative shadowing, a threshold had to be set where we considered vegetative shadowing of the direct component to be present. Shadowing was considered to be present when the data output of the running average process fell below a threshold of -2 dB. Vegetative shadowing of the direct component was considered to be absent above this threshold. Again, this number was chosen by examining at the data. Because of transmitter power fluctuations, receiver fluctuations, data processing errors, or a variety of other reasons, the signal output by the running average tended to drift around the 0 dB threshold (sometimes in excess of 1 dB) when no shadowing was present. Ideally, the direct component should remain at 0 dB when no shadowing is present. If the threshold for determining the presence of shadowing is set too low, much of the unshadowed data will be considered shadowed because of the drifting of the recorded signal mean. Setting the threshold to -2 dB tended to eliminate nearly all the unshadowed data that would otherwise be considered shadowed with a lower threshold. The value was not set any higher so that a minimum of shadowed data falling below the -2 dB threshold would be eliminated from being considered shadowed.

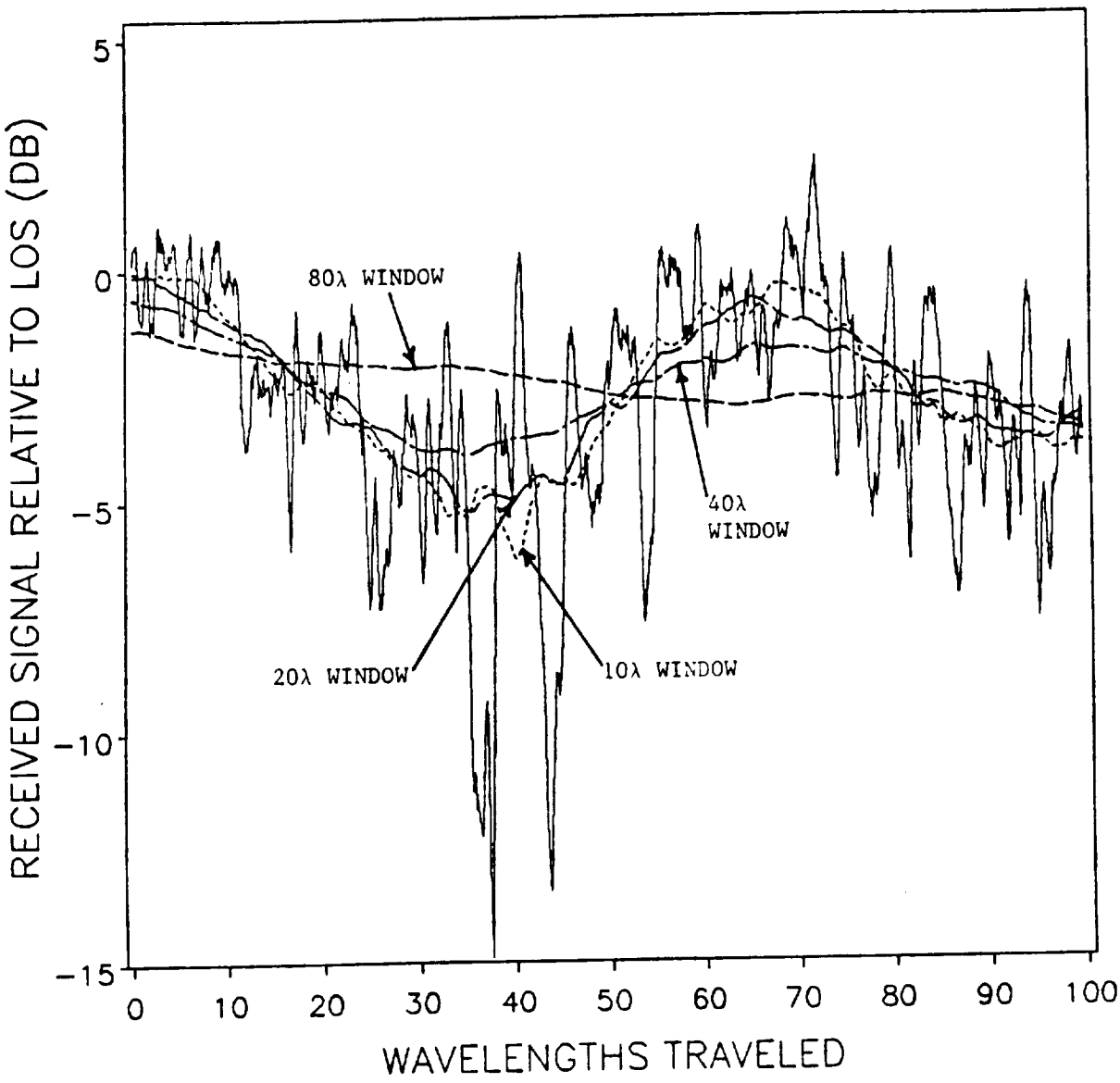

Figure 4.2-2. 100 wavelengths of data set TD090954 and superimposed running averages with various size averaging windows.

After setting the threshold for shadowing, the distribution of the shadowed portion of the direct component output by the running average was tested. To test the distribution of the direct component, when vegetative shadowing is present, only data output by the running average falling below the -2 dB theshold are considered. All other data are excluded from the distribution. It was earlier assumed that the distribution of the vegetatively shadowed direct component was lognormal. Figure 4.2-3 shows the distribution of one minute of Vogel's data where much vegetative shadowing was present. It also shows the distribution of the running average of the shadowed data extracted from this data set. Note the output of the running average, which corresponds to the direct component of the LMSS signal, follows a lognormal distribution very well when vegetative shadowing is present. All other data sets tested also showed the vegetatively shadowed direct component of the signal to follow a lognormal distribution, justifying our earlier assumption of a lognormally-distributed vegetatively-shadowed direct component.

We did not examine the distribution of the direct component phase because earlier processing (described in Appendix A) forced the phase to be essentially zero. The absolute value of the phase of the direct component is, we believe, fairly unimportant in our work because it is essentially constant relative to the phase of the diffuse component and thus plays little role in the fading dynamics of the overall signal.

The program for performing running averages on Vogel's data is called RUNA2.F and a listing may be found in Appendix B.

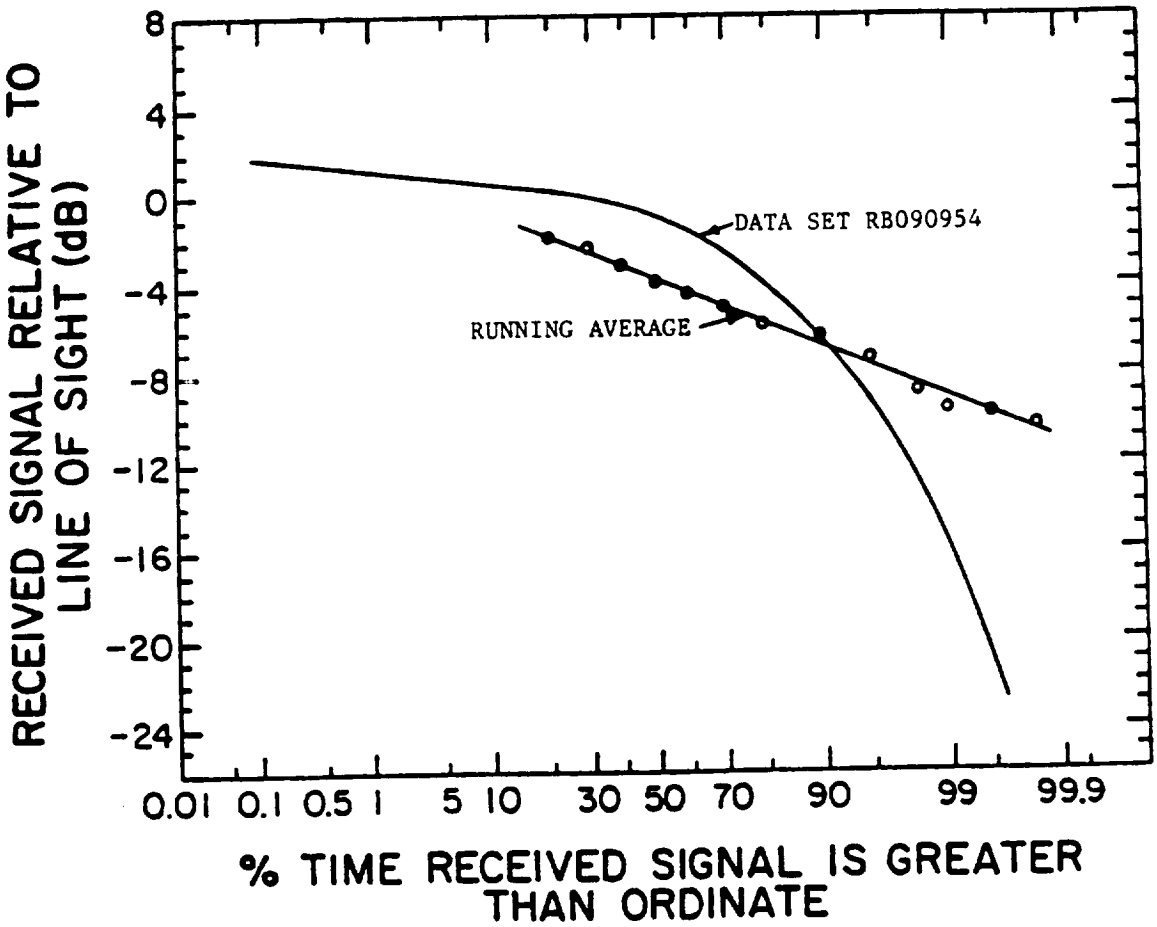

Figure 4.2-3. Cumulative distribution plot of heavily shadowed data set TD090954 and the extracted slow fade component.

4.2.3 Fast Varying, Rayleigh Component

Implicit in the development of the VT simulator is the assumption that the fast varying diffuse component of the LMSS signal is Rayleigh distributed in magnitude and uniformly distributed in phase for both vegetatively shadowed and unshadowed conditions. To test this assumption, we extracted the fast varying component of the signal by subtracting the running average from each member of the original data set. To perform this subtraction, we put both data sets into complex voltage form and took the difference on a point-by-point basis. The result of this subtraction process is the total mobile signal less the direct component, and it corresponds to the fast varying diffuse component of the signal.

We tested the result of the subtraction process for distribution for both shadowed and unshadowed conditions. As before, the threshold for shadowing was set by the running average at -2 dB. Figure 4.2-4 shows the distribution of unshadowed data set TD090517; note that it appears to be Rician distributed because the data is unshadowed. Figure 4.2-5 shows on Rayleigh probability paper the distribution of 4096 points of the magnitude of the diffuse component extracted from data set TD090517. Note it plots as a straight line on the Rayleigh paper and is thus Rayleigh distributed. Figure 4.2-6 shows the probability density (density is used again here instead of a cumulative distribution because a uniform density is more easily recognized when plotted in this manner) of the phase of the diffuse component extracted from 4096 points of data set TD090517. Note the density function plots close to a horizontal straight line, indicating that the phase of the diffuse component is uniformly distributed. We examined each of the 16 unshadowed data sets supplied by Vogel and found the diffuse component in each data set to be Rayleigh distributed in magnitude and uniformly distributed in phase.

We, therefore, conclude that this behavior is a general characteristic of the diffuse component of the received LMSS signal.

Figure 4.2-7 shows the distribution of shadowed data set TD091540. Figure 4.2-8 shows on Rayleigh paper the distribution of the magnitude of the diffuse component extracted only from shadowed data contained in data set TD091540. Note again it plots as a straight line on the Rayleigh paper indicating it is Rayleigh distributed. Figure 4.2-9 shows the probability density of 8096 points of the phase of the diffuse component extracted from data set TD091540. It is not uniformly distributed. The phase tends to group around 0 and 180 degrees in a bimodal distribution. We presently have no explanation for this behavior, but every shadowed data set examined behaves in the same manner (both in magnitude and phase), independent of the fade depth.

Because under vegetatively shadowed conditions the magnitude of the diffuse component was found to be Rayleigh distributed and the phase was found to behave in a consistent manner (although not uniformly distributed), we chose to initially ignore the nonuniform distribution of the phase in our initial simulator development. It turns out that the nonuniformly distributed phase of the extracted diffuse component for the shadowed mobile is important. Although not uniformly distributed, the predictable behavior of the phase independent of fade depths allows it to be incorporated to improve the simulator's performance.

The programs for separating the fast varying fades from the overall data set through use of the running average of the data set is called RICSE3.F and a listing may be found in Appendix B.

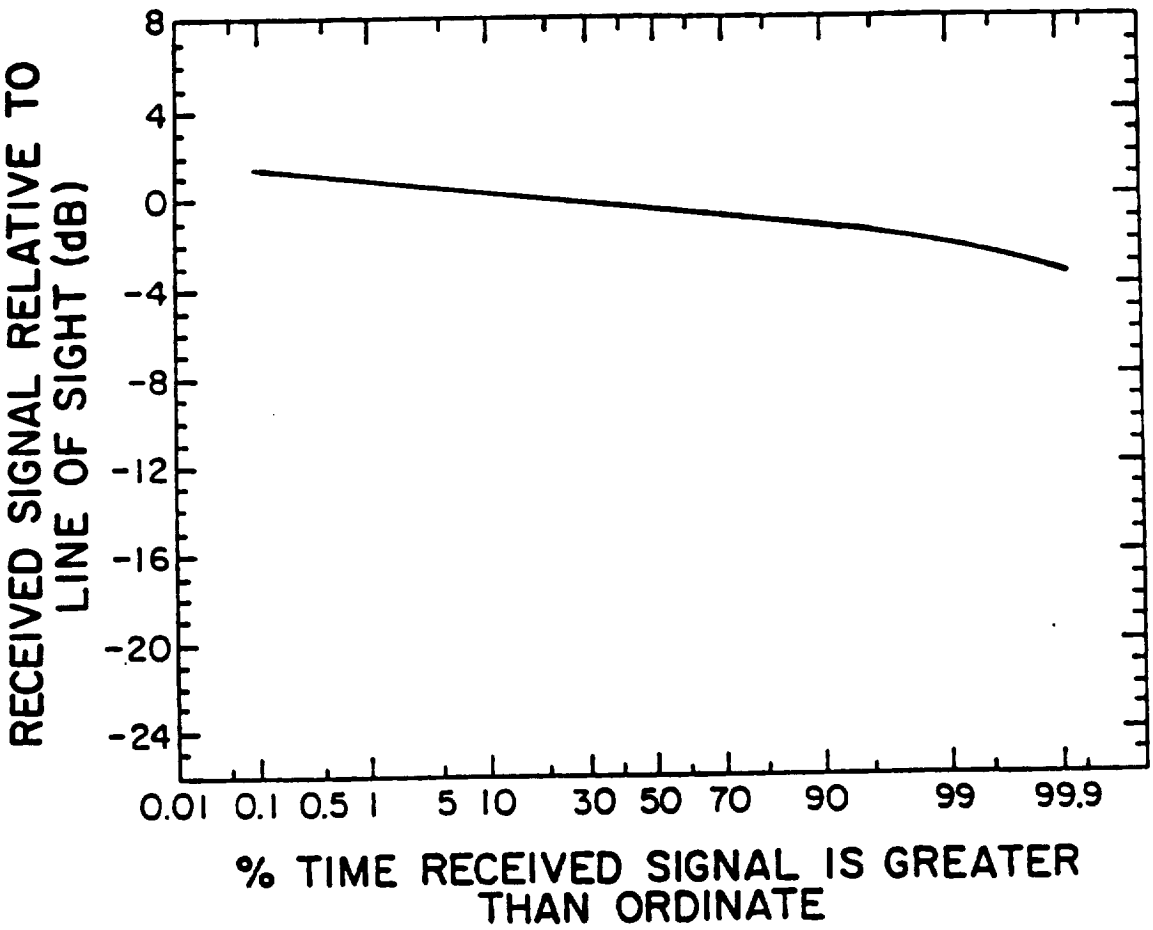

Figure 4.2-4. Cumulative distribution plot of unshadowed data set TD090517.

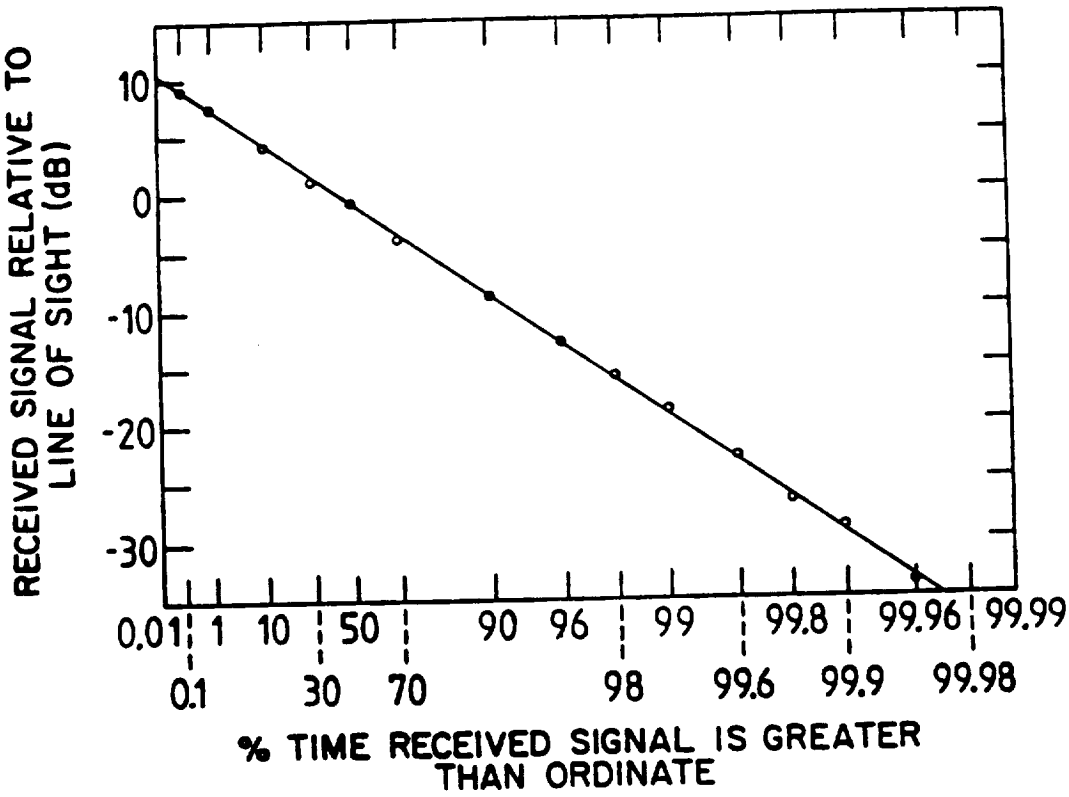

Figure 4.2-5. Cumulative distribution plot of the magnitude of the fast fade component extracted from unshadowed data set TD090517 plotted on Rayleigh probability paper.

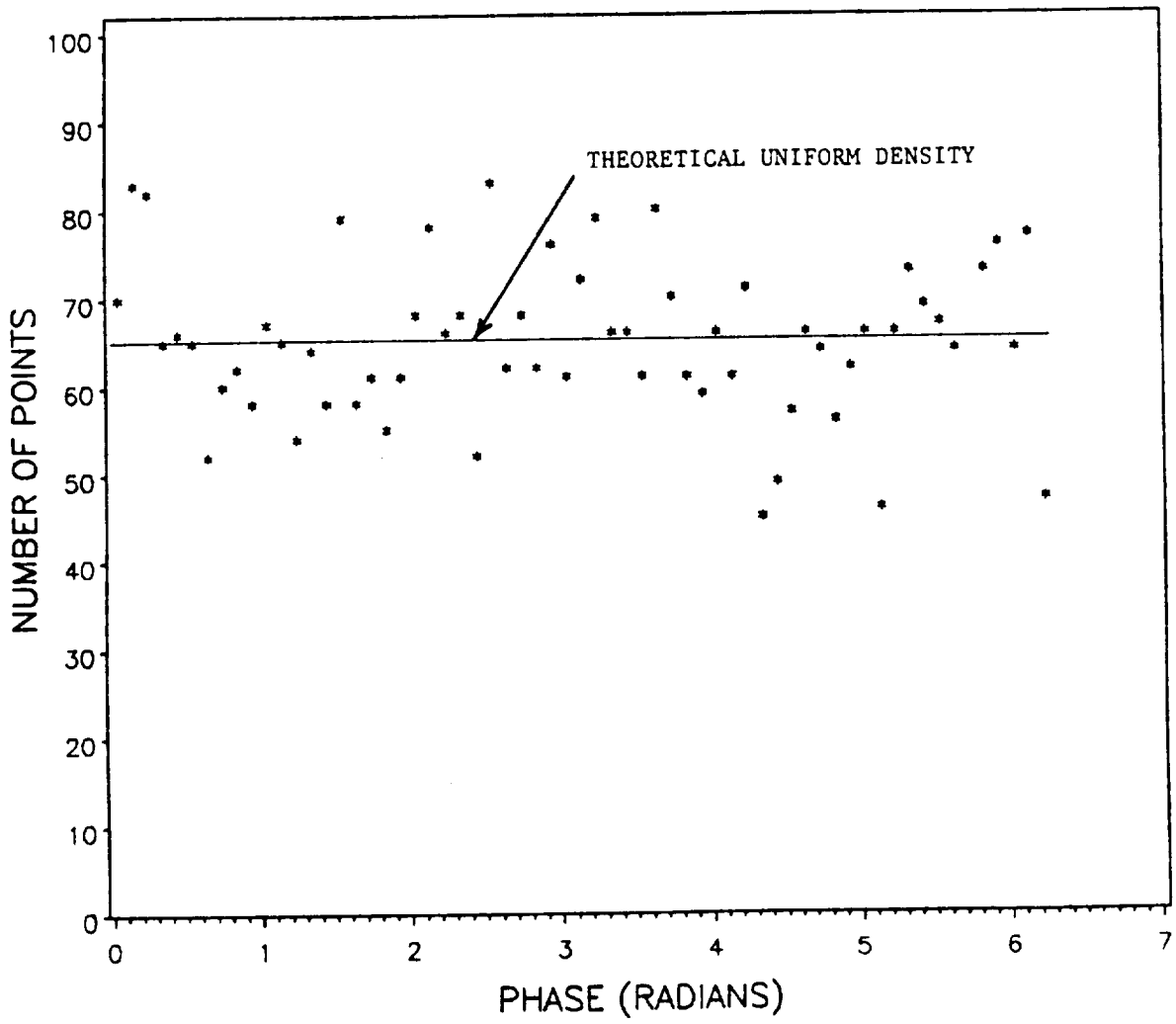

Figure 4.2-6. Density function plot of 4096 points of the phase of the fast fade component extracted from unshadowed data set TD090517.

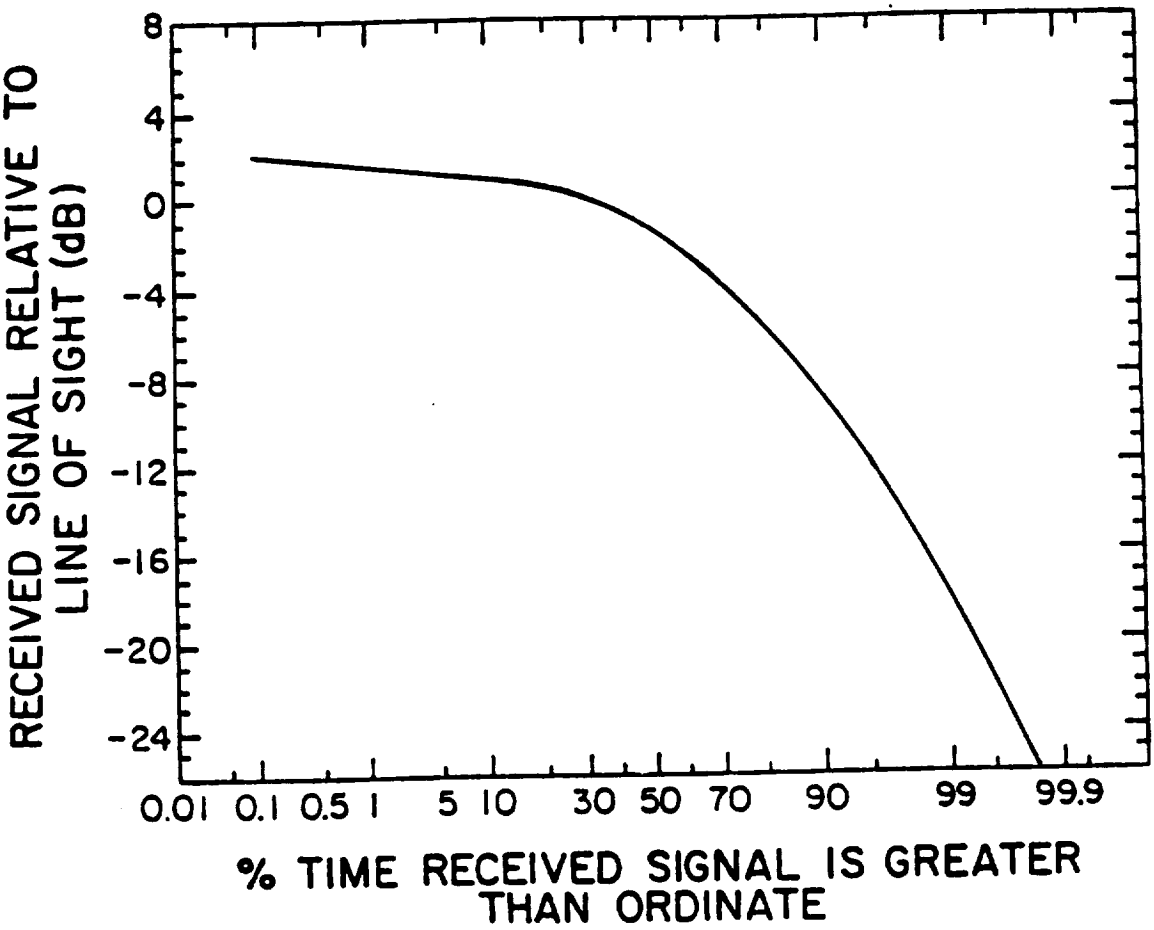

Figure 4.2-7. Cumulative distribution plot of partially shadowed data set TD091540.

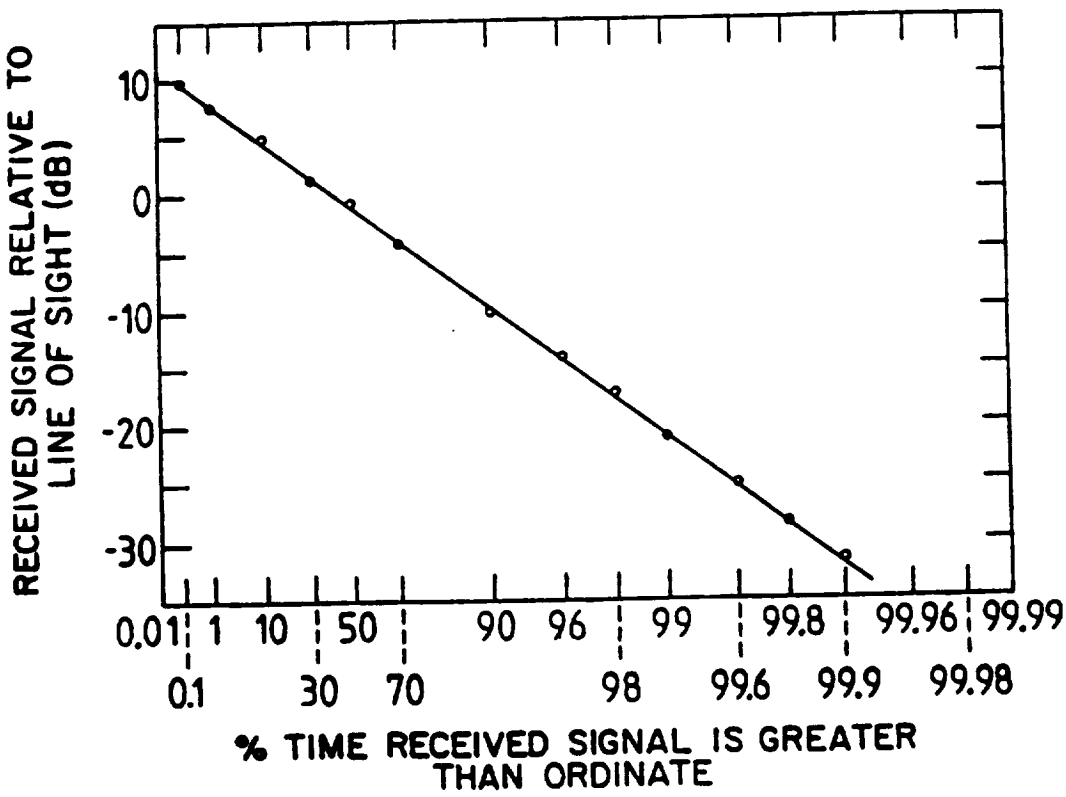

Figure 4.2-8. Cumulative distribution plot of the magnitude of the fast fade component extracted from shadowed data in data set TD091540 plotted on Rayleigh probability paper.

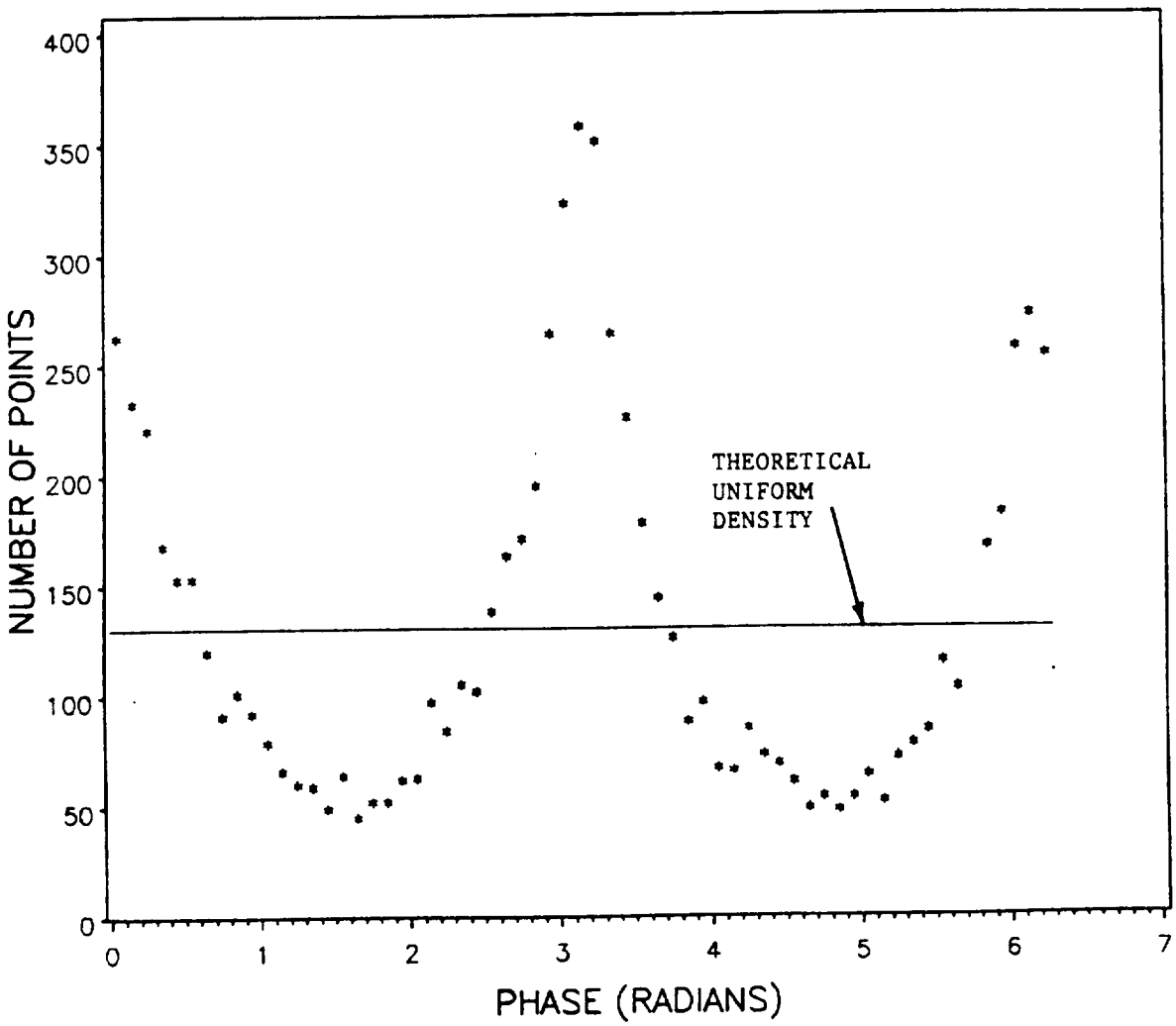

Figure 4.2-9. Density function plot of 8192 points of the phase of the fast fade component extracted from shadowed data in data set TD091540.

4.3 Generation of the Rapidly Varying Component of the LMSS Signal

The fast varying component of the LMSS signal due to multipath fades is, as was shown in Section 4.2, Rayleigh distributed in magnitude and uniformly distributed in phase (at least for the unshadowed case). To create this component of the signal, the VT simulator initially generates a diffuse process exactly like that of the CRC and the JPL simulators. This diffuse process generator, or Rayleigh generator, is covered extensively in the literature and may be found in various forms in [2,5,10,13,14,15]. Figure 4.3-1 shows a block diagram of the Rayleigh generator. All of the Rayleigh generators reviewed, whether developed in hardware or software, are constructed following the basic building blocks in Figure 4.3-1. Our original simulator follows the same block diagram.

To generate the diffuse process, the spectrum of the filters in Figure 4.3-1 must be determined. To determine the spectrum of these filters, the nature of the diffuse process must be examined. Rewriting Equation 2.4-1, the diffuse component may be expressed as

$$R_{dif} = \sum_{i=1}^{N} A_i \exp[j\varphi_i] \tag{4.3-1}$$

where A_i and φ_i are the amplitude and phase (phase measured with respect to the direct component) respectively of component i of the scattered wave. Following [15], this is also equivalent to

$$R_{dif} = N_C(t) + jN_S(t) = N(t)\exp[j\theta(t)] \tag{4.3-2}$$

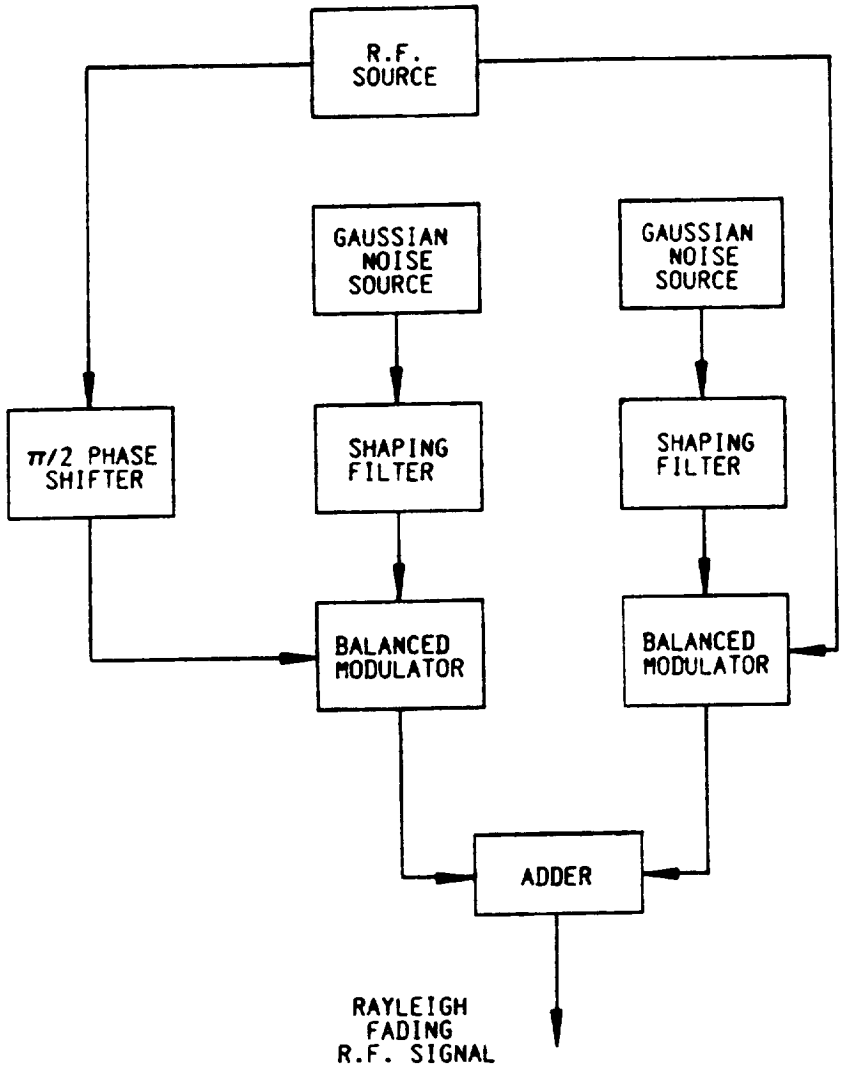

Figure 4.3-1. Block diagram of Rayleigh fading signal generator.

where $N_C(t)$ and $N_S(t)$ are colored Gaussian noise processes, N(t) is the Rayleigh distributed amplitude of the diffuse component, and $\theta(t)$ is the uniformly distributed phase of the diffuse component. The Rayleigh generator attempts to produce the processes $N_C(t)$ and $N_S(t)$ to generate R_{dif} , but to generate such processes, the autocorrelation or power spectral density of the process must be known.

The power spectral density of the diffuse process is developed in detail in [12]. In general, it is given by

$$S(f) = \frac{p(\alpha)\, g(\alpha) + p(\gamma)\, g(\gamma)}{\sqrt{f_m^2 - f^2}}$$

$$\alpha = \cos^{-1}(f/f_m) \qquad (4.3\text{-}3)$$

$$\gamma = -\cos^{-1}(f/f_m)$$

$$f_m = V/\lambda$$

where $p(\alpha)$ is the intensity function of the diffuse waves, $g(\alpha)$ is the power gain of the antenna, f is the frequency, V is the velocity of the mobile, and λ is the wavelength at the frequency of operation. For an omnidirectional antenna, which is the case we are interested in, this reduces to

$$S(f) = \frac{1}{\pi \sqrt{f_m^2 - f^2}} \qquad (4.3\text{-}4)$$

$$f_m = V/\lambda$$

where V is the velocity of the mobile, λ is the wavelength at the frequency of operation, f. The spectrum of Equation 4.3-4 appears as shown in Figure 4.3-2.

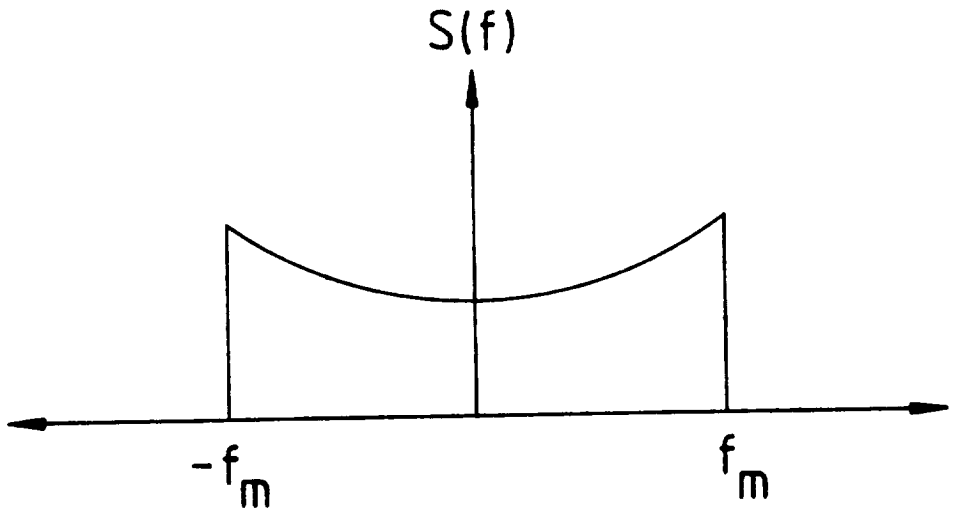

Figure 4.3-2. Spectral density of complex envelope of the received signal used for shaping filters in the Rayleigh generator.

The power spectral density for an omnidirectional antenna given by Equation 4.3-4 determines the spectrum of the shaping filters shown as building blocks in Figure 4.3-1. The frequency response of these filters is given by $\sqrt{S(f)}$. After defining the spectrum of the shaping filters, the diffuse process is generated in software as shown in Figure 4.3-3. The complex white Gaussian noise processes, $n_1(t)$ and $n_2(t)$, input to the complex filter are independent. The output of the diffuse process generator, or Rayleigh generator, is Rayleigh distributed in magnitude, N(t), and uniformly distributed in phase, $\theta(t)$. This approach to generating the diffuse process envelope is the software equivalent to that of Figure 4.3-1.

The distribution of the magnitude of 8192 points of the output of the VT Rayleigh generator, generated as shown in Figure 4.3-3, is shown in Figure 4.3-4 on Rayleigh probability paper. Note it appears as a straight line, hence the magnitude of the data output by the Rayleigh generator is indeed Rayleigh distributed. Figure 4.3-5 shows the density (a density function is used here so that a uniform density can be easily recognized) of 8192 points of the phase output by the Rayleigh generator. The phase closely approximates a uniform distribution.

Figures 4.3-4 and 4.3-5 show that the VT Rayleigh generator has the proper cumulative distributions for magnitude and phase, but it must also be tested for dynamic behavior. To test the dynamic behavior of the VT Rayleigh generator, its output was tested for mean fade duration against the theoretical curve found in [5]. Data were generated at the rate of 10,000 points per second with a vehicle velocity of 55 mph and an operating frequency of 869 MHz to produce 32768 data points. The data were then normalized to signal level as a function of wavelengths traveled, and subsequently tested for mean fade duration. Figure 4.3-6 shows mean fade duration of the data output by the VT

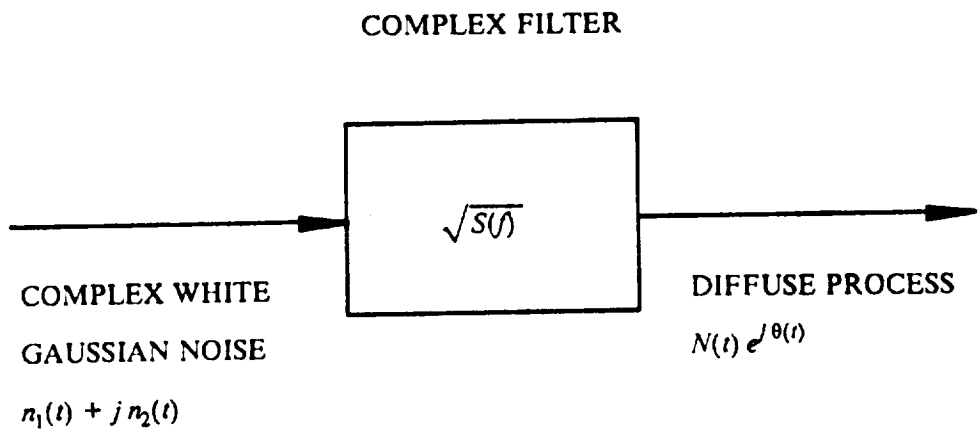

Figure 4.3-3. Block diagram of the software approach used to generate the diffuse process [15].

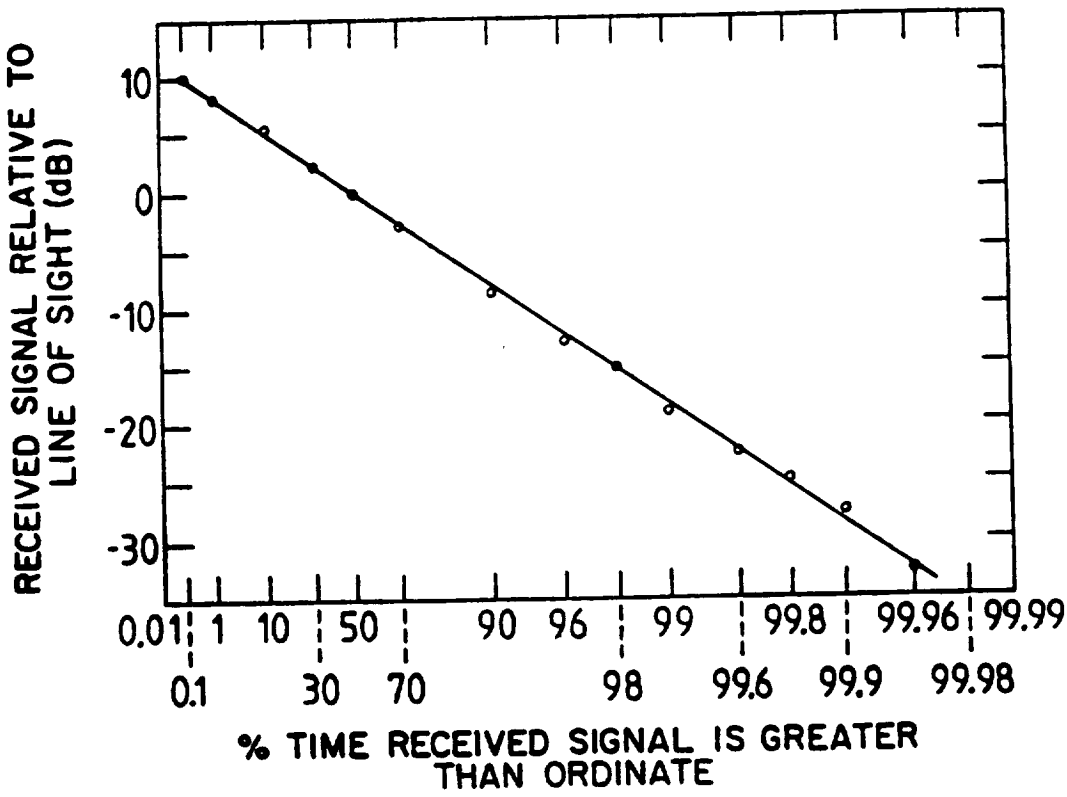

Figure 4.3-4. Cumulative distribution plot of the signal magnitude output by the VT Rayleigh generator plotted on Rayleigh probability paper.

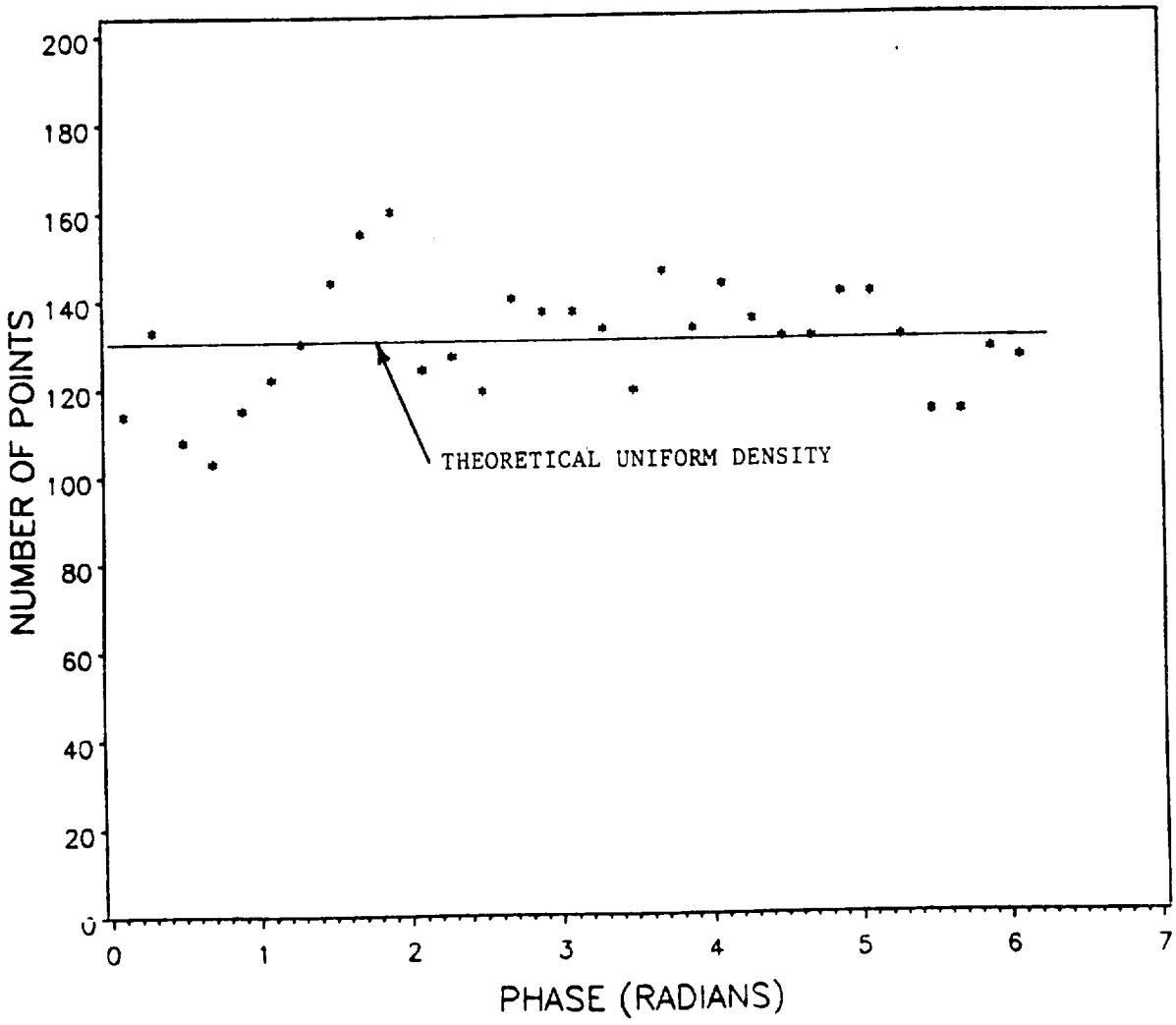

Figure 4.3-5. Density function plot of 8096 points of the signal phase output by the VT Rayleigh generator.

Rayleigh generator compared to the theoretical curve [5]. The close agreement indicates the dynamic output of the Rayleigh generator agrees with theory.

No listing of the Rayleigh generator code at this stage of evolution is provided because of subsequent improvements discussed in Chapter 5.

4.4 Generation of the Slowly Varying Component of the LMSS Signal

It was shown in Section 4.2 that the slowly varying direct component of the LMSS signal due to vegetative fades is lognormally distributed. The VT simulator attempts to generate these slow fades by scaling an existing universal data set of slow fades extracted from Vogel's November 1984, balloon data. The universal data set is scaled in mean and standard deviation to match the distribution of the desired data set. The result is an exact match (or as close as possible) between the distribution of the scaled universal data set and the desired data set, and, we hope, a match between the dynamics of the data set also.

The background and some justification for this scaling procedure (scaled attenuation) are presented in Section 4.4.1. The VT simulator version of this scaling procedure (called the lognormal signal generator) is presented in Section 4.4.2.

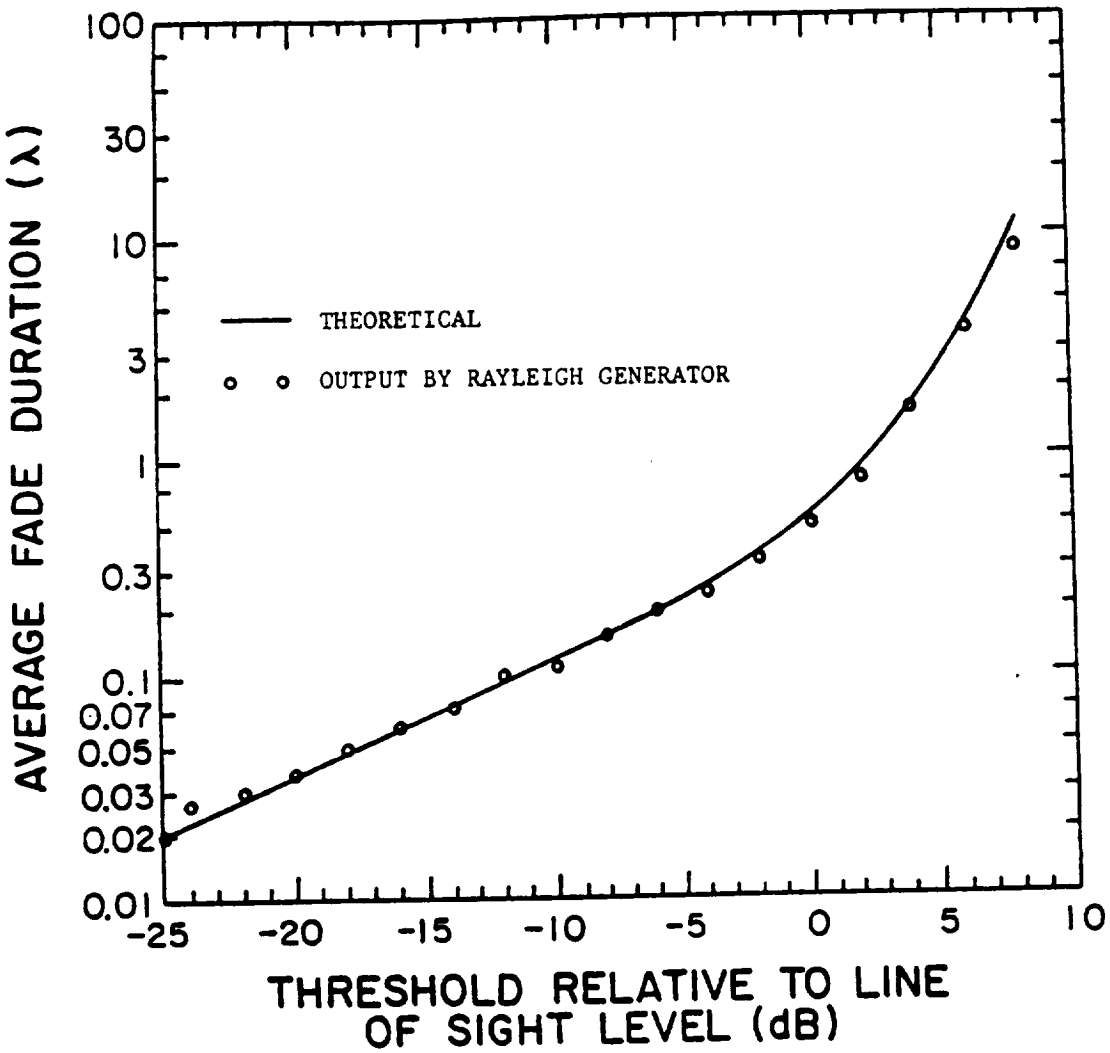

Figure 4.3-6. Calculated mean fade duration of VT Rayleigh signal compared with theoretical result [5].

4.4.1 Background for Scaled Attenuation

All of the background for the scaling procedure used in the VT lognormal generator was drawn from Bottomley's work [6]. The scaling procedure developed by Bottomley was developed from rain attenuation research in which attenuation (in dB) is lognormally distributed (i.e. the log of attenuation is normally distributed). In LMSS, vegetative shadowing of the direct component of a received mobile signal is lognormally distributed (i.e. attenuation, in dB, is normally distributed). Because the time behavior of attenuation in these two cases appears similar, although rain attenuation is lognormally distributed and vegetative attenuation of the direct component of an LMSS signal is normally distributed, we decided to investigate the application of the scaling procedure in [6] to LMSS.

The derivation by Bottomley starts with the assumption that rain attenuation follows the first-order differential equation for a Markov process. To find the necessary parameters of the model, rain attenuation (in dB) is assumed to be lognormally distributed and the rate of change of attenuation is assumed to increase with attenuation level. This leads to a known solution of the Fokker-Planck equation which provides formulas for the model parameters. Because attenuation (in dB) is assumed to be lognormally distributed, Bottomley works with a process proportional to the log of attenuation, called X. This is stated as

$$X_{(k)} = A\,X_{(k-1)} + B\,N_{(k)} \tag{4.4-1}$$

where

$X_{(k)}$ = k th sample of the log of attenuation, attenuation in dB

$N_{(k)}$ = white, Gaussian, zero-mean, unity variance input process

$$A = \exp(-\beta \Delta t)$$

$$B = \sqrt{1 - A^2}$$

$\Delta t = t_{(k)} - t_{(k-1)}$ = sampling period in seconds

$$\beta = E\left\{(\alpha(t + \Delta t) - \alpha(t))^2/\alpha(t)\right\}/(2\sigma_L^2 \Delta t) \qquad (4.4\text{-}2)$$

where $E\{\ \}$ indicates expected value and α is attenuation in dB

σ_L = standard deviation of the log of attenuation not including unshadowed data, attenuation expressed in dB

These equations imply that for discrete samples of rain attenuation, the log of each attenuation sample is a function of the log of the previous value and a random variable generated by a stochastic input process.

One way to simplify the model given in Equations 4.4-1 and 4.4-2 is to assume β, given by Equation 4.4-2, is constant. This is equivalent to fixing the A and B parameters of Equation 4.4-1, but not the standard deviation of the input process N. If β is fixed, only mean μ_L, standard deviation σ_L, and the number of points vary between different data sets. Since statistically, only the mean and standard deviation of the log of attenuation change, the log of rain attenuation in any two data sets can be related both statistically and on a point-to-point basis by

$$L2 = (\sigma_{L2}/\sigma_{L1})(L1 - \mu_{L1}) + \mu_{L2} \qquad (4.4\text{-}3)$$

where

$L2$ = log of attenuation in data set 2, attenuation in dB

$L1$ = log of attenuation in data set 1, attenuation in dB

σ_{L2} = standard deviation of the log of attenuation not including clear weather for data set 2, attenuation in dB

σ_{L1} = standard deviation of the log of attenuation not including clear weather for data set 1, attenuation in dB

μ_{L2} = mean of the log of attenuation not including clear weather for data set 2, attenuation in dB

μ_{L1} = mean of the log of attenuation not including clear weather for data set 1, attenuation in dB

Although the derivation in [6] was performed specifically for rain attenuation studies, we believe it can be easily altered for application to LMSS. To apply the derivation to the slowly varying direct component of the LMSS signal, we must work directly with attenuation instead of with the log of attenuation as Bottomley did in his derivation. Bottomley assumes that attenuation (in dB) is lognormally distributed and that the rate of change of attenuation increases with attenuation level to obtain his model equations. If we assume, for the vegetatively shadowed direct component of the LMSS signal, that attenuation (in dB) is normally distributed (or, equivalently, attenuation as a ratio is lognormally distributed) and the rate of change of attenuation (given as a ratio, not in dB) increases with attenuation level, then we obtain equations almost identical to those previously given in Equations 4.4-1 and 4.4-2. These equations are stated as

$$\alpha_{(k)} = A\,\alpha_{(k-1)} + B\,N_{(k)} \tag{4.4-4}$$

where

$\alpha_{(k)}$ = discrete values of attenuation (in dB) occurring at time t_k where

$$t_{(k)} - t_{(k-1)} = \Delta t$$

$N_{(k)}$ = white, Gaussian, zero-mean, unity variance input process

$$A = \exp(-\beta\,\Delta t)$$

$$B = \sqrt{1 - A^2}$$

Δt = sampling period in seconds

$$\beta = E\left\{(\gamma(t + \Delta t) - \gamma(t))^2/\gamma(t)\right\}/(2\,\sigma^2\,\Delta t) \tag{4.4-5}$$

where $E\{\ \}$ indicates expected value and γ is proportional to attenuation expressed as a ratio

σ = standard deviation of attenuation (in dB) not including unshadowed data

These equations imply that for discrete samples of attenuation, each attenuation sample is a function of the previous value and a random variable generated by a stochastic input process. The assumption that attenuation (in dB) of the vegetatively shadowed direct component of an LMSS signal is normally distributed was shown to be valid in Section 4.2. The assumption that the rate of change of attenuation increases with increasing attenuation level also appears to be valid for the data we analyzed.

If we next go through the same process as Bottomley and fix β, we can relate the attenuation in any two data sets both statistically and on a point-to-point basis by

$$\alpha 2 = (\sigma_2/\sigma_1)(\alpha 1 - \mu_1) + \mu_2 \qquad (4.4\text{-}6)$$

where

$\alpha 2$ = attenuation (in dB) in data set 2

$\alpha 1$ = attenuation (in dB) in data set 1

σ_2 = standard deviation of attenuation (in dB) not including clear weather for data set 2

σ_1 = standard deviation of attenuation (in dB) not including clear weather for data set 1

μ_2 = mean of attenuation (in dB) not including clear weather for data set 2

μ_1 = mean of attenuation (in dB) not including clear weather for data set 1

Thus if we assume for the vegetatively shadowed direct component of an LMSS signal that

1. Attenuation follows a Markov process
2. Attenuation (in dB) is normally distributed
3. The rate of change of attenuation increases with attenuation level
4. The dynamic parameter β can be fixed

then we can relate any two model data sets (of the slowly varying, lognormally distributed, vegetatively shadowed, direct component of the LMSS signal) by a linear scaling procedure using Equation 4.4-6. This in turn assumes that both data sets use the same random number sequence. This implies that we only need a single model data set which we can scale by Equation 4.4-6 to produce any new data set of the slowly varying component of the LMSS signal.

4.4.2 Lognormal Signal Generator

A block diagram of the lognormal signal generator used in the VT simulator to produce the slowly varying, lognormally distributed, vegetatively shadowed direct component of the LMSS signal is shown in Figure 4.4-1. The requirements for the lognormal signal generator are a universal data set of vegetatively shadowed direct component, the mean and standard deviation of the data set to be generated, and the number of shadowed data points to generate. The lognormal signal generator scales the lognormal distributed universal data set according to Equation 4.4-6 to produce a new lognormal data set (with a distribution like those shown in Figure 2.4-1) with the desired mean and standard deviation. The result is a scaled version of the universal data set that we hope possesses the desired dynamic characteristics of the vegetatively shadowed direct component of the signal.

The universal data set used in the lognormal signal generator was derived from the 869 MHz, November 1984, balloon experiment data supplied by Vogel. The data base was constructed by taking a 20 wavelength long running average of all the data supplied.

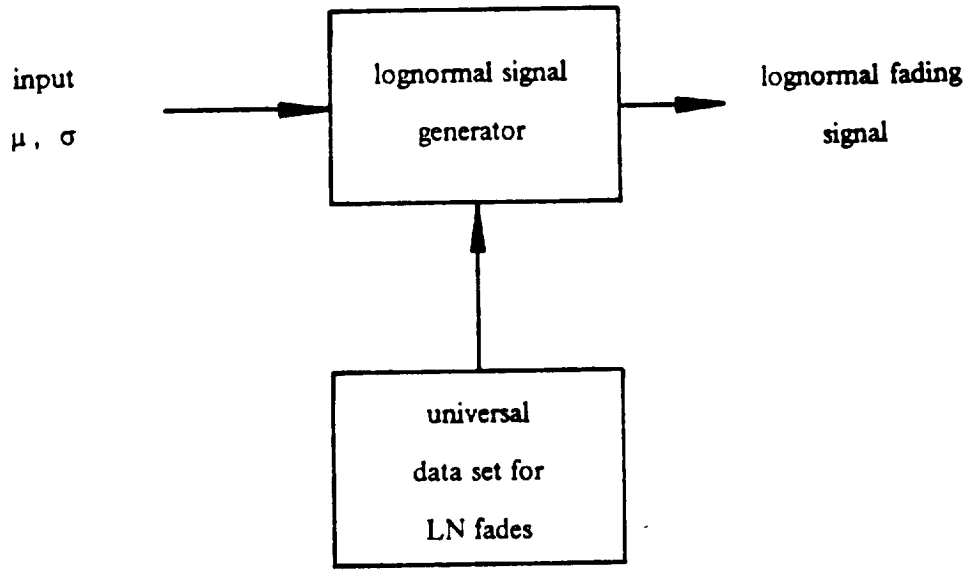

Figure 4.4-1. Block diagram of lognormal signal generator.

Data output by the running average and falling below a -2 dB threshold were considered to be shadowed and were used to construct the universal data base. The reasons for choosing a 20 wavelength window for the running average and a -2 dB threshold for shadowing are discussed in 4.2.2. The universal data base constructed from this process contains data corresponding to 4.5 km of travel and consists of purely vegetatively shadowed direct component of the signal with points spaced 0.1 wavelengths apart. The distribution of this data set is shown in Figure 4.4-2. Note it is lognormally distributed with a mean and standard deviation of -4.1 dB and 2.5 dB respectively. This data base serves as the universal data base to be scaled by the lognormal generator, which assumes that the dynamic behavior of the data base is universal.

4.5 Total Signal Generator

The total fading envelope of the LMSS signal is generated by combining the Rayleigh signal generator and the lognormal signal generator in the proper manner to create the VT simulator. A block diagram of this construction is shown in Figure 4.5-1. The inputs to the simulator are the number of points to generate (the spacing between points is set to 0.1 wavelengths), the percent shadowing, the value of K for the unshadowed Rician data, the value of $\overline{K}$ for the multipath component of the shadowed data, and the mean and standard deviation of the lognormal component of the shadowed data. The output of the simulator is data spaced 0.1 wavelengths apart that represents the total LMSS fading signal.

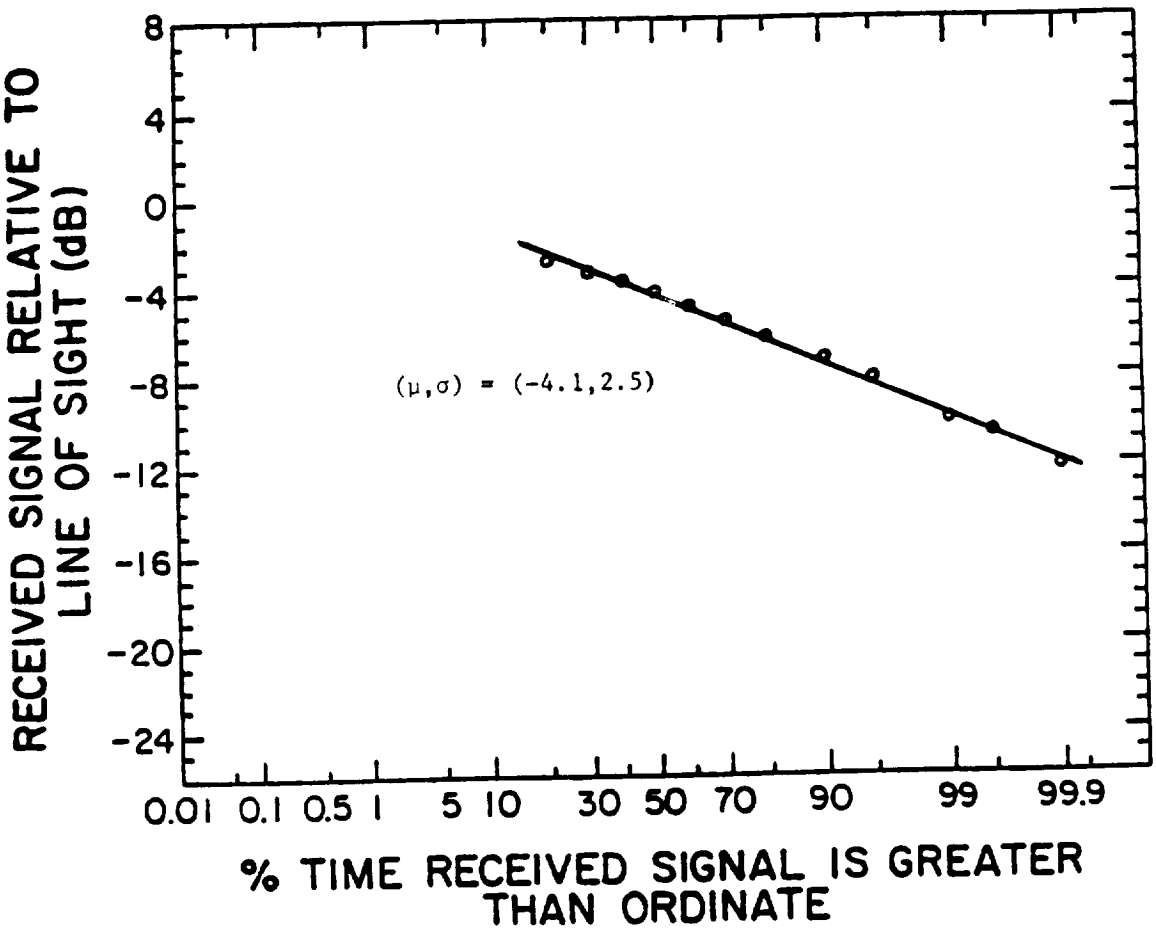

Figure 4.4-2. Distribution of the lognormal data base used in the lognormal signal generator.

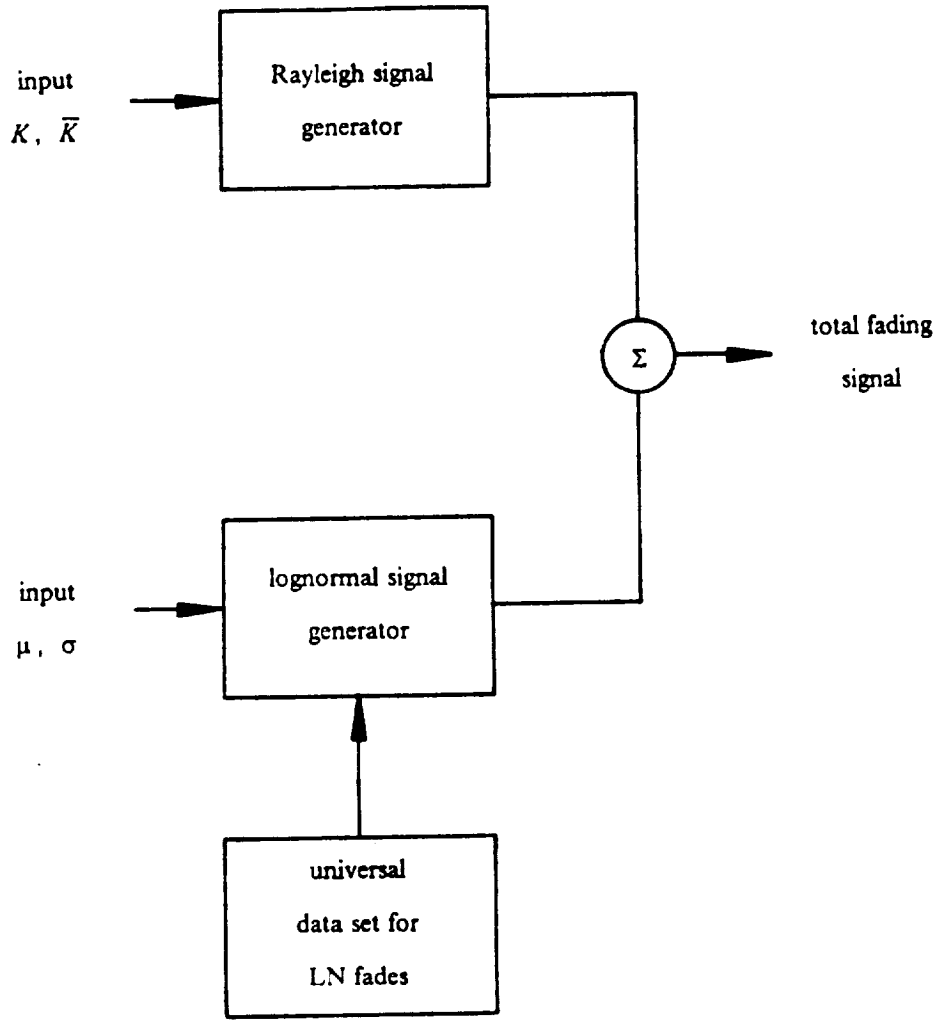

- K, $\overline{K}$, μ, and σ are determined from cumulative distribution information

Figure 4.5-1. Block diagram of total VT simulator.

To construct the shadowed data, the complex voltage of the signal output by the Rayleigh generator is added (phasor addition) to the complex voltage of the scaled signal output by the lognormal signal generator. This corresponds exactly to Equation 2.3-3, restated below for vegetatively shadowed conditions where the diffuse component of the signal is generated by the Rayleigh generator and the lognormally distributed component is generated by the lognormal signal generator.

$$R_1 \approx R_{dir} + R_{dif} \tag{4.5-1}$$

The magnitude of the signal output by the Rayleigh generator is determined by input parameter $\overline{K}$ while the scaling factors for the lognormal signal generator are determined by the input parameters μ_R and σ_R. The total shadowed data set created by the simulator adding the outputs of the Rayleigh generator and the lognormal generator has a VS distribution. The distribution of a sample of vegetatively shadowed data output by the simulator with input parameters $\overline{K} = -12\,\text{dB}$, $\mu_R = -8.1\,\text{dB}$, and $\sigma_R = 2.5\,\text{dB}$ is shown in Figure 4.5-2. Note it appears similar to the plot of a VS distribution shown in Figure 2.4-5.

Construction of the unshadowed data is performed by temporarily suspending the operation of the lognormal signal generator while it outputs a constant. The output of the Rayleigh generator is added as a complex voltage to this constant to produce unshadowed data. Again this corresponds exactly to Equation 2.3-3, but this time for unshadowed conditions where the diffuse component of the signal is generated by the Rayleigh generator and the constant direct component of the signal is generated by the lognormal signal generator (whose normal mode of operation has been temporarily suspended). The magnitude of the signal output by the Rayleigh generator is determined by the parameter K; the constant added to the Rayleigh generator signal is arbitrarily

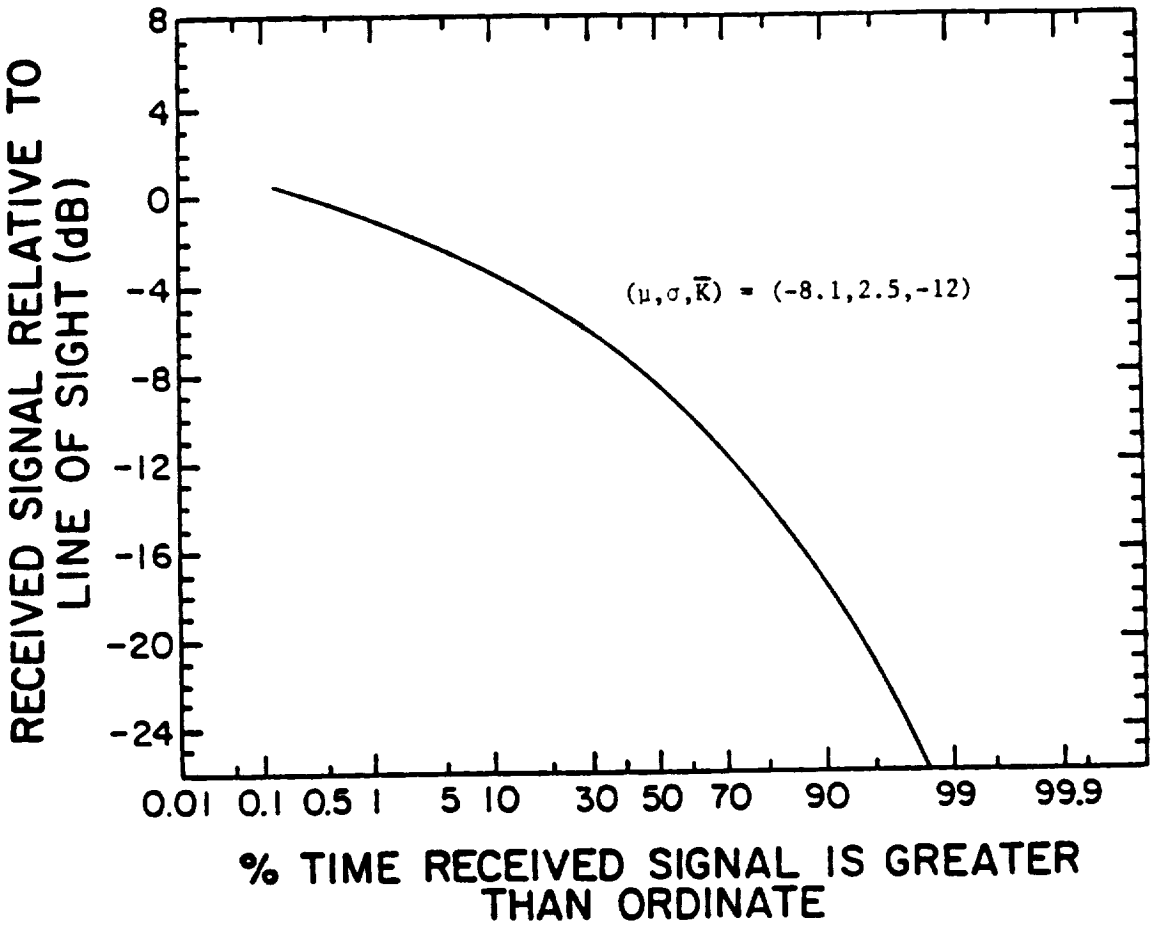

Figure 4.5-2. Cumulative distribution plot of VT simulator output under 100% vegetatively shadowed conditions.

chosen to be 1.0. The total unshadowed data set created by adding the output of the Rayleigh generator to a constant has a Rician distribution. The distribution of a sample of unshadowed data output by the simulator with input parameter K = -11 dB is shown in Figure 4.5-3 along with a theoretical Rician curve with the same K value.

Once the shadowed and unshadowed data sets are generated, they are concatenated in the proper proportion to generate the total data set. If NPTS is the total number of data points desired in the data set and p is the percentage of vegetative shadowing present, the total number of shadowed data points is p(NPTS) and the total number of unshadowed data points is (1 - p)(NPTS). Note NPTS = p(NPTS) + (1 - p)(NPTS). This corresponds to a total probability approach to constructing the overall data set by concatenating shadowed and unshadowed data sets.

4.6 Testing the Simulator

The VT simulator was first tested on unshadowed data since this required knowledge of the fewest number of variables. It was then tested on shadowed data. The initial tests were performed using the same November 1984 balloon data that was used to verify the separability of the data into component parts and to construct the lognormal data base. Using the Vogel data to verify the VT simulator operation for unshadowed data is valid because operation of this portion of the simulator was not derived from the data. Verification of the operation of the simulator for shadowed data, however, is not entirely valid here because the data used to generate the universal lognormal data base is the

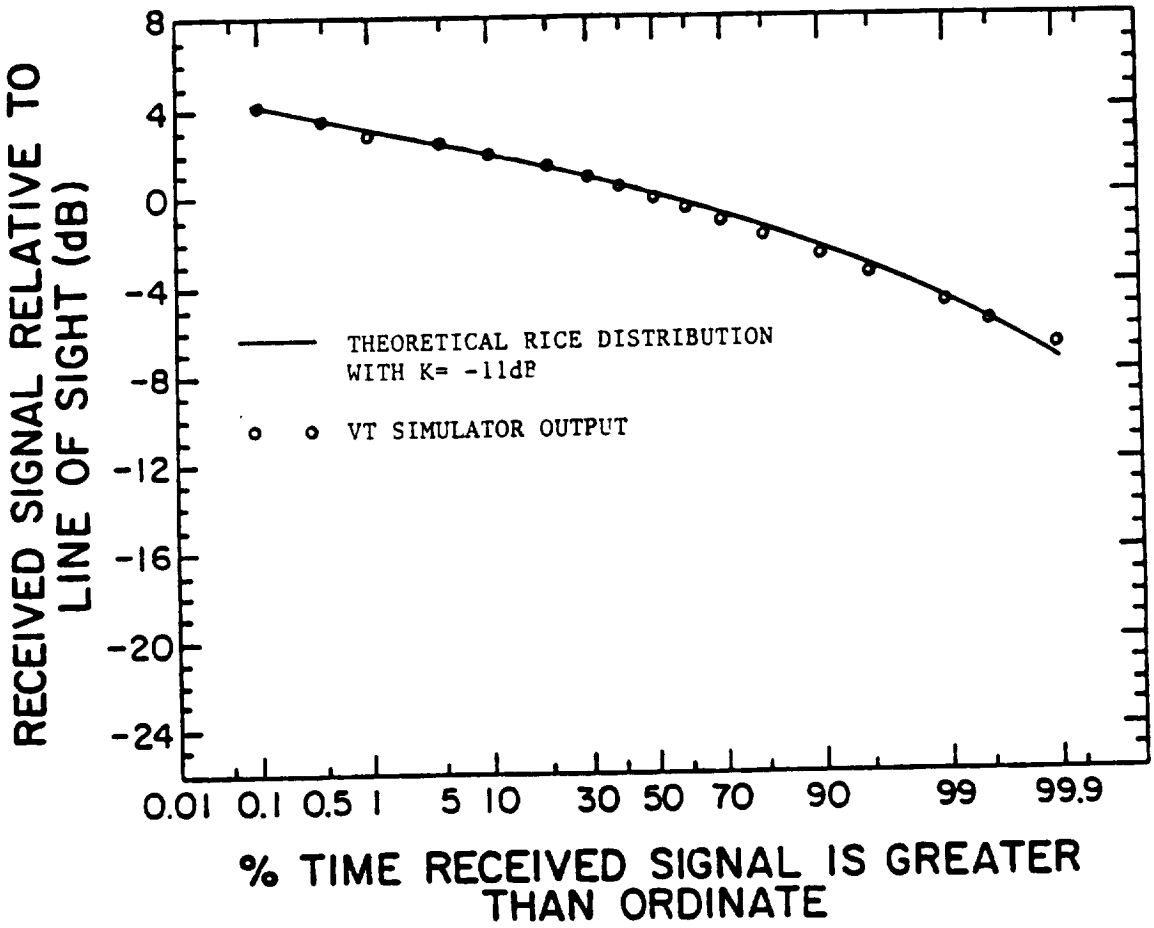

Figure 4.5-3. Cumulative distribution plot of VT simulator output under unshadowed conditions and input parameter K = -11 dB compared with theoretical Rician distribution with K = -11 dB.

same data used to verify the simulator for the shadowed mode of operation. Comparison of the simulator output to the Vogel data for shadowed data is performed anyway to see if the Rayleigh generator output when added to the lognormal signal generator output produces a signal with the proper dynamic behavior.

4.6.1 Unshadowed Data

The performance of the simulator was tested under unshadowed conditions by matching its distribution to the first eaght 1.024 second files of Vogel's data set RB093413. Figure 4.6-1 shows the distribution of the Vogel data and the distribution of the simulator output using a K value of -26 dB for input. Note that the fades in this data set are under 1 dB and insignificant, but they are typical of the fades encountered in the unshadowed data supplied by Vogel and they do serve as an adequate test of the simulator for unshadowed data.

Once the distributions were matched, the fade duration characteristics of the actual and simulated data sets were compared. Figure 4.6-2 shows a cumulative distribution plot of fade durations at -0.2 dB and -0.5 dB thresholds. Figure 4.6-3 shows a cumulative distribution of rise durations (the opposite of fade durations) at +0.2 dB and +0.5 dB thresholds. Table 4.6-1 combines the information in the plots into fade and rise duration tables. The match between the fade and rise durations of the simulator and those of the data is fair, but we believed they could be improved. The improved unshadowed data simulator is discussed in Chapter 5.

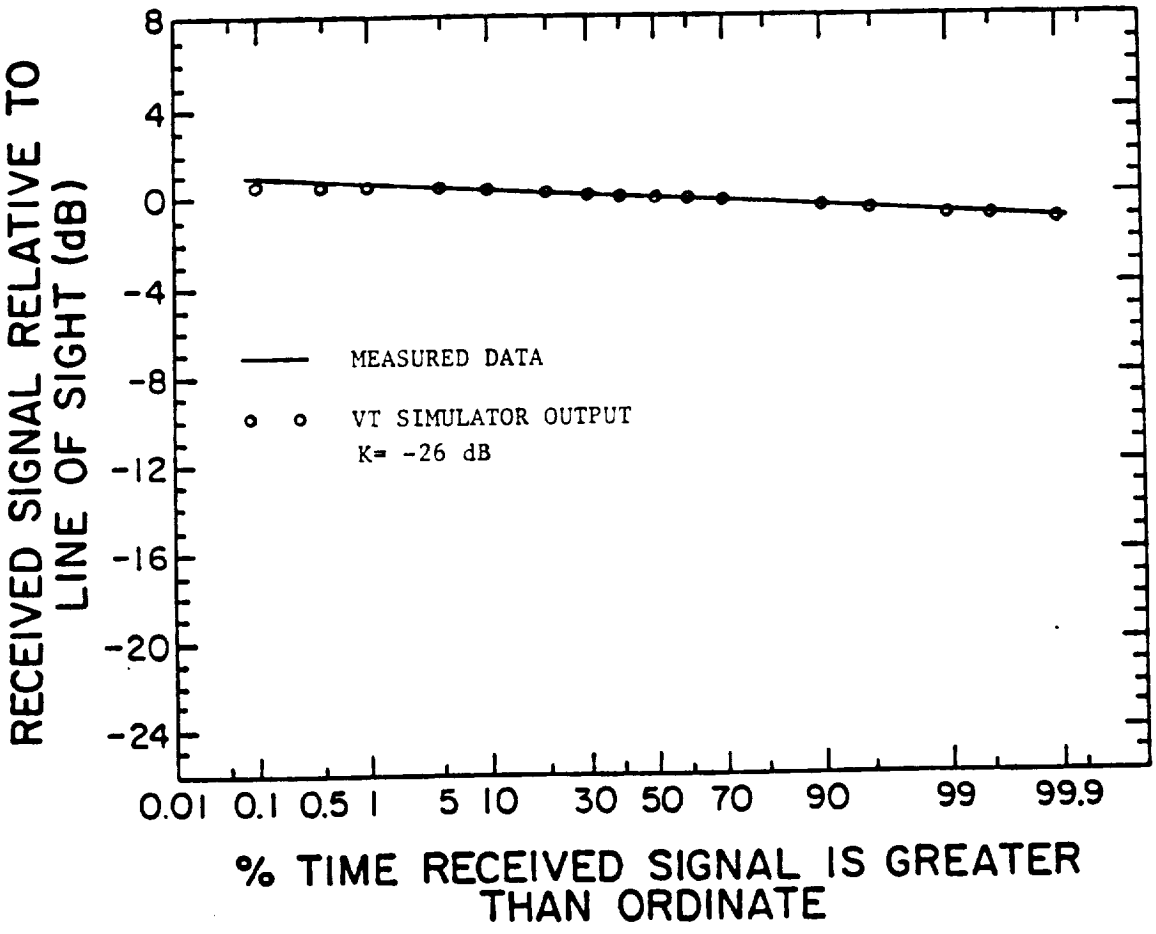

Figure 4.6-1. Cumulative distribution plot of the first eight 1.024 second records of data set RB093413 and the VT simulator match to it.

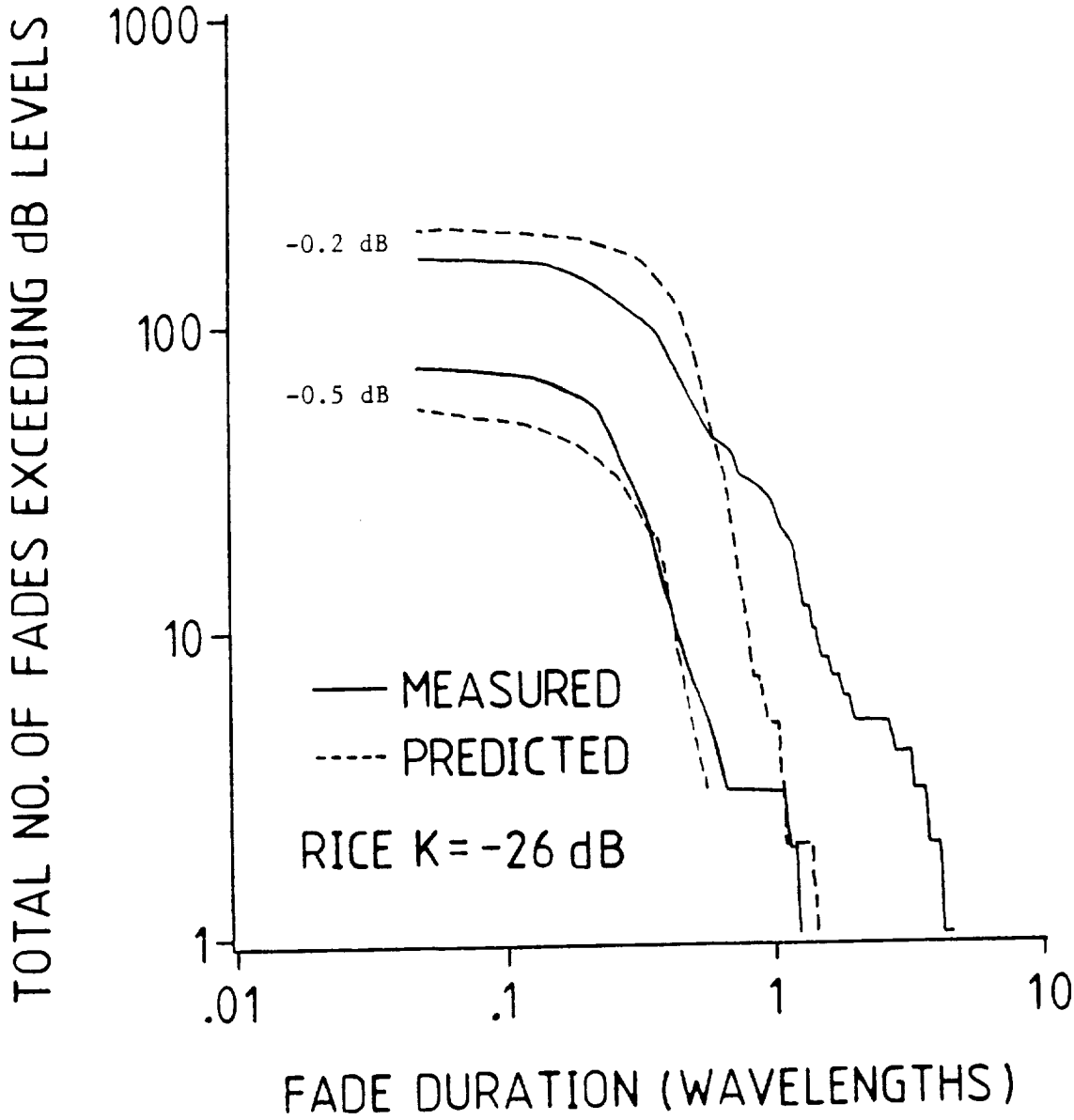

Figure 4.6-2. Cumulative fade duration distribution at two thresholds comparing experimental and simulator predicted fades for the first eight 1.024 second files of Vogel's unshadowed data set RB093413.

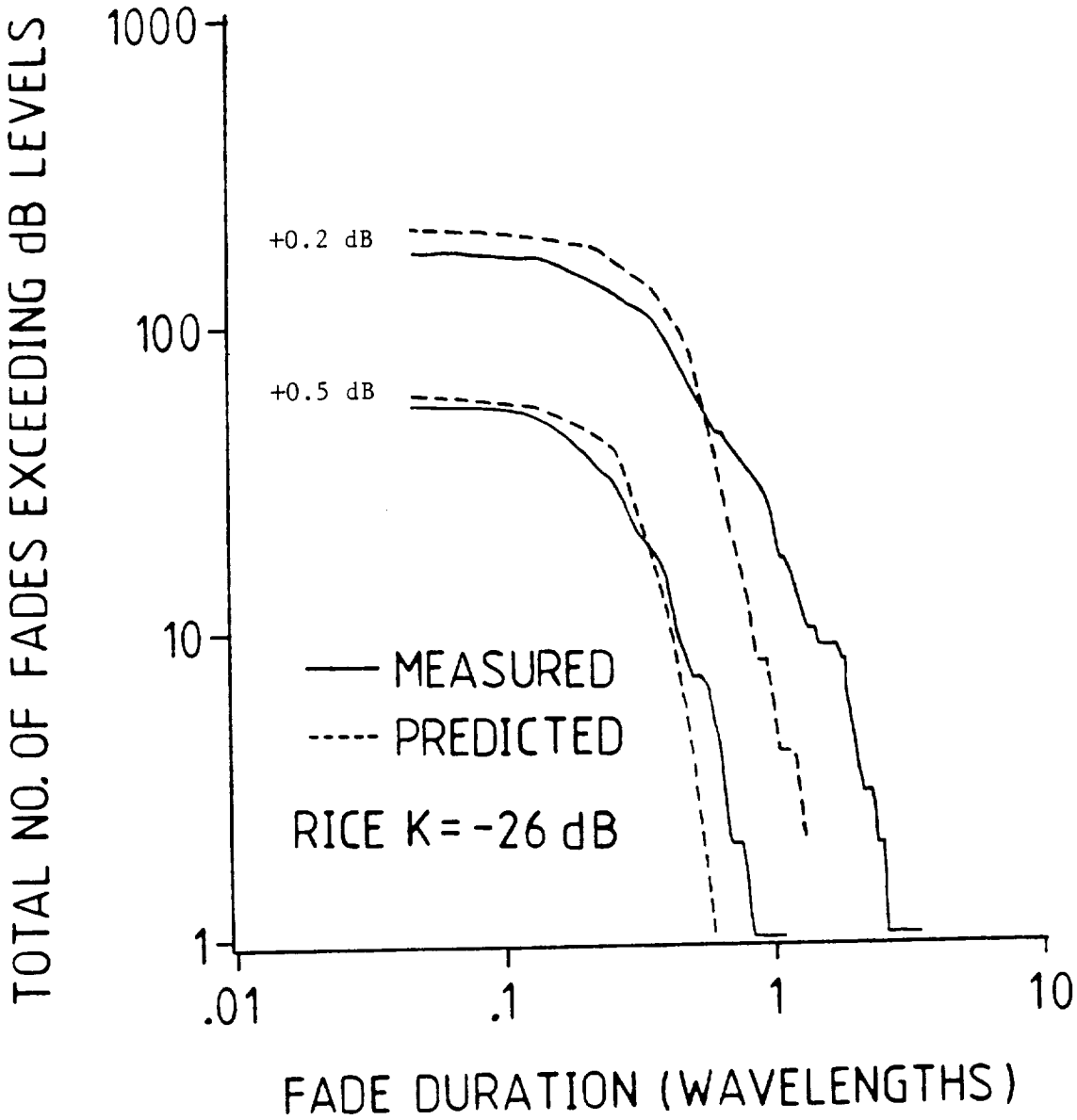

Figure 4.6-3. Cumulative rise duration distribution at two thresholds comparing experimental and simulator predicted fades for the first eight 1.024 second files of Vogel's unshadowed data set RB093413.

Table 4.6-1. Comparison of experimental and Rice generator predicted rises and fades for first eight 1.024 second files of Vogel's data set RB093413.

RISE THRESHOLD	0.5		0.2	
RISE DURATION	NO. EVENTS		NO. EVENTS	
(WAVELENGTHS)	DATA	SIM	DATA	SIM
0.0 - 0.1	5	6	8	15
0.1 - 0.2	16	11	28	17
0.2 - 0.4	19	31	48	62
0.4 - 0.8	14	12	57	101
0.8 - 1.6	1		24	13
1.6 - 3.2			8	
3.2 - 6.4			1	

FADE THRESHOLD	- 0.2		-0.5	
FADE DURATION	NO. EVENTS		NO. EVENTS	
(WAVELENGTHS)	DATA	SIM	DATA	SIM
0.0 - 0.1	8	7	8	7
0.1 - 0.2	28	15	10	15
0.2 - 0.4	54	54	25	41
0.4 - 0.8	48	122	8	11
0.8 - 1.6	24	7	3	
1.6 - 3.2	4	1		
3.2 - 6.4	3			

4.6.2 Shadowed Data

The simulator was tested under vegetatively shadowed conditions by matching the distribution of the output of the simulator to that of a shadowed Vogel data set. After matching the distributions, the fade duration characteristics of the actual and the simulated data sets were compared. Unfortunately, at this point in time, we encountered a crash of the Harris 800 computer used for simulation and the entire hard disk used by the computer was destroyed. In the crash, recent programs and data that had not yet been backed-up were lost. For this reason, no figures of the match between data sets were developed. What we did observe before the computer crash was that although the cumulative distribution of the simulated and empirical data sets matched, the fade duration behavior did not match well. The fades output by the simulator tended to group in large numbers in the low duration bins (0.0-0.1, 0.1-0.2, and 0.2-0.4 wavelength bins) while the fades of the empirical data set were more widely distributed. Consequently, although the total number of fading points matched (i.e. the cumulative distributions matched), the dynamic behavior of the simulated and empirical data sets did not match acceptably. Fortunately, we were able to improve the dynamic behavior of the simulator for vegetatively shadowed data so we chose not to regenerate the software and data lost in the computer crash (important previous programs and data were not lost because they had been backed-up).

V. IMPROVED SIMULATOR

The initial version of the VT simulator had, we felt, unacceptable dynamic characteristics when generating vegetatively shadowed data. We felt that the dynamics of the simulator could be improved when generating the shadowed data and also when generating the unshadowed data. These improvements were made by altering the Rayleigh generator to run using empirical data.

In Section 5.1, refinement of the Rayleigh generator is discussed. The Rayleigh generator is refined for use in both shadowed and unshadowed conditions. Section 5.2 introduces a new, independent, data set supplied by Vogel and employs it to verify the operation of the VT simulator.

5.1 Refined Rayleigh Generator

The initial Rayleigh generator constructed, because of its purely mathematical deviation, is very artificial in its generation of the diffuse process. We believe that a Rayleigh generator based on actual LMSS data would produce improved simulator output for both shadowed and unshadowed conditions. This section discusses this data-derived Rayleigh generator for both shadowed and unshadowed conditions.

5.1.1 Unshadowed Rayleigh Generator

In Section 4.1.3, we showed that the total unshadowed mobile signal could be separated into a constant direct component and a diffuse component that is Rayleigh distributed in magnitude and uniformly distributed in phase. The Rayleigh generator we developed attempts to construct this diffuse component of the signal. Why attempt artificially to construct the diffuse component when we have already extracted it from the data? The data extracted from the unshadowed data sets are properly distributed in magnitude and phase to serve as Rayleigh generated data. It also has the proper dynamic behavior since it is empirical data (assuming the data provided by Vogel is valid and accurate). So in place of the artificial Rayleigh generator, we can place a generator that extracts the diffuse component of empirical data to produce the diffuse process for the simulator. This is essentially what is done in the improved VT Rayleigh generator, but instead of separating the data every time the simulator is run, a large data base of diffuse data is constructed from the unshadowed Vogel data. The improved generator draws from this

data base and the input value K or $\overline{K}$, precisely like the initial generator, to output data of the proper magnitude. As far as the overall simulator is concerned, the improved Rayleigh generator operates like its predecessor, but now the Rayleigh generator is based on empirical data. Verification of this improved simulator is presented in 5.2.

5.1.2 Shadowed Rayleigh Generator

The improved Rayleigh generator discussed in Section 5.1.1 was used in conjunction with the lognormal generator to produce vegetatively shadowed data. Again, as with the initial Rayleigh generator, the dynamics of the data output by the simulator were not acceptable. As with the initial Rayleigh generator, the vegetatively shadowed data output by the simulator tended to have a large number of fades in the short duration bins which the empirical data did not have. So although the cumulative distributions of measured and empirical vegetatively shadowed data sets could be well matched with the improved simulator, the dynamic behavior could not.

Our inability to generate vegetatively shadowed data with the proper dynamic behavior using the initial and improved Rayleigh generators results from neglecting the nonuniformly distributed phase of the diffuse component found in Section 4.2.3. In Section 4.2.3, we found that the magnitude of the diffuse component extracted from the shadowed empirical data is Rayleigh distributed in magnitude, but it is not uniformly distributed in phase. The Rayleigh generator we have been using to generate the diffuse component for both unshadowed and shadowed data outputs data with a uniformly

distributed phase. This is appropriate for unshadowed data, but not for the shadowed data which was found to have a nonuniformly distributed phase.

Although the phase of the diffuse component of the shadowed data was found to have a bimodal distribution instead of a uniform distribution (whether the phase is actually nonuniformly distributed or if it appears so because of our processing of the data is impossible to tell), it was found to behave in a predictable manner. In all of the shadowed data examined, the magnitude of the diffuse component of the data was found to be Rayleigh distributed and the diffuse component phase was found to have a consistent distribution (the density of the phase was shown in Figure 4.2-9). These distributions were found to be independent of the fade depths, depending only on the fact that vegetative fading is present. Because of this uniform behavior, we decided to extract the diffuse component of the vegetatively shadowed data and use it for input to the Rayleigh generator precisely as we did in Section 5.1.1 for unshadowed data. The resulting Rayleigh generator, when used in conjunction with the lognormal signal generator has dynamic behavior much closer to that of the empirical data. Verification of this improved dynamic behavior is presented in Section 5.2.

5.1.3 Total Improved Rayleigh Generator

The final version of the Rayleigh generator incorporates two data bases, one for unshadowed data and one for shadowed data. The generator still operates similar to the initial Rayleigh generator, but now it draws data from the unshadowed diffuse data base when generating unshadowed data and it draws data from the shadowed diffuse data

base when generating shadowed data. The simulator configuration and operation is exactly like the initial configuration, but now additional data bases have been added. The final configuration is shown in Figure 5.1-1.

The program used to implement the final simulator configuration is called SIGGE2.F and a listing may be found in Appendix B.

5.2 Verification of Simulator Using the November 1984, Balloon Data

The final version of the simulator, shown in Figure 5.1-1, was first tested on the original data set received from Vogel. The results of comparisons between the simulator output and these data sets are discussed in this section.

To test the improved simulator for operation under unshadowed conditions, we chose to try to match its output to the entire unshadowed data set TD093523. This data set is not contained in the unshadowed Rayleigh data base. The simulator output was first matched to the cumulative distribution of the data precisely as in Section 4.6. A Rician K of -28 dB gave the best match between simulator output and data distributions. Figure 5.2-1 compares the cumulative fade duration of the simulated and empirical data. Comparing this figure to Figure 4.6-3 shows that the performance of the simulator for unshadowed conditions has been improved by using data to drive the Rayleigh generator.

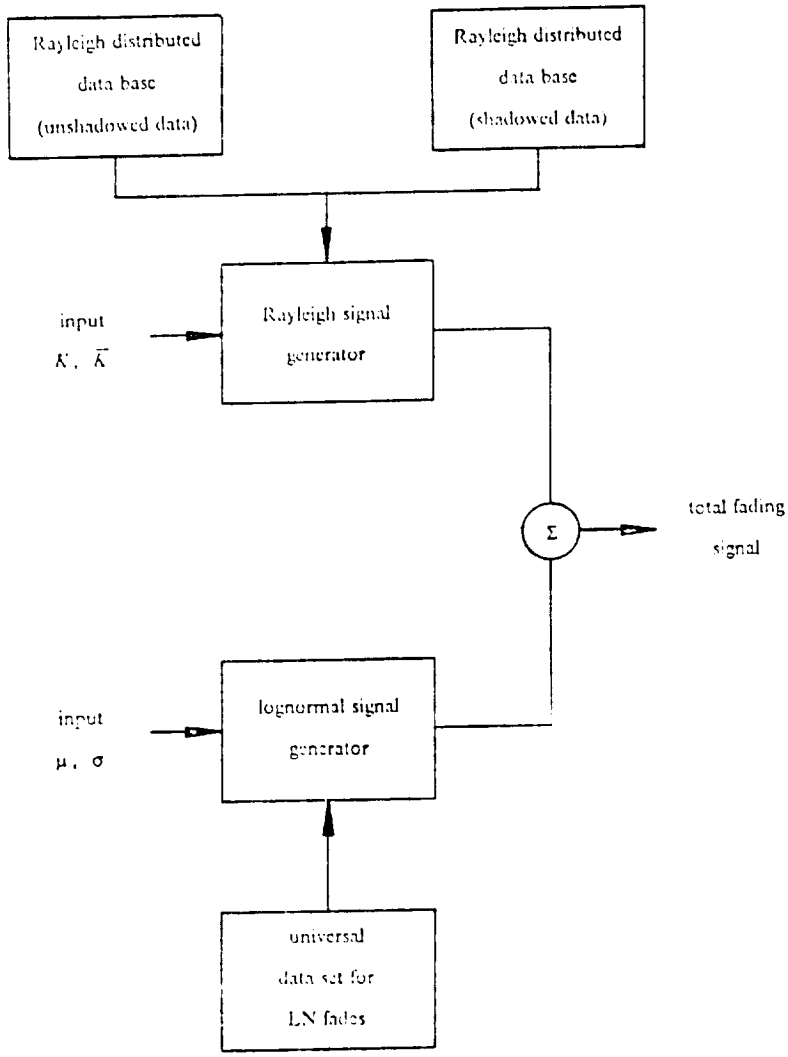

- K, $\overline{K}$, μ, and σ are determined from cumulative distribution information

Figure 5.1-1. Block diagram of the final version of the VT simulator.

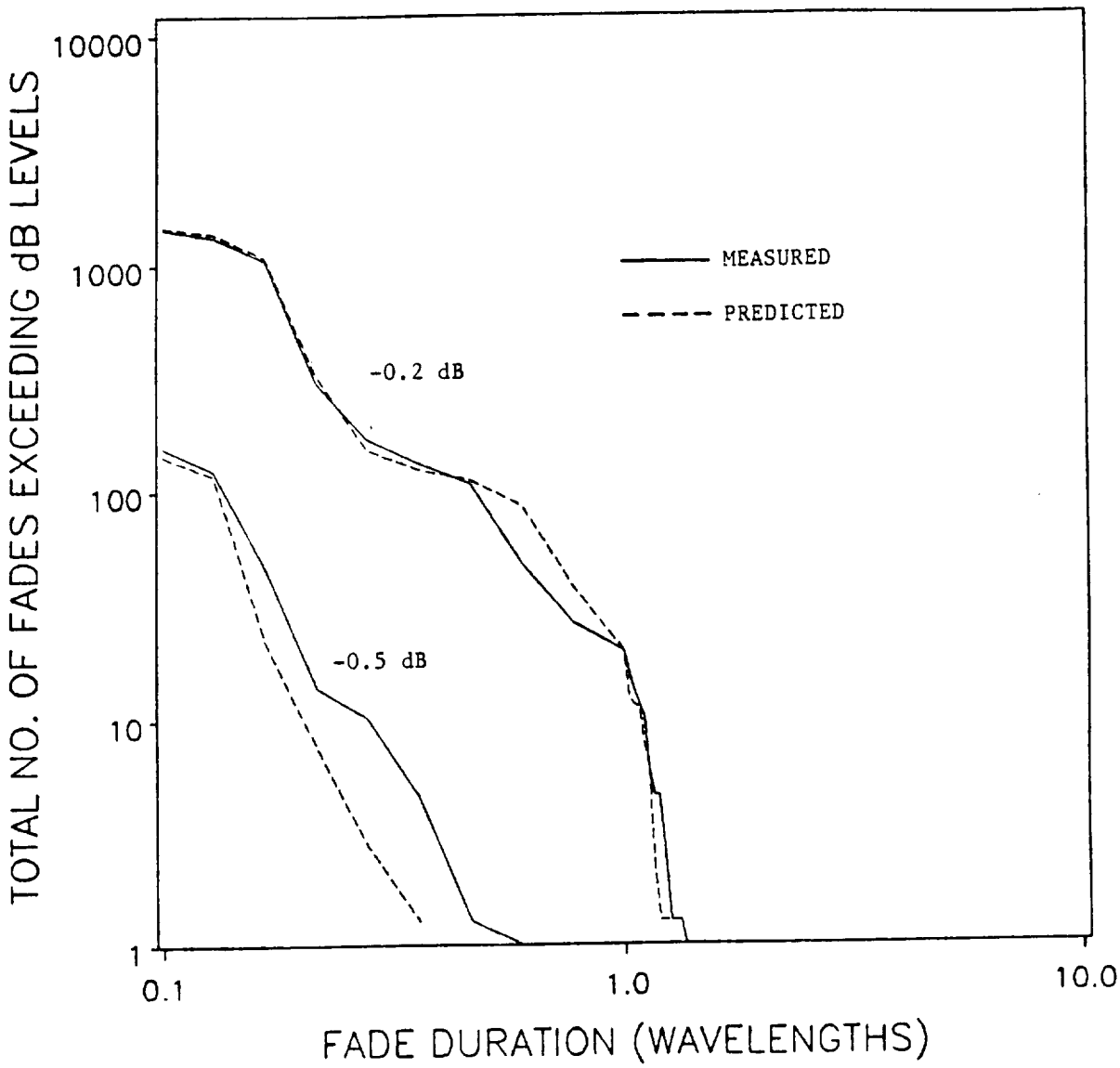

Figure 5.2-1. Cumualtive fade duration distributions at two thresholds comparing experimental and simulator predicted fades for Vogel's unshadowed data set TD093523.

To test the improved simulator for operation under shadowed conditions, we chose to match the distribution of its output to an entire data set containing both shadowed and unshadowed data. Data set TD091759 was chosen for this purpose. It contains 46.6% of vegetatively shadowed data. Figure 5.2-2 shows the distribution of this data set and our match to it. The simulator output is matched to the data by a fairly complex procedure outlined in Appendix C. The procedure outlined in Appendix C describes a method for determining the simulator input parameters K, $\overline{K}$, μ_R, and σ_R assuming the percent shadowing is known. If the percent shadowing cannot be estimated, a trial and error method must be used to determine the simulator inputs.

Once the distribution between simulator output and data set TD091759 were matched, their fade duration characteristics were compared. Figure 5.2-3 shows a cumulative plot of fade durations for both the empirical data and the simulator output at five different fade thresholds. The good agreement between the empirical and simulated data indicates proper operation of our simulator both statistically and dynamically, at least for the Vogel, 1984 balloon experiment data. The real test of the simulator's universal application follows in the next section as its distribution is first matched to a totally unrelated data set and then tested for its dynamic match to the data set as is discussed in the next section.

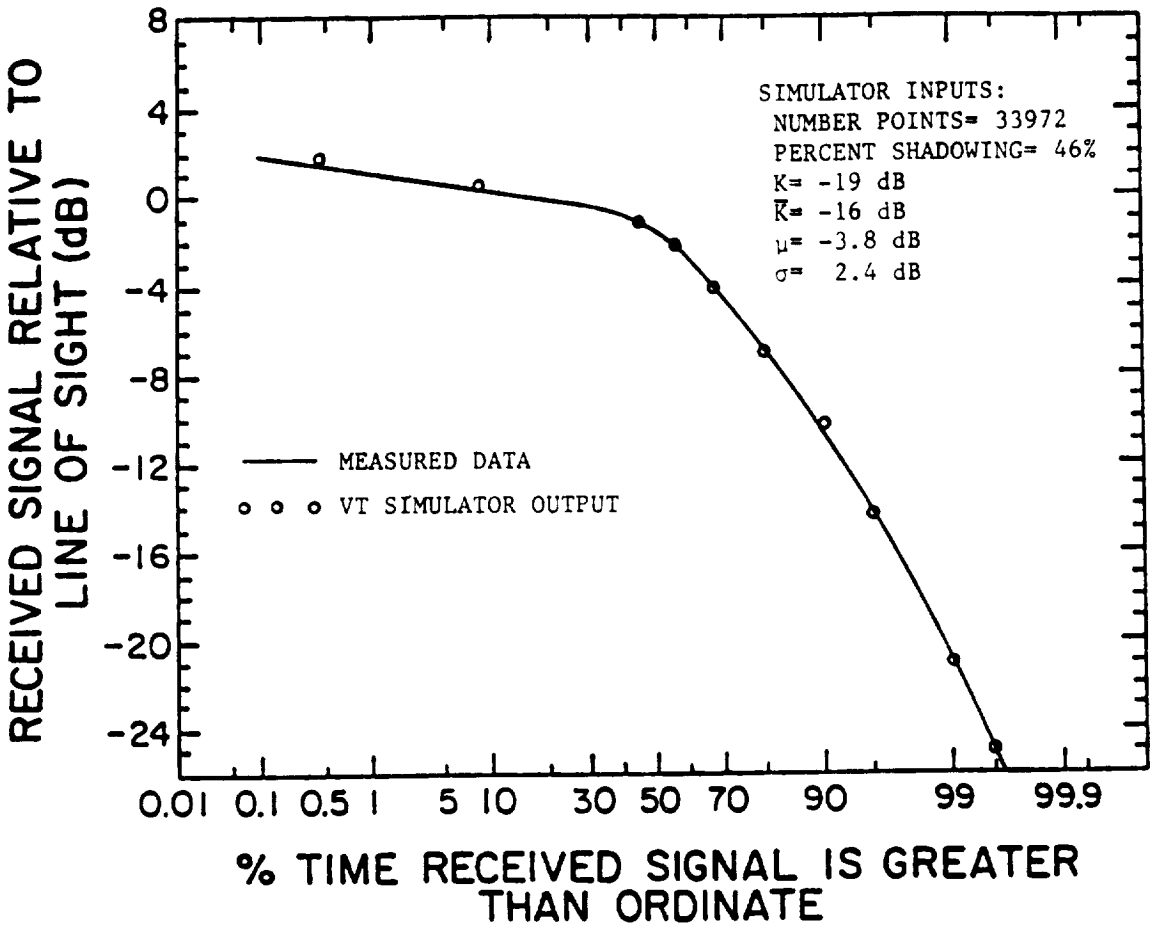

Figure 5.2-2. Cumulative distribution plot of partially shadowed data set TD091759 and the VT simulator match to it.

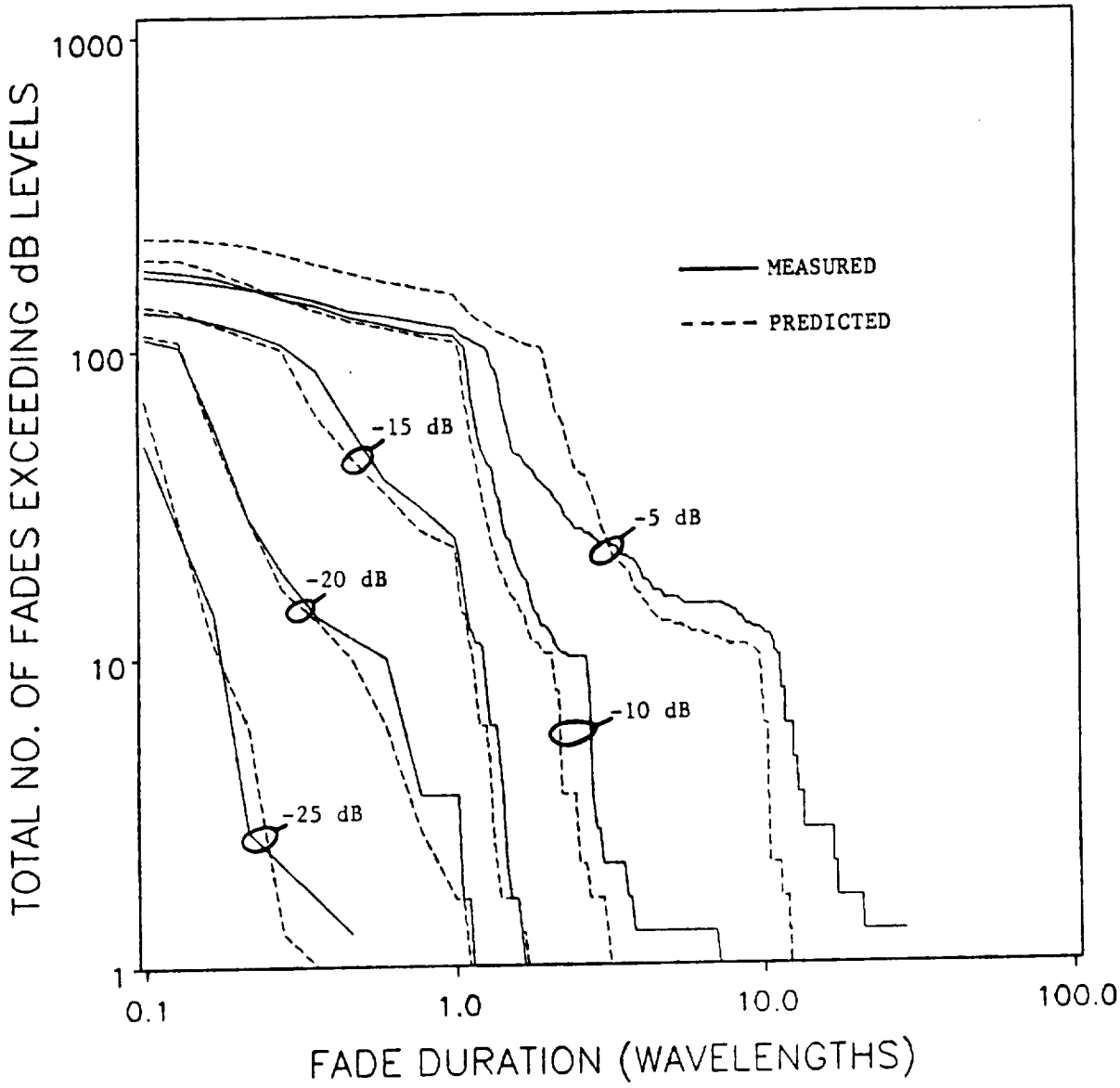

Figure 5.2-3. Cumulative fade duration distributions at five thresholds comparing experimental and simulator predicted fades for partially shadowed data set TD091759.

5.3 Verification of Simulator Using an Independent Data Set

A new data set independent of the November 1984, Balloon data was required to adequately test the simulator. This section introduces the new data set and uses the data set to verify the operation of the VT simulator.

5.3.1 The Independent Data Set

The new data set used to verify the operation of our simulator was generously supplied by Vogel and Goldhirsch. The data are from their March, 1986, helicopter experiments. The data consists of two helicopter runs taken on the Baltimore-Washington Parkway, heading south, with the van in the right lane and the helicopter to the right of the van. The data were taken between the intersection with Highway 32 and the New Carrolton exit.

Data from the first helicopter run are contained in eight files. Each file consists of 87 records which in turn consist of 1.024 seconds of magnitude and phase data spaced 1 ms apart. Data for this run were taken with the elevation angle to the transmitter about 30°.

Data from the second helicopter run are again contained in eight files. The format of these data are the same as the first run. Data for the second run were taken with the elevation angle to the transmitter about 45°.

5.3.2 Verification of Simulator Using Helicopter Data

To test the improved simulator for operation using the new data, the procedure outlined in Section 4.6 was again used. The simulator output cumulative distribution was first matched to data containing both shadowed and unshadowed conditions. The fade duration statistics of the measured and simulated data were then compared.

The first data set used for simulator validation was TD110534. These data were taken with a 45° elevation angle and correspond to 2.25 km of travel with approximately 50% shadowing. Figure 5.3-1 shows the cumulative distribution plot of TD110534 and the simulator match to it. Figure 5.3-2 compares the cumulative fade durations at five different thresholds for the simulated and measured data.

Next we concatenated four data sets with 45° elevation angles. Data sets TD110534, TD111039, TD111220, and TD111401 were concatenated to produce data which correspond to 9.08 km of travel with approximately 42% shadowing. Figure 5.3-3 shows the distribution plot of the concatenated data and the simulator match to it. Figure 5.3-4 compares the cumulative fade durations at five different thresholds for the simulated and measured data. Again, the agreement is very good.

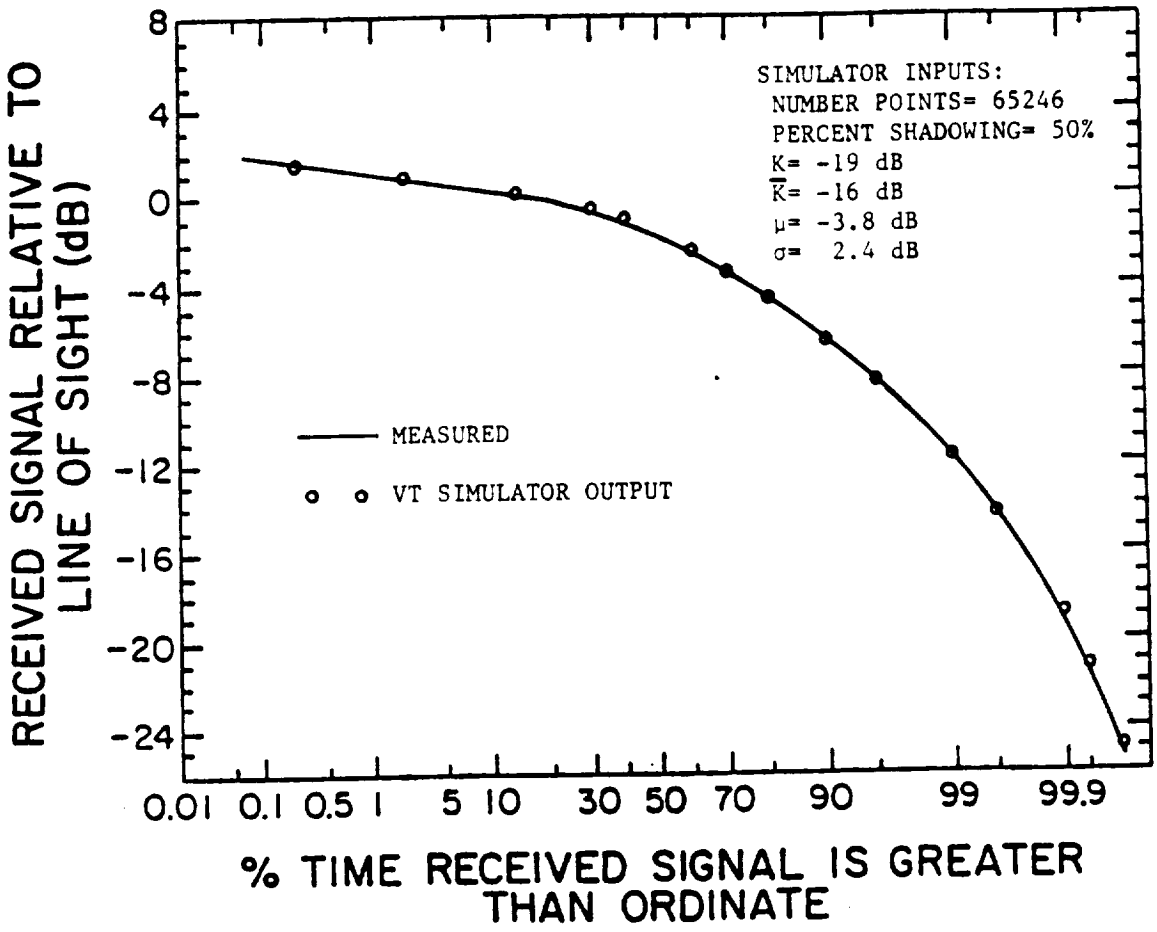

Figure 5.3-1. Cumulative distribution plot of data set TD110534 and the VT simulator match to it.

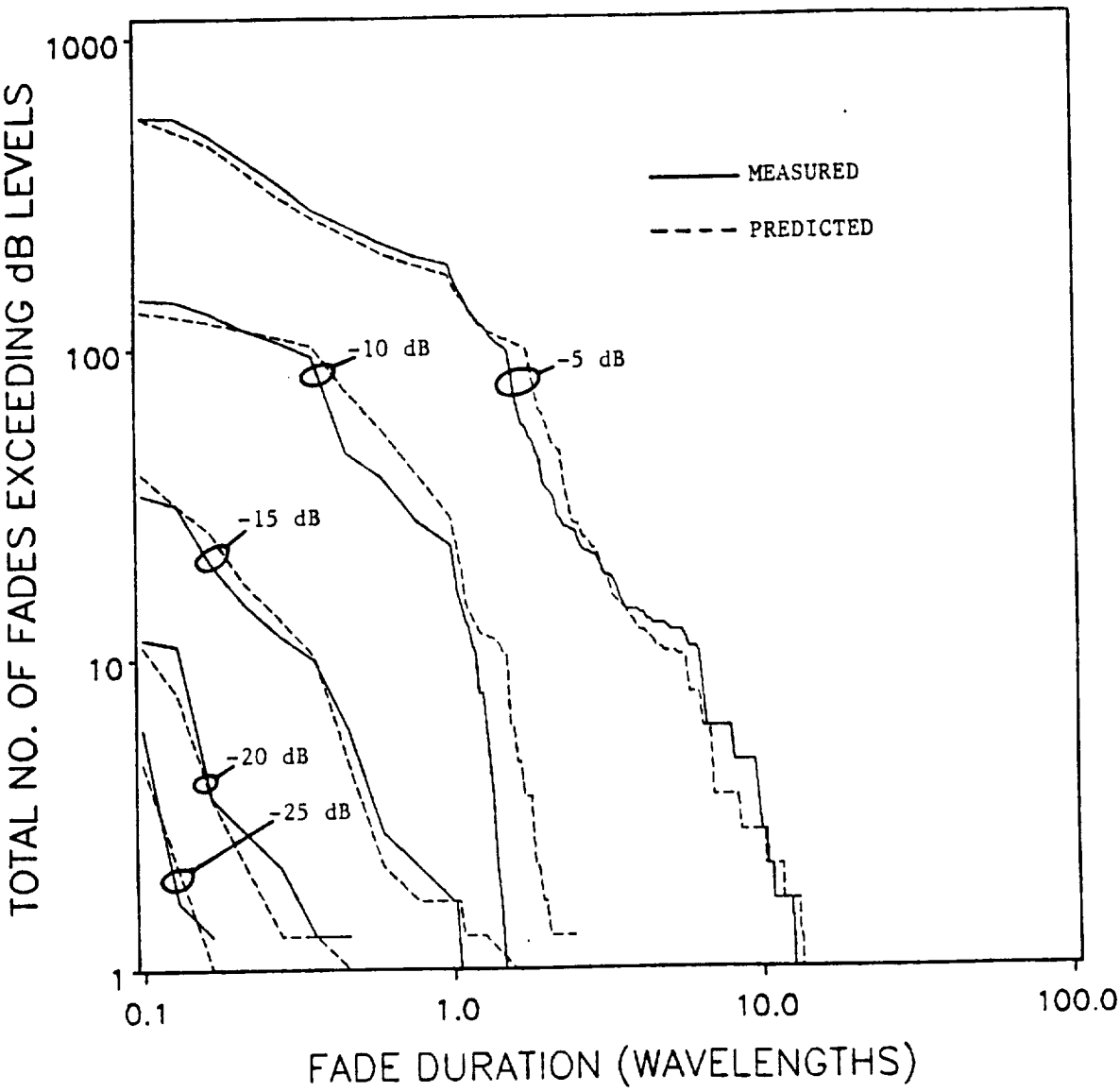

Figure 5.3-2. Cumulative fade duration distribution at five thresholds comparing experimental and simulator predicted fades for data set TD110534.

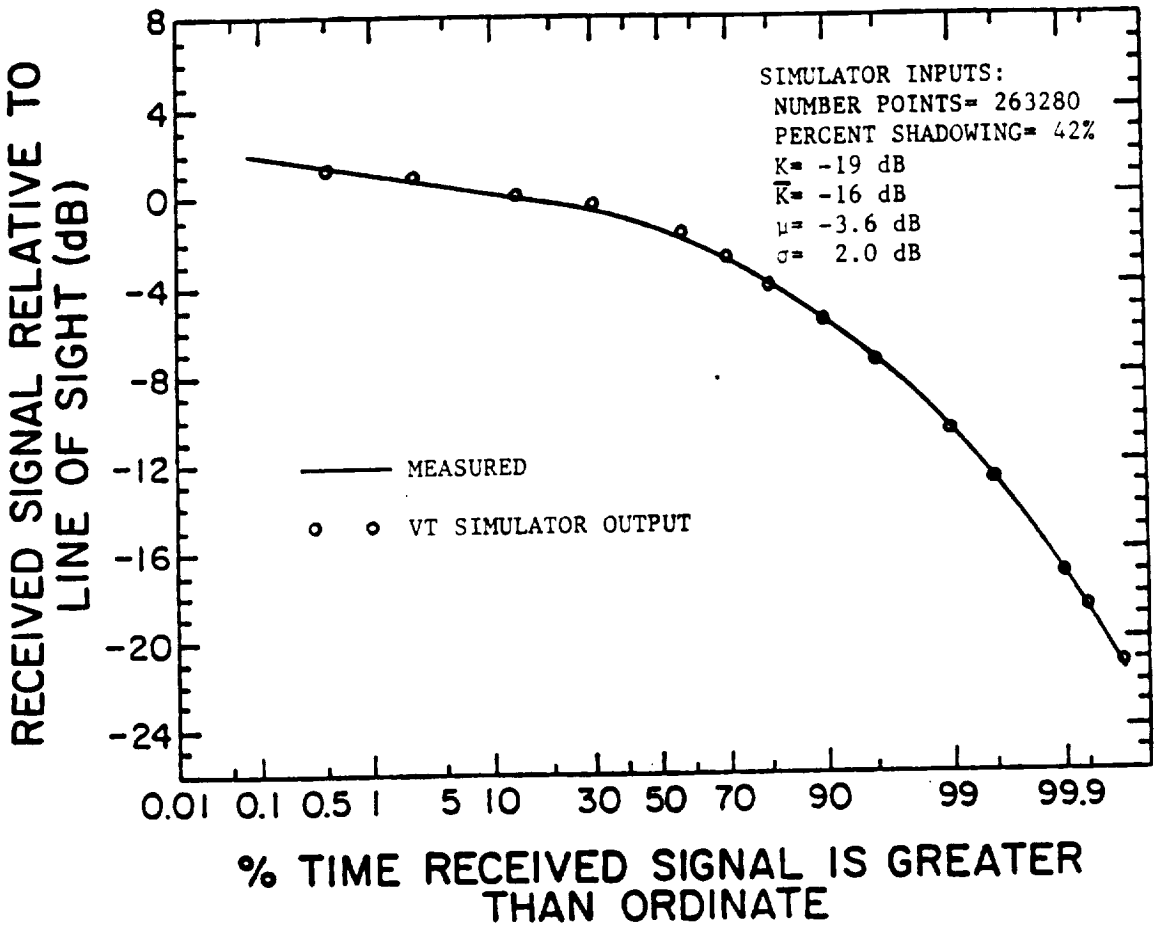

Figure 5.3-3. Cumulative distribution plot of concatenated data data sets TD110534, TD111039, TD111220, and TD111401 and the VT simulator match to them.

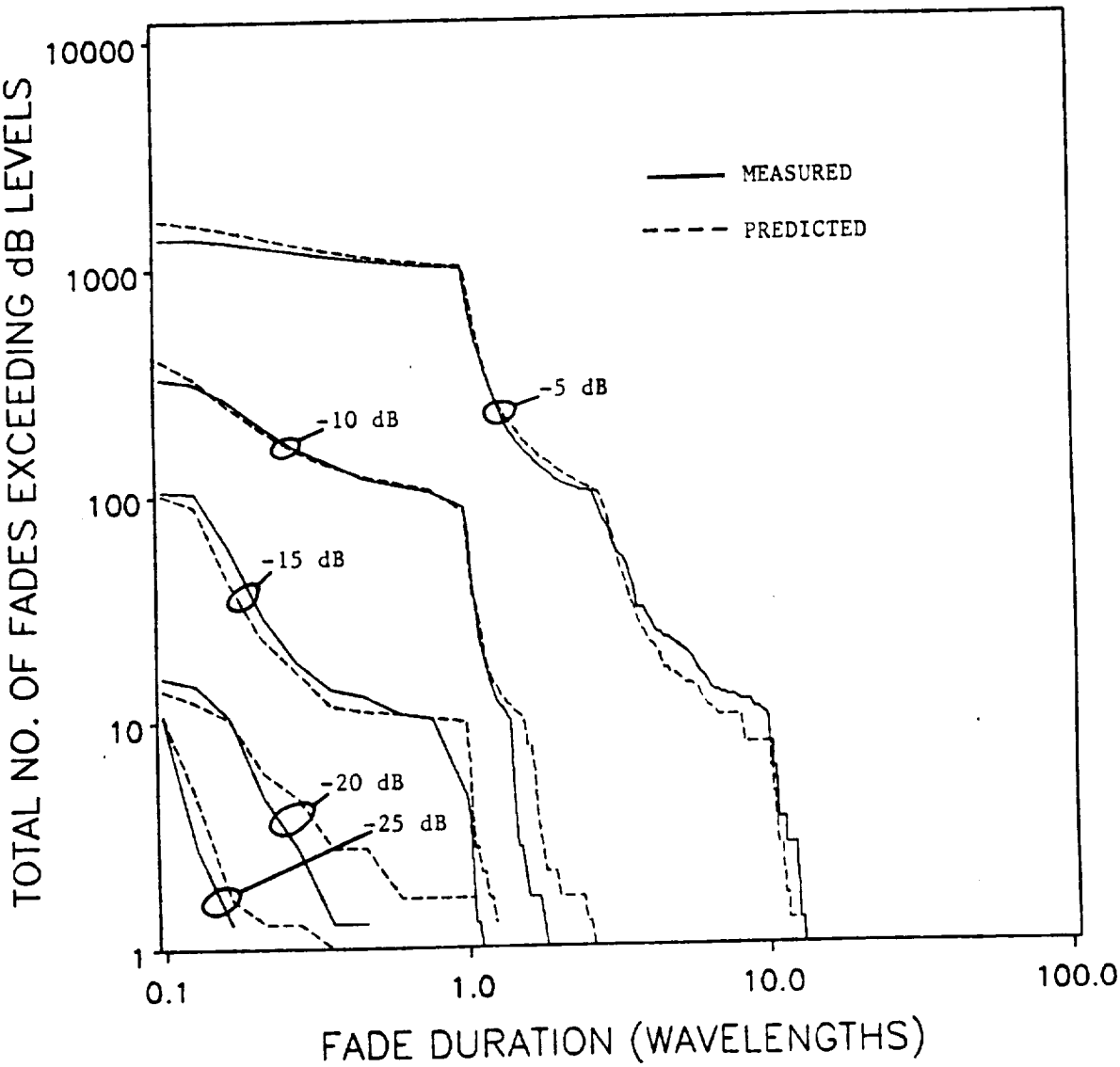

Figure 5.3-4. Cumulative fade duration distribution at five thresholds comparing experimental and simulator predicted fades for concatenated data sets TD110534, TD111039, TD111220, and TD111401.

To test the operation of the simulator for data collected at 30° elevation angle, we matched the cumulative distribution of the simulator output to data set TD103416. Data set TD103416 contains data for 2.01 km of travel with approximately 55% shadowing. Figure 5.3.5 shows the distribution of these data and the simulator match. The cumulative fade durations at five thresholds for the simulated and measured data are compared in Figure 5.3-6.

The final test was performed using three data sets with 30° elevation angles. These include TD103416, TD103745, and TD103927. The concatenation of these data sets produced data which correspond to 6.97 km of travel with approximately 71% shadowing. Our simulator match to the cumulative distribution of the concatenated data is shown in Figure 5.3-7. Figure 5.3-8 compares the cumulative fade durations for the simulated and measured data. Agreement is excellent.

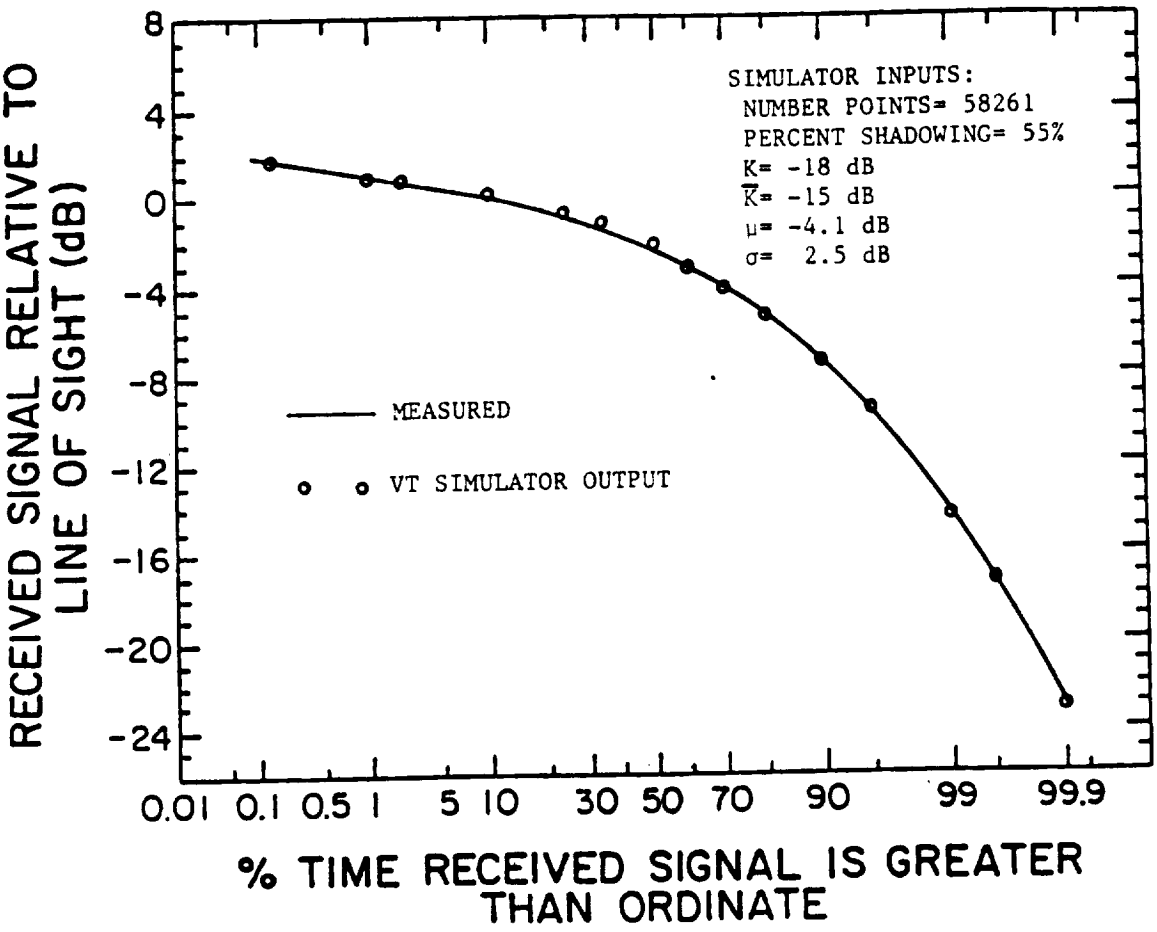

Figure 5.3-5. Cumulative distribution plot of data set TD103416 and the VT simulator match to it.

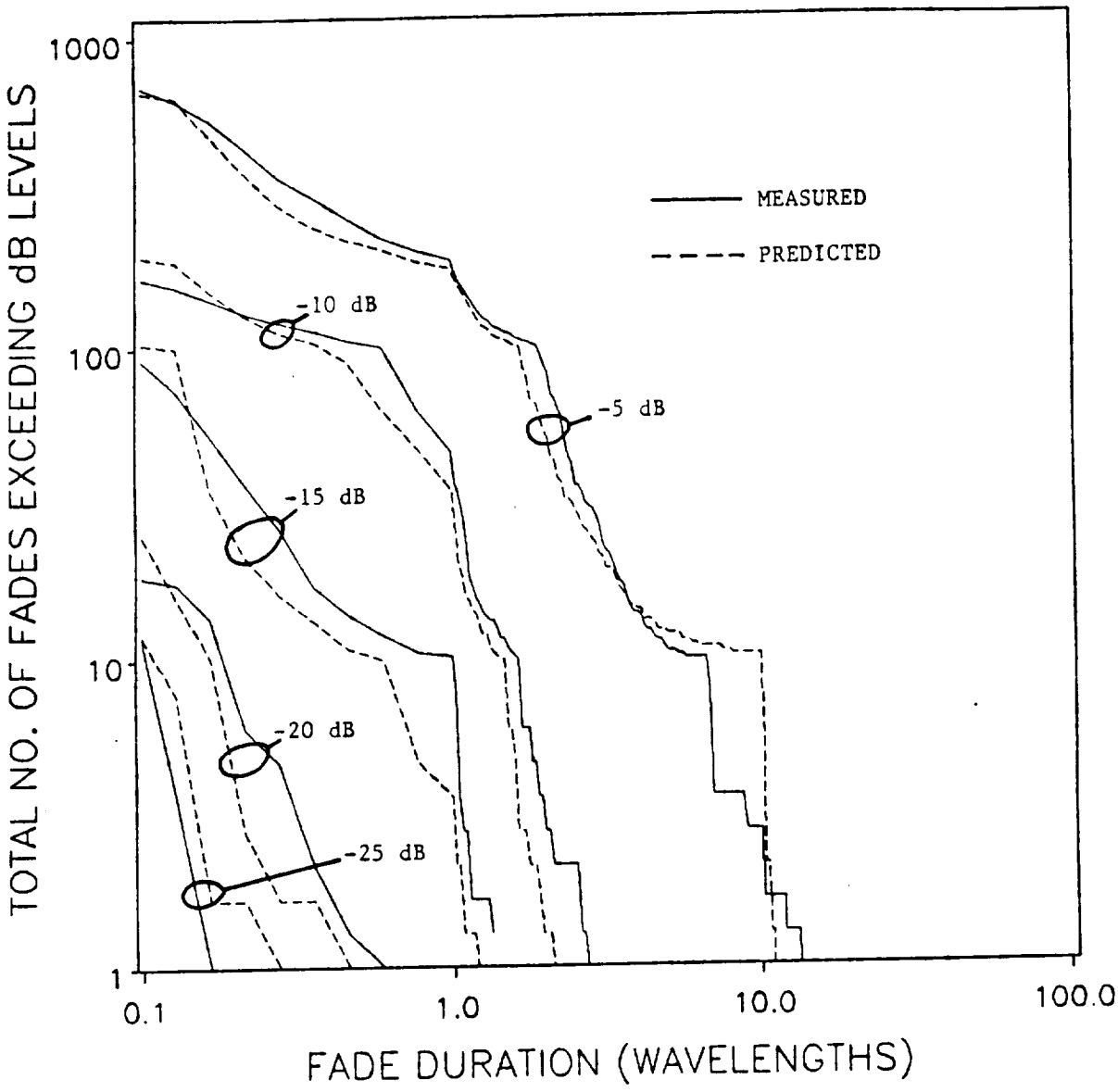

Figure 5.3-6. Cumulative fade duration distribution at five thresholds comparing experimental and simulator predicted fades for data set TD103416.

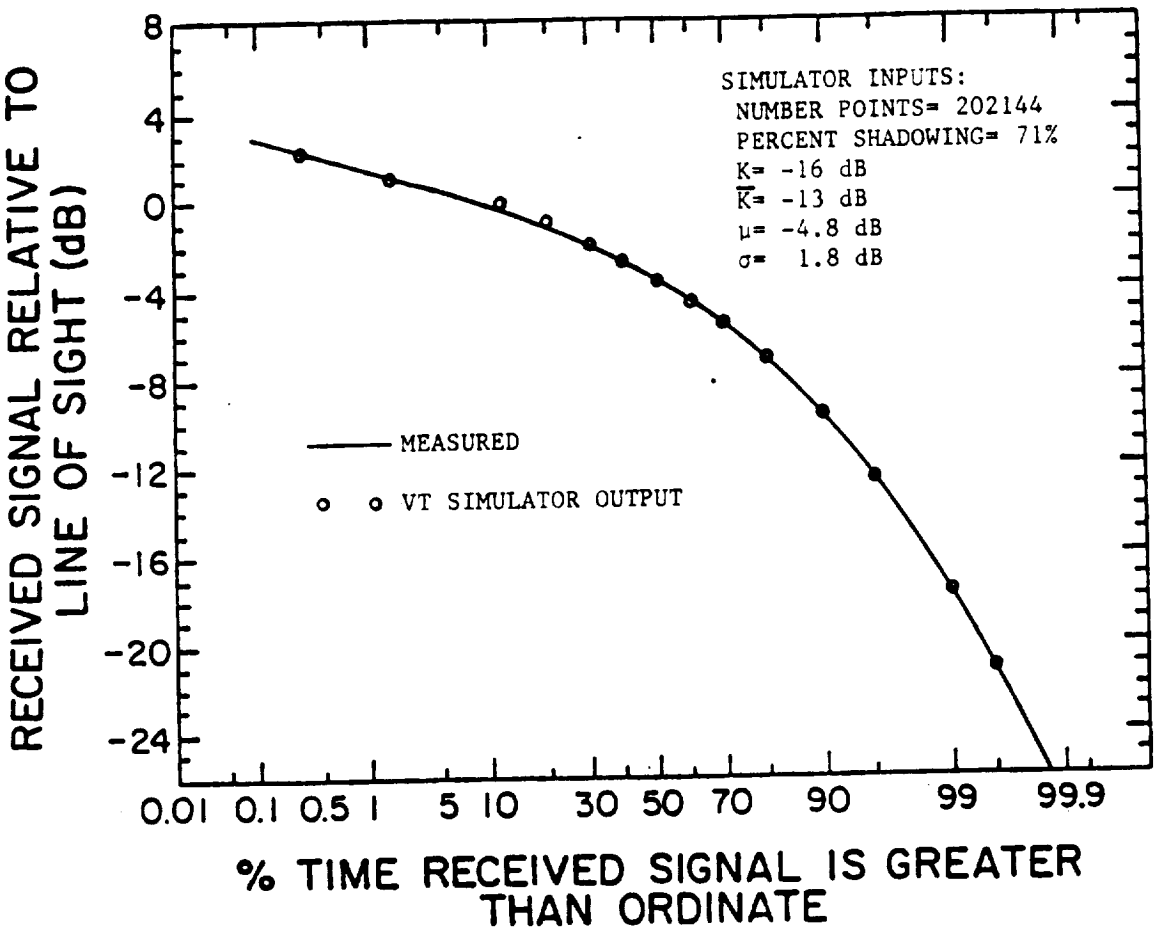

Figure 5.3-7. Cumulative distribution plot of concatenated data sets TD103416, TD103745, and TD103927 and the VT simulator match to them.

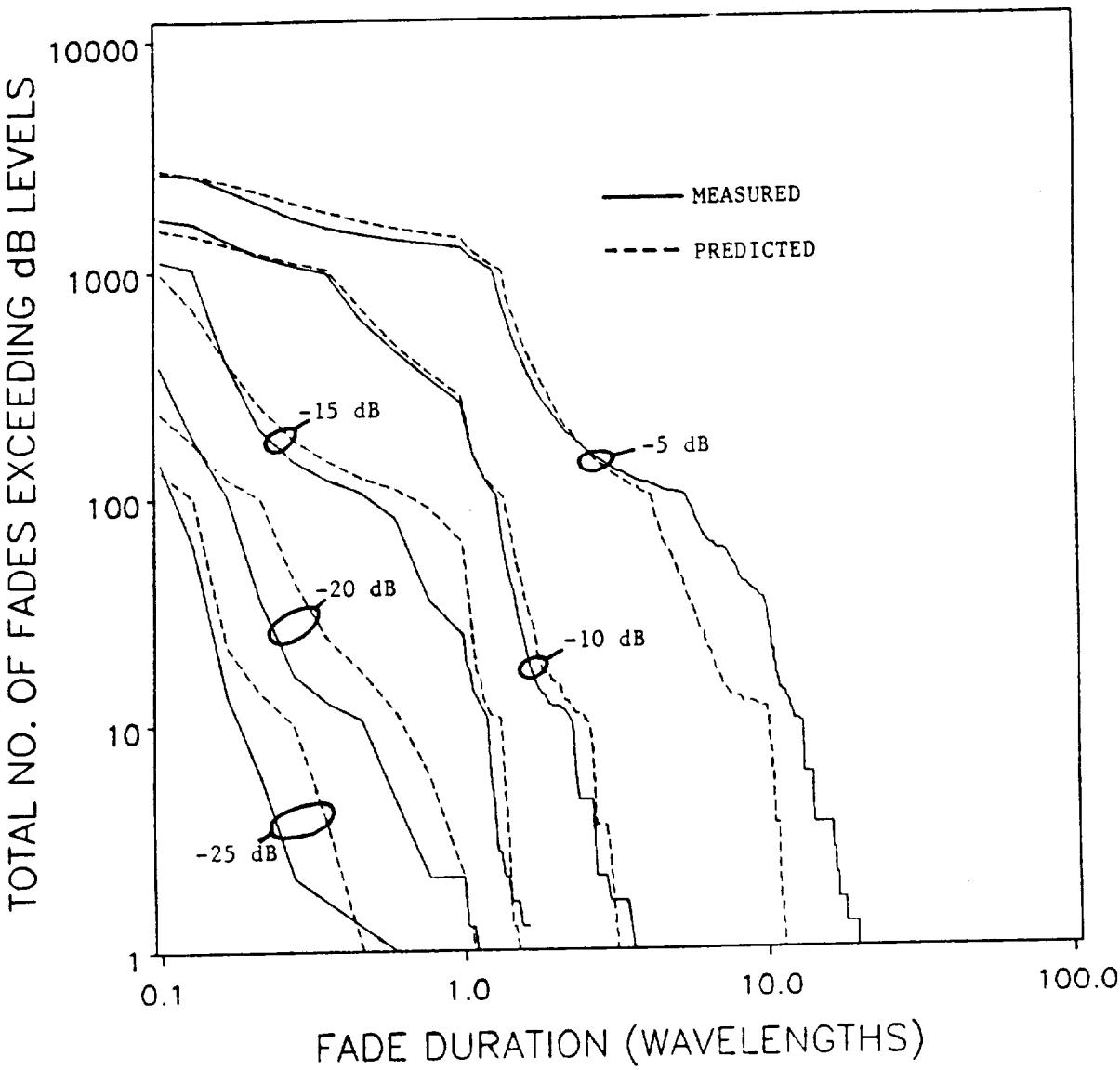

Figure 5.3-8. Cumulative fade duration distribution at five thresholds comparing experimental and simulator predicted fades for concatenated data sets TD103416, TD103745, and TD103927.

VI. CONCLUSIONS AND RECOMMENDATIONS

In this report, we described a software simulator that generates a received LMSS signal that is used for predicting fade duration statistics. The only simulator input is a cumulative distribution plot of the data to be generated. We started the simulator development by following the efforts of the JPL and CRC simulators and generating the diffuse component in precisely the same manner as these simulators. We then added to previous efforts by using a scaled attenuation approach to generate the direct component of vegetatively shadowed data. To improve the simulator, we found that we needed to abandon the original approach to generating the diffuse process and use data to generate the diffuse component of the signal. The final simulator is based entirely on data, using universal data sets to generate both the direct component and the diffuse component of the LMSS signal.

Some of the most significant results noted in the simulator development are:

1. In all of the data examined and simulated by us, the unshadowed data seldom contained fades in excess of 5 dB. Thus, in data we examined, it appears that the unshadowed Rician distributed fades are not important, but other data have indicated more severe unshadowed fading which make inclusion of a unshadowed data generator a necessary part of the simulator.

2. To produce good simulator data with the proper dynamic behavior, the distribution of the simulator output must be closely matched to that of the desired measured data. Essentially, this means that the simulator appears to have universal dynamic characteristics, but it must be tuned by K, $\overline{K}$, μ_R, and σ_R to produce output with the same characteristics as the desired data. The cumulative distribution plot is the tool used to tune the simulator and determine the proper values of the input parameters. This tuning process requires knowledge of the percentage of vegetative shadowing fairly well and following the matching procedure outlined in Appendix C.

3. The dynamic characteristics of the LMSS signal envelope appear to be universal. The VT simulator, since it is based entirely on data, relies on the assumption that the dynamic characteristics of the data are universal. In Section 5.3, we showed that the simulator (based entirely on data collected in Texas) predicted fading dynamics for data collected in Maryland at two different elevation angles extremely well. This indicates to us that indeed the dynamic behavior is universal and that the simulator may be employed to generate data for any area of the country where a cumulative fade duration curve is available.

Although the simulator is basically complete, we have a few recommendations for further investigation. First, the simulator should be modified slightly for operation at L-band (the present frequency of operation is 869 MHz). The only change necessary for

this is to change the lognormal data base so it is a function of distance traveled instead of wavelengths traveled as it presently is. After this modification, the operation of the simulator at L-band must be tested by using a measured L-band data set. Finally, distribution curves, based on vegetation and terrain, should be obtained for various parts of the country so that the simulator can be used to predict dynamic fade characteristics for the curves.

REFERENCES

1. J. Aitchison, and J. A. C. Brown, *The Lognormal Distribution*, Cambridge University Press, London, 1957.

2. G. A. Arredondo, W. H. Chriss, and E. H. Walker, "A multipath fading simulator for mobile radio, " *IEEE Trans. on Vehicular Technology*, vol. VT-22, pp. 241-244, Nov. 1973.

3. P. Beckmann and A. Spizzichino, *The Scattering of Electromagnetic Waves from Rough Surfaces*, Pergamon Press, New York, 1963.

4. P. Beckmann, *Probability in Communication Engineering*, Harcourt, Brace and World, New York, 1967.

5. W. F. Bodtmann and H. W. Arnold, "Fade duration statistics of a Rayleigh distributed wave, " *IEEE Trans. Comm.*, vol. COM-30, pp. 349-353, March 1982.

6. G. E. Bottomley, "Modeling the dynamic behavior of rain attenuation, " Masters Thesis, VPI & SU, June 1985.

7. W. S. Bradley and W. L. Stutzman, "Propagation modeling for land mobile satellite communications, " Virginia Tech Report EE Satcom 85-3, performed for JPL sponsored by NASA under Contract 956512, August 1985.

8. J. S. Butterworth, "Propagation measurements for land-mobile satellite services in the 800 MHz band, " Communications Research Centre, Department of Communications, Canada, Aug. 1984.

9. J. S. Butterworth, "Propagation measurements for land-mobile satellite systems at 1542 MHz, " Communications Research Centre, Department of Communications, Canada, Aug. 1984.

10. J. S. Butterworth, "The description and evaluation of a mobile communications channel simulator, " *Proceedings of the Propagation Workshop in Support of MSAT-X,* JPL, Pasadena, CA, pp. 4.3-4.21, Jan. 1985.

11. CCIR Interim Working Party 5/2, "Propagation data for land-mobile satellite systems for frequencies above 100 MHz, " Document 5/12-E, Mar. 1983.

12. R. H. Clarke, "A statistical theory of mobile-radio reception, " *Bell Syst. Tech. J.,* vol. 47, pp.957-1000, July/Aug. 1968.

13. F. Davarian and J. Sumida, "Channel simulator tests digital mobile radios, " *Microwaves and RF,* vol. 23, pp. 115-118, Aug. 1984.

14. F. Davarian, "JPL's mobile communications channel hardware simulator, " *Proceedings of the Propagation Workshop in Support of MSAT-X,* JPL, Pasadena, CA, pp. 2.5-2.18, Jan. 1985.

15. D. Divsalar, "Software simulation of the LMSS propagation channel, " *Proceedings of the Propagation Workshop in Support of MSAT-X,* JPL, Pasadena, CA, pp. 2.19-2.46, Jan. 1985.

16. W. L. Flock, "Propagation effects on satellite systems at frequencies below 10 GHz: A handbook for satellite system design, " *NASA Reference Publication 1108,* Dec. 1983.

17. J. G. Gardiner, "Satellite services for mobile communication, " *Telecommunications,* North American Edition, vol. 20, no. 8, pp. 34-41, Aug. 1986.

18. V. Jamnejad, "Ground multipath in TOPEX's precision orbit determination tracking system, " JPL Interoffice Memorandum 3365-84-003, Jet Propulsion Lab., Pasadena, CA, Jan. 9, 1985.

19. W. C. Y. Lee, *Mobile Communications Engineering,* Mcgraw Hill, New York, 1982.

20. C. Loo, "A statistical model for a land mobile satellite link, " *Proceedings of the 1984 IEEE International Communication Conference,* pp. 588-594, 1984.

21. "MSAT-X Quarterly, " Jet Propulsion Lab., Pasadena, CA, no. 1, Oct. 1984.

22. A. Papoulis, *Probability, Random Variables, and Stochastic Processes,* Mcgraw-Hill, New York, 1965.

23. A. B. Salmasi, A. B. Springett, J. C. Sumida, and J. J. Richter, "Land mobile satellite service (LMSS) channel simulator: An end-to-end hardware simulator and study of the LMSS communications link, " Jet Propulsion Lab., Pasadena, CA, NASA-CR-173744, May 1984.

24. E. K. Smith, J. F. Cavanagh, and W. L. Flock, "Propagation effects for land mobile satellite systems, " *Proceedings of the National Radio Science Meeting*, Jan. 1983.

25. W. T. Smith and W. L. Stutzman, "Statistical Modeling for Land Mobile Satellite Communications, " Virginia Tech Report EE Satcom 86-3, performed for JPL sponsored by NASA under Contract 956512, August 1986.

26. W. J. Vogel, "CTS attenuation and cross polarization measurements at 11.7 GHz, " *Final Report Covering the Period 1 February 1978 to 31 January 1979*, The University of Texas at Austin, Electrical Engineering Research Lab, Prepared for Goddard Space Flight Center under contract NAS5-22576.

27. W. J. Vogel and G. W. Torrence, "Measurement results from a balloon experiment simulating land mobile satellite transmissions, " MSAT-X Report No. 101, (submitted for JPL Contract 956520), Apr. 1984.

28. W. J. Vogel and E. K. Smith, "Propagation considerations in land-mobile satellite transmission, " MSAT-X Report No. 105, NASA-JPL, Pasadena, CA, pp. 1.5-1.18, Jan. 1985.

29. W. J. Vogel, "Land mobile satellite transmission measurements at 869 MHz " Technical Report, JPL, contact no. 956520, Mar. 1985.

Appendix A. PROCESSING THE VOGEL NOVEMBER 1984, BALLOON EXPERIMENT DATA

The 869 MHz signal envelope data supplied by Vogel from his November 1984, balloon experiments was sent as a group of 37 floppy disks, each containing a file of 259,560 bytes of data. Each file consists of 63 records of 4120 bytes or 2060 integers. Each record contains a 24 byte header and 1024 samples of the signal level and the phase. The format of each record is shown in Table A-1. The sampling rate was 1000 Hz, so each record represents 1.024 seconds of data, and each file represents slightly over one minute of data. Of the files received, 21 out of the 37 contain at least a small amount of vegetatively shadowed data. In this appendix, the collection and processing of the data by Vogel is described. This is followed by a discussion of some of our special processing of the data to get it into an acceptable form for the simulator development.

Table A-1. Format of Vogel's November, 1984, balloon experiment data.

Integer No.	Length (Bytes)	Content
1	2	A sequence number (2...65)
2	2	Receiver antenna used 1=drooping dipole 2=microstrip 3=heli bowl
3-5	6	Time: Hour Minute Second
6	2	Van speed in 0.1 mph
7	2	n/a
8	2	n/a
9	2	n/a
10	2	A power level in 0.01 dB
11	2	n/a
12	2	n/a
13-1036	2048	Signal level in 0.01 dB relative to level in integer #10
1037-2060	2048	Phase in 0.04 degrees

A.1 Collection and Processing of the Data by Vogel

A description of the data collection and processing by Vogel prior to our receiving it is given in [29] and is partly repeated here. The data was collected on analog tapes by recording the in-phase and quadrature components continuously. The tapes were then digitized with 12-bit resolution at 1000 samples per second for the in-phase and quadrature channels and a lower rate for the speed and rf-gain control voltages. The digitized data were organized into files, each one of which consists of 65 records of 1.024 seconds of data. The A/D converter outputs stored in the files were converted to received power and phase through a sequence of programs, making use of a calibration table. Each record was screened by graphic presentation to avoid contamination of the data base [29].

During the data collection, the transmitter and receiver oscillators slowly drifted with respect to each other because they were free running. This resulted in the two detector outputs having a slowly varying offset frequency ω_0. Another cause of varying frequency offset is a change in the Doppler frequency due to a change in the relative velocity between the balloon-borne transmitter and the receiver in the van. If the inphase and quadrature voltages are viewed on an x-y oscilloscope display, a phasor r results and rotates at a radial frequency ω_0 , and amplitude and phase variations can be seen as changes in the length of r and in the frequency of rotation ω_0 [29].

The received power can be calculated from the sum of the squares of the two orthogonal components. To get the phase, calculated as the arc-tangent of the in-phase and quadrature component, however, one has to eliminate the frequency offset ω_0 , which

produces a linear increase or decrease with time of the phase. To determine the offset frequency, a FFT was performed on one of the two output channels for each 1024 point record. The peak frequency multiplied by the time represents the phase shift due to the difference in frequency. It was added or subtracted from the calculated phase, depending on which output was leading the other. Further, any residual phase sawtooth appearance due to an error in the estimate of the offset frequency and the 2π ambiguity of the arc-tangent was eliminated and finally the remaining linear trend in the phase data was removed [29].

A.2 Additional Processing of the Data by Virginia Tech

The data supplied by Vogel had to be further processed for use in our simulator development. The majority of the processing was performed on the phase data. This processing includes forcing the phase to be continuous between 1.024 second records and removing slow variations in the phase as discussed in Section A.2.1. Additional processing, as discussed in Section A.2.2, put the data in the form of signal level as a function of wavelengths traveled with data points spaced 0.1 wavelengths apart.

A.2.1 Phase Processing

The phase data, as supplied by Vogel, were processed as discrete 1.024 second records. Because the data were processed as discrete records, the phase was discontinuous between the 1.024 second records. In reality, the phase should be continuous between the records since the records follow each other continuously in time. The processing of the data by Vogel, which was adequate for his uses, left arbitrary constants (or phase references) in the phase data which caused the phase discontinuity between records. We forced the phase to be continuous between the records by adding an appropriate constant to the phase of each record. The constant was determined so that the value of the first phase data point in a record was set equal to the value of the last phase data point in the previous record. The result is data with the phase discontinuities due to processing removed. Each file of 65 seconds of data was processed in the manner just described to remove the phase discontinuities.

Processing data to remove slow phase variations was not obvious initially. A few figures should illustrate the problems we encountered because of slow variations in the raw phase data. Figure A-1 shows 100 wavelengths of unshadowed data from TD090517. Overlayed on the empirical data is a 20 wavelength long running average of the complex signal voltage. For the running average shown in this figure, the only phase processing that has been done is to make the phase continuous between records. The running average does not follow the mean of the data as it should. This error in the running average is due to slow variations of the phase data.

The phase of the signal data in Figure A-1 is shown in Figure A-2. Note the mean phase drifts around slowly, uncorrelated to the magnitude data. We hypothesize that these

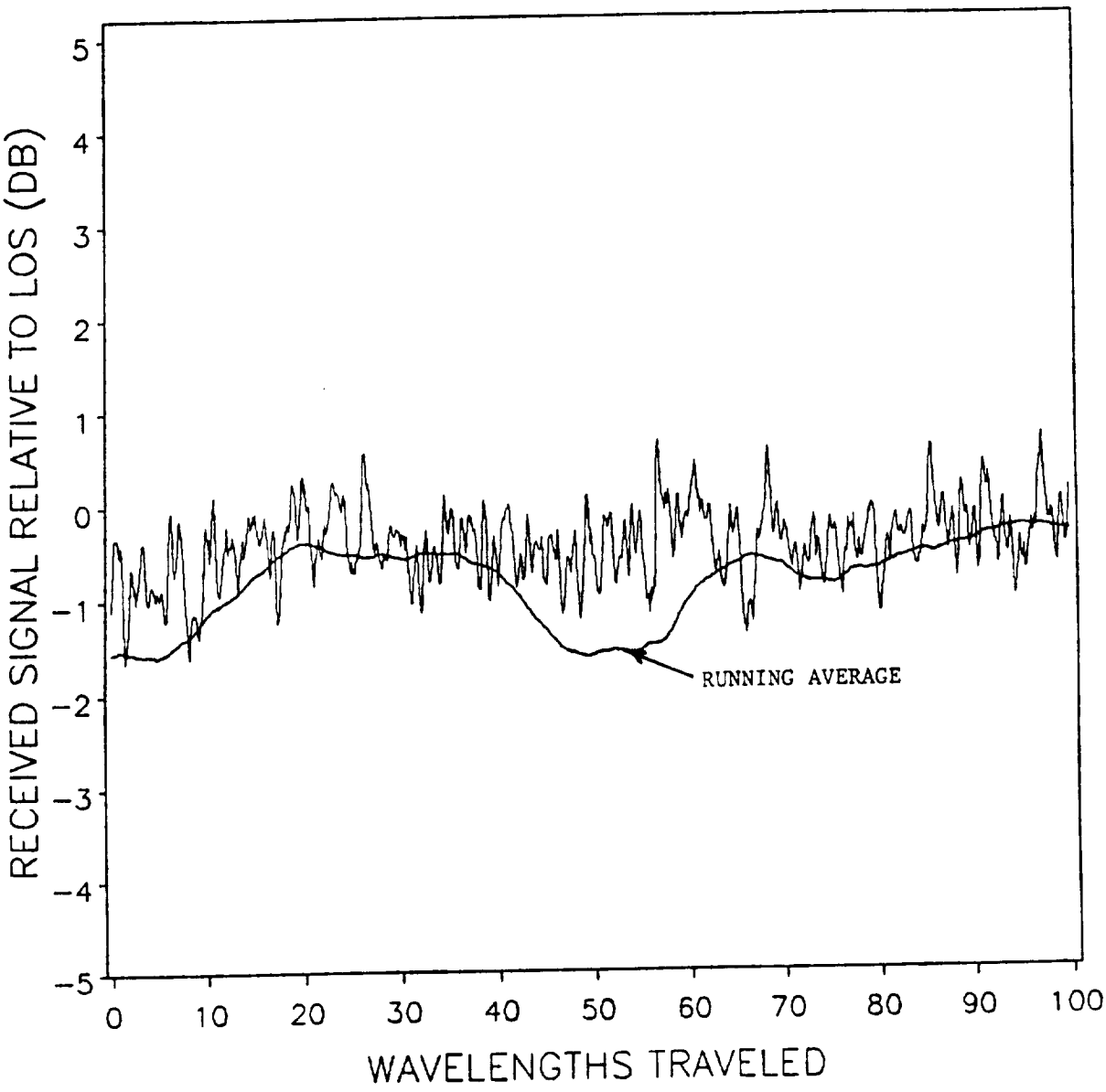

Figure A-1. 100 wavelengths of unshadowed data set TD090517 and superimposed running average prior to processing the signal phase.

slow phase variations are due to path length changes between the balloon and the mobile as the mobile travels or to slow oscillator drifts not completely removed from the data by Vogel. Regardless of the reason for the slow phase drifts, they had to be removed so that the running average could operate properly. They were removed by highpass filtering the phase data with a 20 Hz highpass digital filter (the filtering program is named HIGPAS.F and a listing may be found in Appendix B). The resulting phase data retained its high frequency component due to multipath, but all slow phase variations were removed. Figure A-3 shows the same data as Figure A-1, but in Figure A-3 the phase has been forced to be continuous and slow variations have been removed. Overlayed on the data is the running average. Note that it follows the mean of the data well as is desired. Figure A-4 shows the raw phase of four records of a typical Vogel data set from the November 1984, balloon data and the same data after each step in our data processing.

A.2.2 Changing the Data Format

Once the phase data were completely processed, the format of the data was changed from signal level as a function of time at a given vehicle velocity to signal level as a function of wavelengths traveled. The data are normalized into this format by multiplying the time at which a data point is recorded by a constant obtained by dividing the vehicle velocity by the wavelength at the frequency of operation (the constant gives velocity as wavelengths traveled per second). This puts the data into a format of signal level as a function of wavelengths traveled.

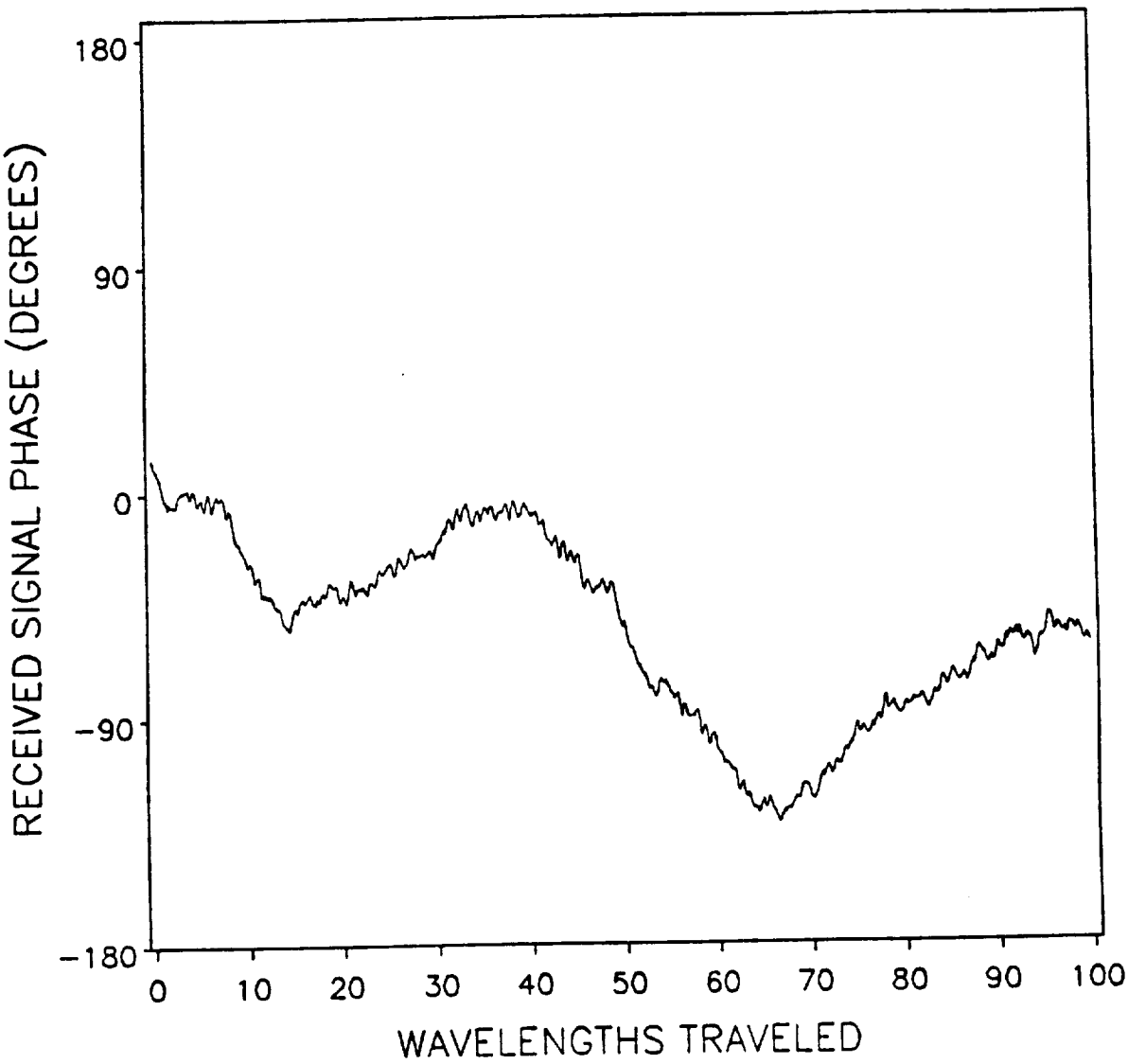

Figure A-2. Phase of the signal data shown in Figure A-1 prior to processing the phase data.

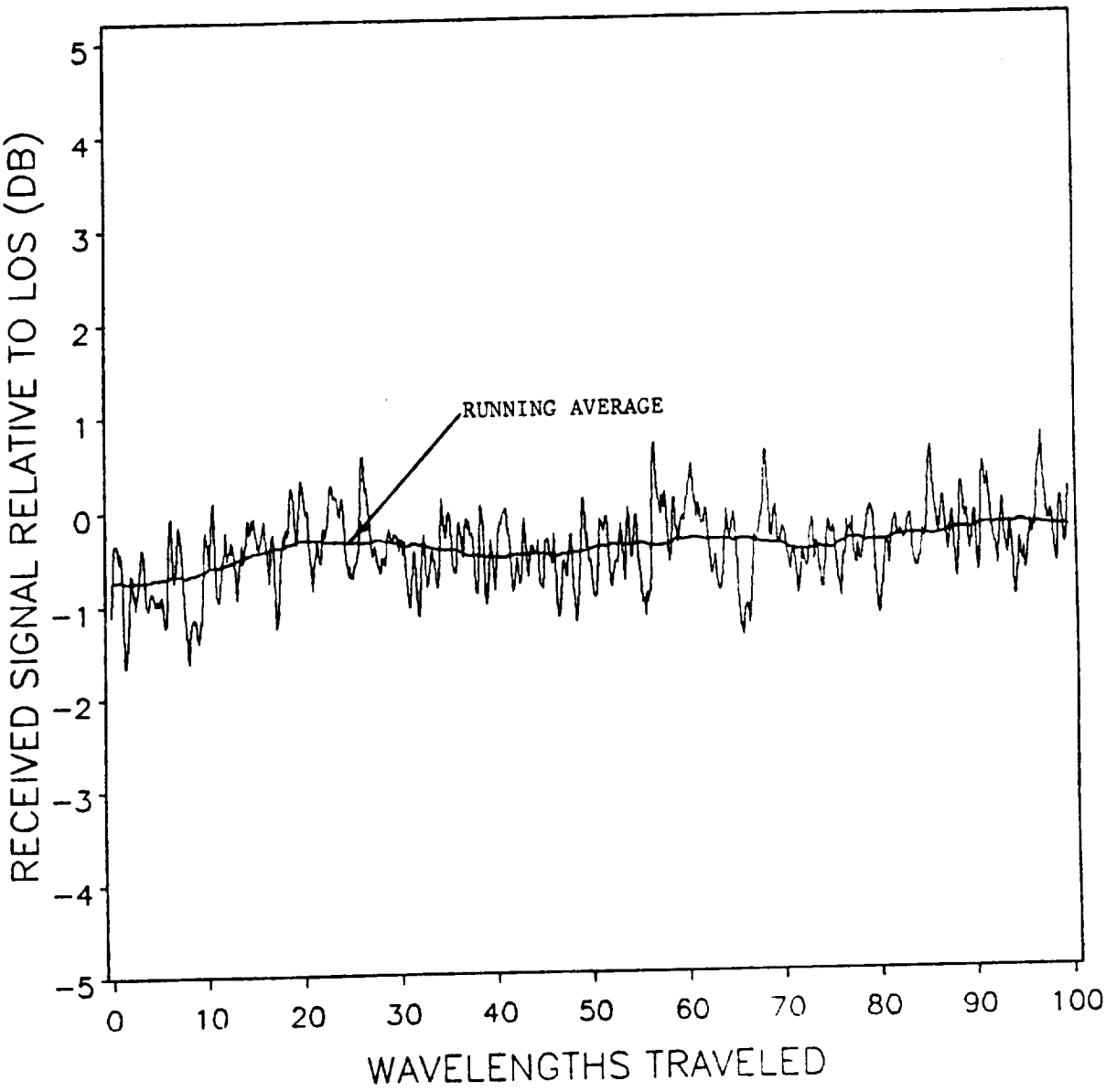

Figure A-3. 100 wavelengths of unshadowed data set TD090517 and superimposed running average after we processed the signal phase.

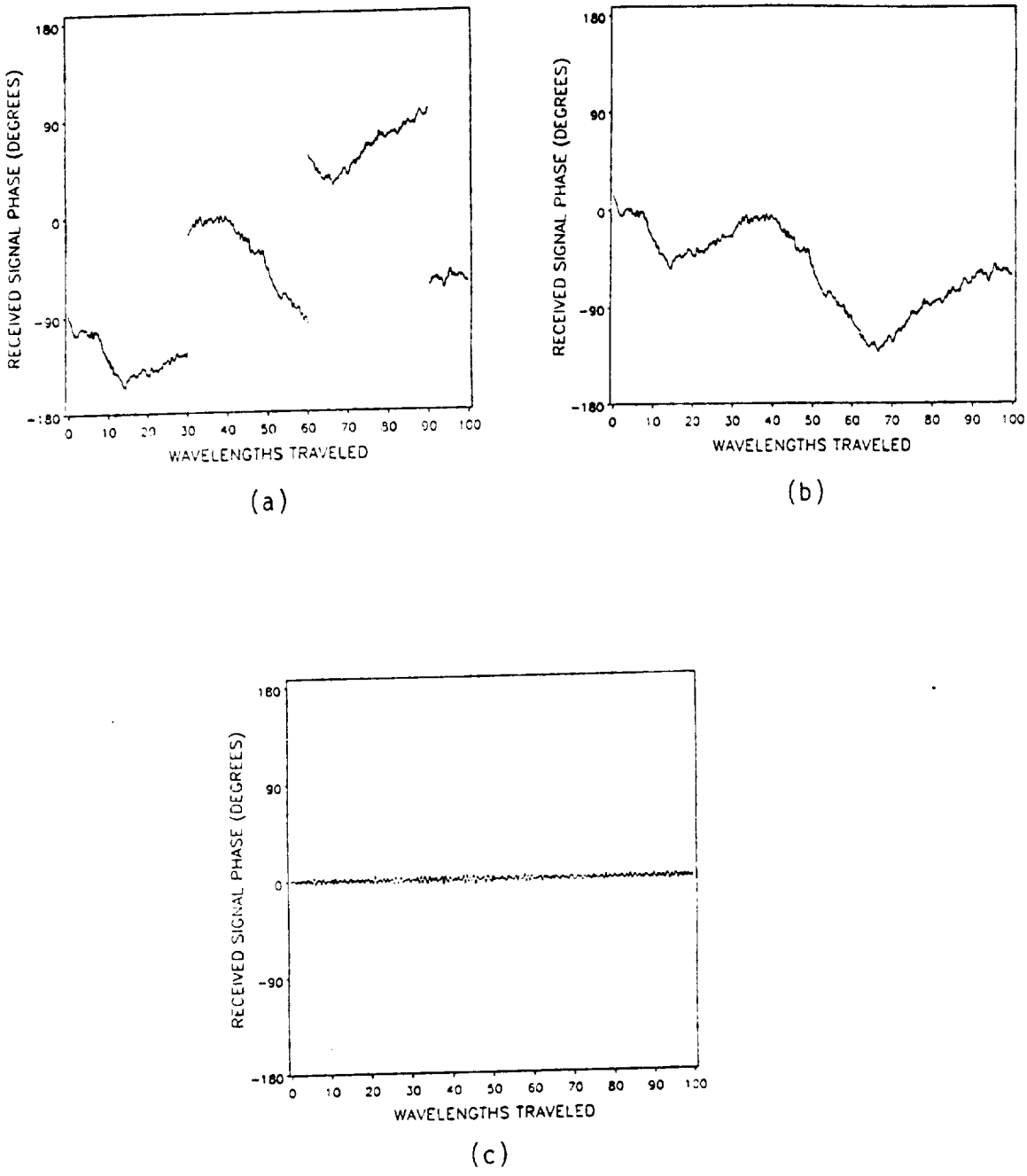

Figure A-4. Processing the phase data. (a) Four records of raw phase from Vogel's November 1984, balloon experiments. (b) Phase is forced to be continuous between records. (c) Phase is then highpass filtered.

After the format of the data has been changed to eliminate the velocity variable, a process of interpolation is used to get data that is spaced 0.1 wavelengths apart. This process very simply puts the data into complex voltage form, does a simple interpolation if the data points do not fall exactly 0.1 wavelengths apart (which they never do), and puts the data back into phase and magnitude in its original format. The resulting data is used for all processing in the simulator development.

Appendix B. COMPUTER PROGRAMS

RUNA2.F

```
C RUNA2.F
C PROGRAM TO PERFORM A RUNNING AVERAGE OF DATA THAT IS SPACED 0.1
C WAVELENGTHS APART. THE PROGRAM WAS WRITTEN SPECIFICALLY TO HANDLE
C VOGEL'S NOVEMBER, 1984, BALLOON DATA, BUT MINOR MODIFICATIONS WILL
C ALLOW IT TO BE USED WITH ANY DATA SET.
C EACH DATA RECORD IS ASSUMED TO BE PRECEDED BY
C A 12 LINE HEADER, LINE 7 OF WHICH CONTAINS THE NUMBER OF POINTS IN
C THE RECORD. THE RECORDS ARE ASSUMED TO BE CONTINUOUS.
      INTEGER COUNT,HEADER(30,12),NUMPTS(30),SUMPTS,MAG(4000),
     &PHASE(4000),PROMAG(4000),PROFAS(4000),A
      COMPLEX POINT(4000),SUM,PROVOL,SUMMER
C INPUT THE LENGTH OF THE AVERAGING WINDOW
      WRITE(10,3)
 3    FORMAT(1X,'INPUT NUMBER OF WAVELENGTHS LONG AVERAGE IS, REAL')
      READ(10,*) ALENTH
      LENTH = NINT(ALENTH/0.1)
C INITIALIZE SOME COUNTERS
      LL = 1
      COUNT = 0
      SUM = (0.0,0.0)
      SUMPTS = 0
      IB = 0
      FUDGE = 3.141593*0.04/180.0
C START GETTING DATA
 5    READ(20,10,END = 999) (HEADER(LL,J),J = 1,12)
 10   FORMAT(I6)
      NUMPTS(LL) = HEADER(LL,7)
      IF (LL .GT. 1) THEN
        INIT = SUMPTS + 1
        IFIN = SUMPTS + NUMPTS(LL)
      ELSE
        INIT = 1
        IFIN = NUMPTS(LL)
      END IF
      READ(20,20) (MAG(I),I = INIT,IFIN)
      READ(20,20) (PHASE(I),I = INIT,IFIN)
C CHANGE DATA FROM LOGARITHMIC FORM TO A COMPLEX VOLTAGE FORM.
      CALL PTOV(MAG,PHASE,INIT,IFIN,POINT)
 20   FORMAT(8I6)
C KEEP TRACK OF TOTAL NUMBER OF POINTS READ
      SUMPTS = SUMPTS + NUMPTS(LL)
      IF (SUMPTS.LE.LENTH) THEN
        IF (SUMPTS.LE.LENTH/2) THEN
          COUNT = LL
        END IF
        LL = LL + 1
        GO TO 5
      END IF
C THE RUNNING AVERAGE OF THE FIRST AND LAST HALF WINDOW LENGTH
C CANNOT BE DETERMINED SO THEY ARE SET TO 9999 JUST FOR EASY ID.
      DO 40 I = 1,LENTH/2
        PROMAG(I) = 9999
```

```
      PROFAS(I) = 9999
 40   CONTINUE
C OUTPUT RESULTS
     IF (COUNT.GT.0) THEN
       DO 50 I = 1,COUNT
         WRITE(30,10) (HEADER(I,J),J = 1,12)
         WRITE(30,20) (PROMAG(J),J = 1,NUMPTS(I))
         WRITE(30,20) (PROFAS(J),J = 1,NUMPTS(I))
         IB = IB + NUMPTS(I)
 50    CONTINUE
       DO 3000 K = 1,LL-COUNT
         NUMPTS(K) = NUMPTS(K + COUNT)
         DO 3010 J = 1,12
           HEADER(K,J) = HEADER(K + COUNT,J)
 3010    CONTINUE
 3000  CONTINUE
     LL = LL-COUNT
     END IF
C KEEP TRACK OF SUM FOR RUNNING AVERAGE
     DO 60 I = 1,LENTH
       SUM = SUM + POINT(I)
 60  CONTINUE
     KK = 0
     MM = LENTH
     JJ = LENTH/2 - IB
 65  MM = MM + 1
     KK = KK + 1
     JJ = JJ + 1
C IF WE RUN OUT OF DATA IN THE RECORD, GO TO THE NEXT RECORD AND
C THEN RESET.
     IF (MM.GT.SUMPTS) THEN
       LL = LL + 1
       READ(20,10,END = 99) (HEADER(LL,J),J = 1,12)
       NUMPTS(LL) = HEADER(LL,7)
       READ(20,20) (MAG(I),I = MM,MM + NUMPTS(LL)-1)
       READ(20,20) (PHASE(I),I = MM,MM + NUMPTS(LL)-1)
       CALL PTOV(MAG,PHASE,MM,MM + NUMPTS(LL)-1,POINT)
       DO 70 I = 1,LENTH + NUMPTS(LL)
         POINT(I) = POINT(MM + I-1-LENTH)
 70    CONTINUE
       SUMPTS = LENTH + NUMPTS(LL)
       KK = 0
       MM = LENTH
       JJ = JJ-1
       GO TO 65
     END IF
C TAKE THE DATA FROM COMPLEX VOLTAGE FORM AND PUT IT BACK INTO
C LOGARITHMIC FORM TO OUTPUT.
     PROVOL = SUM/FLOAT(LENTH)
     VOLMAG = CABS(PROVOL)
     PWRDB = 20.0*LOG10(VOLMAG)
     PROMAG(JJ) = NINT(PWRDB*100.0)
     ANGLE = ATAN2(AIMAG(PROVOL),REAL(PROVOL))
     PROFAS(JJ) = NINT(ANGLE/FUDGE)
     SUM = SUM + POINT(MM)-POINT(KK)
C     WRITE (10,*) SUM,MM,KK,POINT(MM),POINT(KK)
```

```
      IF (JJ.EQ.NUMPTS(1)) THEN
        WRITE(30,10) (HEADER(1,J),J = 1,12)
        WRITE(30,20) (PROMAG(I),I = 1,NUMPTS(1))
        WRITE(30,20) (PROFAS(I),I = 1,NUMPTS(1))
        JJ = 0
        DO 80 K = 1,LL-1
          NUMPTS(K) = NUMPTS(K + 1)
          DO 90 J = 1,12
            HEADER(K,J) = HEADER(K + 1,J)
90        CONTINUE
80      CONTINUE
        LL = LL-1
      END IF
      GO TO 65
999   WRITE(10,100)
100   FORMAT(1X,'NOT ENOUGH DATA')
      GO TO 9999
C WRITE OUT THE LAST HALF WINDOW LENGTH WITH 9999'S
99    A = LENTH/2
      DO 9000 I = 1,LL-1
        IF (NUMPTS(LL-I) .LT. A) THEN
          DO 9010 J = 1,NUMPTS(LL-I)
            PROMAG(JJ + A-J) = 9999
            PROFAS(JJ + A-J) = 9999
9010      CONTINUE
          A = A-NUMPTS(LL-I)
        ELSE
          DO 9020 J = 1,A
            PROMAG(NUMPTS(LL-I)-J + 1) = 9999
            PROFAS(NUMPTS(LL-I)-J + 1) = 9999
9020      CONTINUE
        END IF
9000  CONTINUE
      MMM = 0
      DO 9030 J = 1,LL-1
      WRITE(30,10,END = 9999) (HEADER(J,K),K = 1,12)
      WRITE(30,20,END = 9999) (PROMAG(I),I = MMM + 1,MMM + NUMPTS(J))
      WRITE(30,20,END = 9999) (PROFAS(I),I = MMM + 1,MMM + NUMPTS(J))
      MMM = MMM + NUMPTS(J)
9030  CONTINUE
9999  STOP
      END
C
C
C
C SUBROUTINE TO TAKE SIGNAL LEVEL IN DB AND PHASE IN RADIANS AND
C CONVERT IT TO COMPLEX VOLTAGE.
      SUBROUTINE PTOV(MAG,PHASE,BEGIN,LAST,POINT)
      INTEGER MAG(4000),PHASE(4000),BEGIN,LAST
      COMPLEX POINT(4000)
      FUDGE = 3.141593*0.04/180.0
      DO 10 I = BEGIN,LAST
        VOLTS = 10.0**(FLOAT(MAG(I))/2000.0)
        ANGLE = FLOAT(PHASE(I))*FUDGE
        POINT(I) = CMPLX(VOLTS*COS(ANGLE),VOLTS*SIN(ANGLE))
10    CONTINUE
```

```
RETURN
END
```

RICSE3.F

```
C RICSE3.F
C PROGRAM TO TAKE A VOGEL, NOVEMBER, 1984, BALLOON DATA SET AND A
C RUNNING AVERAGE OF THE DATA SET AND EXTRACT THE FAST FADE COMPONENT
C OF THE DATA SET. THIS IS ACCOMPLISHED BY PUTTING THE DATA INTO
C COMPLEX VOLTAGE FORM AND SUBTRACTING THE RUNNING AVERAGE DATA
C FROM THE RAW DATA SET ON A POINT-BY-POINT BASIS.
      INTEGER HEADER(12),VOGHED(12),VOGMAG(5120),VOGFAS(5120),
     *        LOGHED(12),LOGMAG(5120),LOGFAS(5120),TOTPTS,MAG(4096),
     *        AFAS(4096)
      REAL MEAN,MEANSQ,AMAG(4096)
      COMPLEX DATA1,DATA2,DIF
      LPTS = 1024
      TOTPTS = 0
      MM = 0
C FUDGE FACTOR TO GET PHASE DATA INTO RADIANS
      FUDGE = 3.141593*0.04/180.0
      DO 50 I = 1,12
        HEADER(I) = 0
 50   CONTINUE
C GET THE DATA
 5    READ (10,10,END = 99) (VOGHED(I),I = 1,12)
 10   FORMAT(I6)
      NPTS = VOGHED(7)
C RAW DATA FIRST
      READ(10,20) (VOGMAG(I),I = TOTPTS + 1,TOTPTS + NPTS)
      READ(10,20) (VOGFAS(I),I = TOTPTS + 1,TOTPTS + NPTS)
 20   FORMAT(8I6)
C NEXT GET THE RUNNING AVERAGE DATA
      READ(20,10) (LOGHED(I),I = 1,12)
      READ(20,20) (LOGMAG(I),I = TOTPTS + 1,TOTPTS + NPTS)
      READ(20,20) (LOGFAS(I),I = TOTPTS + 1,TOTPTS + NPTS)
      IF ((LOGMAG(1) .EQ. 9999) .OR. (LOGMAG(TOTPTS + NPTS) .EQ. 9999))
     *          GO TO 5
      TOTPTS = TOTPTS + NPTS
      IF (TOTPTS .GE. LPTS) THEN
        MM = MM + 1
        SUM = 0.0
        SUMSQ = 0.0
C PUT THE DATA INTO COMPLEX VOLTAGE FORM AND PERFORM THE SUBTRACTION
        DO 30 I = 1,LPTS
          VOLTS1 = 10.0**(FLOAT(VOGMAG(I))/2000.0)
          ANG1 = FLOAT(VOGFAS(I))*FUDGE
          DATA1 = VOLTS1*CMPLX(COS(ANG1),SIN(ANG1))
          VOLTS2 = 10.0**(FLOAT(LOGMAG(I))/2000.0)
          ANG2 = FLOAT(LOGFAS(I))*FUDGE
          DATA2 = VOLTS2*CMPLX(COS(ANG2),SIN(ANG2))
          DIF = DATA1-DATA2
          AMAG(I) = CABS(DIF)
          SUM = SUM + AMAG(I)
          SUMSQ = SUMSQ + AMAG(I)**2
          X = REAL(DIF)
          Y = AIMAG(DIF)
```

```
      IF ((X .EQ. 0.0) .AND. (Y .EQ. 0.0)) THEN
       AFAS(I) = 0
      ELSE
       AFAS(I) = NINT(ATAN2(Y,X)/FUDGE)
      END IF
30    CONTINUE
C DETERMINE THE MEAN AND MEAN SQUARE VALUE OF THE RESULTING DATA
      MEAN = SUM/FLOAT(LPTS)
      MEANSQ = SUMSQ/FLOAT(LPTS)
C IF THE COMPLEX VOLTAGE SUBTRACTION YIELDS 0 VOLTS, THEN THIS
C CORRESPONDS TO MINUS INFINITY OR -9999 DB.
C NORMALIZE THE MAGNITUDE BY ITS MEAN AND CALCULATE ITS
C MAGNITUDE IN DB.
      DO 40 I = 1,LPTS
       IF (AMAG(I) .EQ. 0.0) THEN
        MAG(I) = -9999
       ELSE
        MAG(I) = NINT(2000.0*LOG10(AMAG(I)/MEAN))
       END IF
40    CONTINUE
      MEANSQ = MEANSQ/(MEAN**2)
      HEADER(1) = MM
      HEADER(2) = NINT(MEANSQ*10000.0)
      HEADER(7) = LPTS
C OUTPUT RESULTS
      WRITE(30,10) (HEADER(J),J = 1,12)
      WRITE(30,60) (MAG(J),J = 1,LPTS)
      WRITE(30,60) (AFAS(I),I = 1,LPTS)
60    FORMAT(8I6)
      LEFTOVR = TOTPTS-LPTS
C RESET
      DO 70 I = 1,LEFTOVR
       VOGMAG(I) = VOGMAG(TOTPTS-LEFTOVR + I)
       VOGFAS(I) = VOGFAS(TOTPTS-LEFTOVR + I)
       LOGMAG(I) = LOGMAG(TOTPTS-LEFTOVR + I)
       LOGFAS(I) = LOGFAS(TOTPTS-LEFTOVR + I)
70    CONTINUE
      TOTPTS = LEFTOVR
     END IF
     GO TO 5
99   STOP
     END
```

SIGGE2.F

```
C SIGGE2.F
C THIS IS THE SIMULATOR PROGRAM. IT CONTAINS BOTH THE RAYLEIGH
C GENERATOR AND THE LOGNORMAL SIGNAL GENERATOR. BESIDES REQUIRING
C RAYLEIGH AND LOGNORMAL SIGNAL DATA BASES, IT REQUIRES SIX
C INPUTS. THEY ARE:
C
C    TOTPTS - TOTAL NO. OF PTS. TO GENERATE
C    PERCSHA - PERCENT VEGETATIVE SHADOWING
C    UNSHADK - K VALUE FOR RICE DISTRIBUTION
C    SHADK - K OVERBAR VALUE FOR MULTIPATH COMPONENT OF VEGETATIVE
C          SHADOWING
C    MEAN2 - DESIRED MEAN OF THE LOGNORMAL COMPONENT OF VEGETATIVE
C          SHADOWING
C    STDEV2 - DESIRED STANDARD DEVIATION OF THE LOGNORMAL COMPONENT
C          OF VEGETATIVE SHADOWING
C
C NOTE I ONLY OUTPUT THE SIGNAL MAGNITUDE, SINCE THIS IS ALL I NEED
C TO DETERMINE FADE DURATIONS, BUT PHASE MAY ALSO BE OUTPUT IF
C DESIRED.
C
C
     REAL MEANSQ,MAG(4096),PHASE(4096),MEAN1,MEAN2
     INTEGER TOTPTS,SHAPTS,UNSHAPT,HEADER(12),RSIG(8),LOS(8)
     COMPLEX RAYLEI(8),CSIG(8),ALOS(8)
     WRITE(10,10)
 10   FORMAT(1X,'INPUT TOTAL NUMBER OF POINTS SPACED 0.1 WAVELENGTHS ',
    *'APART')
     READ (10,*) TOTPTS
     TOTPTS = 8*NINT(FLOAT(TOTPTS)/8.0)
     WRITE(10,20)
 20   FORMAT(1X,'INPUT PERCENT SHADOWING')
     READ(10,*) PERCSHA
     PERCSHA = PERCSHA/100.0
     WRITE(10,30)
 30   FORMAT(1X,'INPUT RICE K FOR UNSHADOWED')
     READ(10,*) UNSHADK
     WRITE(10,40)
 40   FORMAT(1X,'INPUT RICE K FOR SHADOWED')
     READ(10,*) SHADK
     WRITE(10,200)
 200  FORMAT(1X,'INPUT MEAN AND STANDARD DEVIATION FOR SCALED',/,
    *1X,      'LOGNORMAL FADES. PRESENT DATA BASE',/,1X,
    *'MEAN = -4.1',/,1X,'STANDARD DEVIATION = 2.5')
     READ(10,*) MEAN2,STDEV2
C MEAN AND STANDARD DEVIATION OF LOGNORMAL DATA BASE
     MEAN1 = -4.1
     STDEV1 = 2.5
C CALCULATE THE NUMBER OF SHADOWED AND UNSHADOWED POINTS
     SHAPTS = 8*NINT(PERCSHA*FLOAT(TOTPTS)/8.0)
     UNSHAPT = TOTPTS-SHAPTS
C READ UNSHADOWED RAYLIEGH DATA FROM DATA BASE
     READ(20,50) (HEADER(I),I = 1,12)
```

```
      MEANSQ = FLOAT(HEADER(2))/10000.0
      NUMPTS = HEADER(7)
      M = NUMPTS/8
C GET K AND K OVERBAR OUT OF DB FORM
      UNSHADK = 10.0**(UNSHADK/20.0)
      SHADK = 10.0**(SHADK/20.0)
      READ(20,60) (MAG(I),I = 1,NUMPTS)
 50   FORMAT(I6)
      READ(20,60) (PHASE(I),I = 1,NUMPTS)
 60   FORMAT(8F7.4)
      UNSCONS = UNSHADK/SQRT(MEANSQ)
      MM = 0
C IF WE RUN OUT OF RAYLEIGH DATA GET MORE
      DO 70 I = 1,UNSHAPT/8
       IF (MM .EQ. M) THEN
        MM = 0
 65      READ(20,50,END = 999) (HEADER(K),K = 1,12)
        GO TO 67
 999      REWIND 20
        GO TO 65
 67      MEANSQ = FLOAT(HEADER(2))/10000.0
        UNSCONS = UNSHADK/SQRT(MEANSQ)
        READ(20,60) (MAG(K),K = 1,NUMPTS)
        READ(20,60) (PHASE(K),K = 1,NUMPTS)
       END IF
C GENERATE RICE DATA
       DO 80 J = 1,8
        RAYLEI(J) = MAG(MM*8 + J) * CMPLX(COS(PHASE(MM*8 + J)),
     *                    SIN(PHASE(MM*8 + J)))*UNSCONS
        CSIG(J) = (1.0,0.0) + RAYLEI(J)
        RSIG(J) = NINT(2000.0*LOG10(CABS(CSIG(J))))
 80   CONTINUE
C OUTPUT RICE DATA MAGNITUDE ONLY
      WRITE(40,90) (RSIG(J),J = 1,8)
 90   FORMAT(8I6)
      MM = MM + 1
 70   CONTINUE
      MM = 0
C GET SHADOWED RAYLEIGH DATA FROM DATA BASE
      READ(50,50) (HEADER(I),I = 1,12)
      MEANSQ = FLOAT(HEADER(2))/10000.0
      NUMPTS = HEADER(7)
      M = NUMPTS/8
      READ(50,60) (MAG(I),I = 1,NUMPTS)
      READ(50,60) (PHASE(I),I = 1,NUMPTS)
      SHACONS = SHADK/SQRT(MEANSQ)
      DO 100 I = 1,SHAPTS/8
C IF WE RUN OUT OF SHADOWED RAYLEIGH DATA, GET MORE
       IF (MM .EQ. M) THEN
        MM = 0
 75      READ(50,50,END = 9995) (HEADER(K),K = 1,12)
        GO TO 77
 9995      REWIND 50
        GO TO 75
 77      MEANSQ = FLOAT(HEADER(2))/10000.0
        SHACONS = SHADK/SQRT(MEANSQ)
```

```
      READ(50,60) (MAG(K),K = 1,NUMPTS)
      READ(50,60) (PHASE(K),K = 1,NUMPTS)
     END IF
C GET THE LOGNORMAL DISTRIBUTED DATA
 85   READ(30,90,END = 9997) (LOS(K),K = 1,8)
     GO TO 87
9997   REWIND 30
     GO TO 85
C SCALE THE LOGNORMAL DATA, PUT IT INTO COMPLEX VOLTAGE FORM, AND
C ADD THE SHADOWED RAYLEIGH DATA TO GENERATE THE SHADOWED DATA
 87   DO 110 J = 1,8
      RAYLEI(J) = MAG(MM*8 + J) * CMPLX(COS(PHASE(MM*8 + J)),
     *                    SIN(PHASE(MM*8 + J)))*SHACONS
      A1 = FLOAT(LOS(J))/100.0
      A2 = (STDEV2/STDEV1)*(A1-MEAN1) + MEAN2
      ALOS(J) = CMPLX(10.0**(A2/20.0),0.0)
      CSIG(J) = ALOS(J) + RAYLEI(J)
      RSIG(J) = NINT(2000.0*LOG10(CABS(CSIG(J))))
110   CONTINUE
C OUTPUT THE SHADOWED DATA MAGNITUDE
     WRITE(40,90) (RSIG(J),J = 1,8)
     MM = MM + 1
100  CONTINUE
    STOP
    END
```

HIGPAS.F

```
C HIGPAS.F
C PROGRAM TO FILTER PHASE OF VOGEL'S DATA. THE PHASE DATA IS HIGHPASS
C FILTERED AT 20 HZ, WITH THE FILTER FREQUENCY RESPONSE BEING READ
C IN ARRAY FILTER(). THIS ARRAY MAY BE ALTERED SO THAT ANY FILTER
C FREQUENCY RESPONSE MAY BE USED. THE FILTER IS DESIGNED BY USING
C THE PROGRAM EQFIR:F, WHICH IS AN IEEE PROGRAM FOR DESIGNING AN
C OPTIMUM FILTER'S IMPULSE RESPONSE. THE IMPULSE RESPONSE MUST
C BE PUT INTO THE FREQUENCY DOMAIN TO USE IN THIS PROGRAM.
C VERY IMPORTANT - THIS PROGRAM IS SET UP TO RUN WITH A FILTER
C THAT IS 113 POINTS LONG - THINGS SUCH AS JJ AND NN MUST BE ALTERED
C TO RUN WITH A DIFFERENT FILTER LENGTH. ALSO, SINCE THE FILTER IS
C 113 POINTS LONG, THERE IS A (N-1)/2 DELAY OR 56 POINT DELAY IN
C THE FILTERED OUTPUT THAT IS THROWN OUT IN THIS PROGRAM. THAT IS,
C I THROW AWAY THE FIRST 56 POINTS OUTPUT BY THE FILTER BECAUSE
C THEY CORRESPOND TO A TIME DELAY. BY DOING THIS, THE PHASE THAT I
C FILTER ALIGNS IN TIME WITH THE MAGNITUDE DATA. ALSO, REALIZE THAT
C THE FINAL 56 PONTS OR SO OUTPUT AT THE END  OF THE FILTERING
C ROUTINE ARE GARBAGE AND MUST BE THROWN AWAY - THIS MEANS AT THE
C THE VERY END WHEN WE RUN OUT OF DATA THE OUTPUT IS GARBAGE, NOT
C IN BETWEEN WHEN WE ARE DOING THE OVERLAP SAVE ROUTINE.
      INTEGER PHASE(1024),PROFAS(1024)
      COMPLEX FILTER(1024),CPHAS(1024),TEMP(112)
      IFLAG = 0
      JJ = 912
      NN = 57
      DO 10 I = 1,112
        TEMP(I) = (0.0,0.0)
 10   CONTINUE
C GET THE FILTER FREQUENCY RESPONSE
 20   READ (40,*) (FILTER(I),I = 1,1024)
C GET THE PHASE DATA
 30   READ (30,40,END = 99) (PHASE(I),I = 1,JJ)
 40   FORMAT (8I6)
C PUT THE PHASE INTO COMPLEX FORM
      DO 50 I = 1,JJ
        CPHAS(I) = CMPLX(FLOAT(PHASE(I)),0.0)
 50   CONTINUE
C ADD ON THE ZEROS SO THAT PROPER UNALIASED FILTERING CAN BE PERFORMED
      DO 60 I = JJ + 1,1024
        CPHAS(I) = (0.0,0.0)
 60   CONTINUE
C PUT THE PHASE INTO THE FREQUENCY DOMAIN
 65   CALL FT(CPHAS,1024,10,0,0.001)
C MULTIPLY PHASE IN THE FREQUENCY DOMAIN BY FILTER FREQUENCY RESPONSE
C TO PERFORM THE ACTUAL FILTERING
      DO 70 I = 1,1024
        CPHAS(I) = CPHAS(I)*FILTER(I)
 70   CONTINUE
C DO INVERSE FFT TO GET BACK TO THE TIME DOMAIN
      CALL FT(CPHAS,1024,10,1,0.001)
C DO THE OVERLAP SAVE AND ADD
      DO 80 I = 1,112
```

```
      CPHAS(I)=CPHAS(I) + TEMP(I)
 80   CONTINUE
C GET THE FILTER PHASE DATA INTO INTEGER FORM
      DO 90 I=1,JJ
       PROFAS(I) = NINT(REAL(CPHAS(I)))
 90   CONTINUE
C RESET THE OVERLAP SAVE
      DO 100 I=JJ+1,1024
       TEMP(I-JJ) = CPHAS(I)
 100  CONTINUE
C OUTPUT THE FILTERED PHASE
      WRITE (50,40) (PROFAS(I),I=NN,JJ)
      NN=1
      IF (IFLAG .EQ. 1) STOP
      GO TO 30
 99   I=I-1
      N=1024-I
      DO 110 J=1,I
       CPHAS(J)=CMPLX(FLOAT(PHASE(J)),0.0)
 110  CONTINUE
      DO 120 J=I+1,I+N
       CPHAS(J)=(0.0,0.0)
 120  CONTINUE
      IFLAG = 1
      JJ = 1024
      GO TO 65
      END
C
      SUBROUTINE FT(FFT,N,NF,IBF,DT)
C
C     SUBROUTINE FT COMPUTES THE FFT OF A FUNCTION. THE ROUTINE IS BASED
C     OF THEM (N ANY INTEGER). TO USE FFT ENTER THE SAMPLE DATA ALONG
C     WITH THE NUMBER OF SAMPLES (N), THE POWER OF 2 (NF) AND IBF (FORWARD
C     OR INVERSE). DT RETURNS AS THE FREQUENCY SAMPLING INCREMENT.
C
      COMPLEX FFT(8192),CEXP,IMAG,A,B,W,PP,QQ
      IMAG=(0.0,1.0)
      PI=3.1415927
C     N=NUMBER OF SAMPLE POINTS
C     NF=POWER OF 2
C     IBF=0 FOR FORWARD TRANSFORM
C     IBF=1 FOR INVERSE TRANSFORM
      IF (IBF.EQ.0) GO TO 900
      DO 900 I=1,N
      IF (REAL(FFT(I)).EQ.0.0) FFT(I) = -IMAG*AIMAG(FFT(I))
      IF (AIMAG(FFT(I)).EQ.0.0) GO TO 900
      IF (REAL(FFT(I)).EQ.0.0) GO TO 900
      FFT(I)=CONJG(FFT(I))
 900  CONTINUE
C     CALCULATE P AND W**P
      TN=N
      W=CEXP(-IMAG*2.*PI/TN)
C     CALCULATE THE FAST FOURIER TRANSFORM
      DO 902 II=1,NF
       J=N/(2**II)
       NS=2**(II-1)
```

```
      DO 902 KK = 1,NS
        DO 902 JJ = 1,J
          LL = JJ + 2*J*(KK-1)
          MM = (LL-1)/2**(NF-II)
          CALL IB(MM,NF)
          PP = FFT(LL) + (W**MM)*FFT(LL+J)
          QQ = FFT(LL) - (W**MM)*FFT(LL+J)
          FFT(LL) = PP
 902    FFT(LL+J) = QQ
C      UNSCRAMBLE
       DO 903 I = 1,N
        K = I-1
        CALL IB(K,NF)
        IF(K + 1.LT.I) GO TO 903
        QQ = FFT(I)
        FFT(I) = FFT(K + 1)
        FFT(K + 1) = QQ
 903    CONTINUE
C      SORTING AND PRINTING ROUTINES
       RN = N
       DT = 1./(RN*DT)
       DO 904 I = 1,N
       IF (IBF.EQ.0) FFT(I) = (1./RN)*FFT(I)
       IF (IBF.EQ.1) FFT(I) = CONJG(FFT(I))
 904   CONTINUE
       RETURN
       END
C
C      SUBROUTINE FOR BIT REVERSING
       SUBROUTINE IB(LM,LP)
       ML = 0
       DO 909 I = 1,LP
        M = LM/2**(I-1)
        RM = M
        MM = RM/2.
        RMM = MM
        RL = RM-2.*RMM
        LLL = 0
        IF (RL.NE.0.) LLL = 1
 909    ML = ML + LLL*2**(LP-I)
       LM = ML
       RETURN
       END
```

Appendix C. MATCHING DISTRIBUTION OF THE SIMULATOR OUTPUT TO EMPIRICAL DATA

For the VT simulator to estimate the dynamic behavior of a LMSS signal envelope, the distribution of its output must first be matched to the distribution of an empirical data set (or an estimated distribution). Matching the empirical distribution with Rician and VS distribution components can be difficult and time consuming. This appendix outlines a fairly simple and quick procedure for matching the simulator output to any cumulative distribution plot, assuming the percent shadowing is known fairly well. Figure C-1 shows the distribution of one minute of the Vogel November 1984 balloon data containing 47% shadowing which we will try to match.

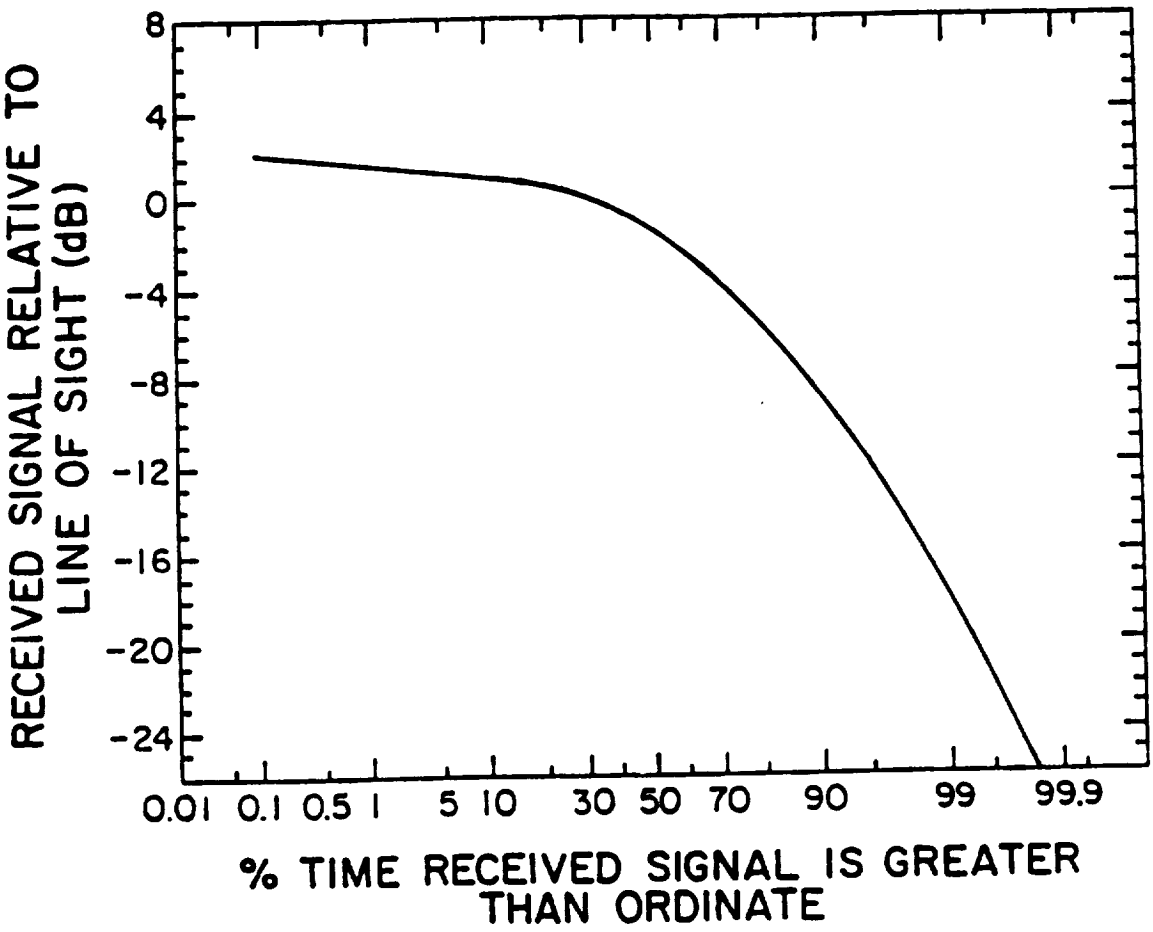

Figure C-1. Cumulative distribution plot of partially shadowed data set TD091540.

C.1 Obtaining the Rician Distributed Portion

As noted in Section 3.1, the portion of the distribution to the left of the knee of an LMSS distribution plot where shadowing is present follows a Rician shape (the entire plot appears Rician if no shadowing is present) and is relatively insensitive to the amount of shadowing. This portion of the curve is used to determine the K parameter for generating unshadowed data in the VT simulator. To determine the value of K (in dB), the simulator is set to generate about 10,000 points of unshadowed data (0% shadowing) and the value of K in the simulator is varied until the distribution of the generated data matches the left portion of the empirical distribution. The value of K that produces this match corresponds to the K of the unshadowed multipath fading signal. Figure C-2 shows the distribution of the data output by the simulator with an input of K = -16 dB overlayed on the distribution of the data set we are trying to match.

C.2 Obtaining the VS Distributed Portion

Obtaining the VS portion of the distribution is much more complicated because it requires determination of three input parameters to the simulator. Assuming the percent shadowing is known, these parameters are $\overline{K}$ for the Rayleigh generator and μ_R and σ_R for the lognormal generator. These parameters are determined by matching the simulator output under 100% shadowed conditions to a portion of a VS distribution curve extracted from the overall empirical data set.

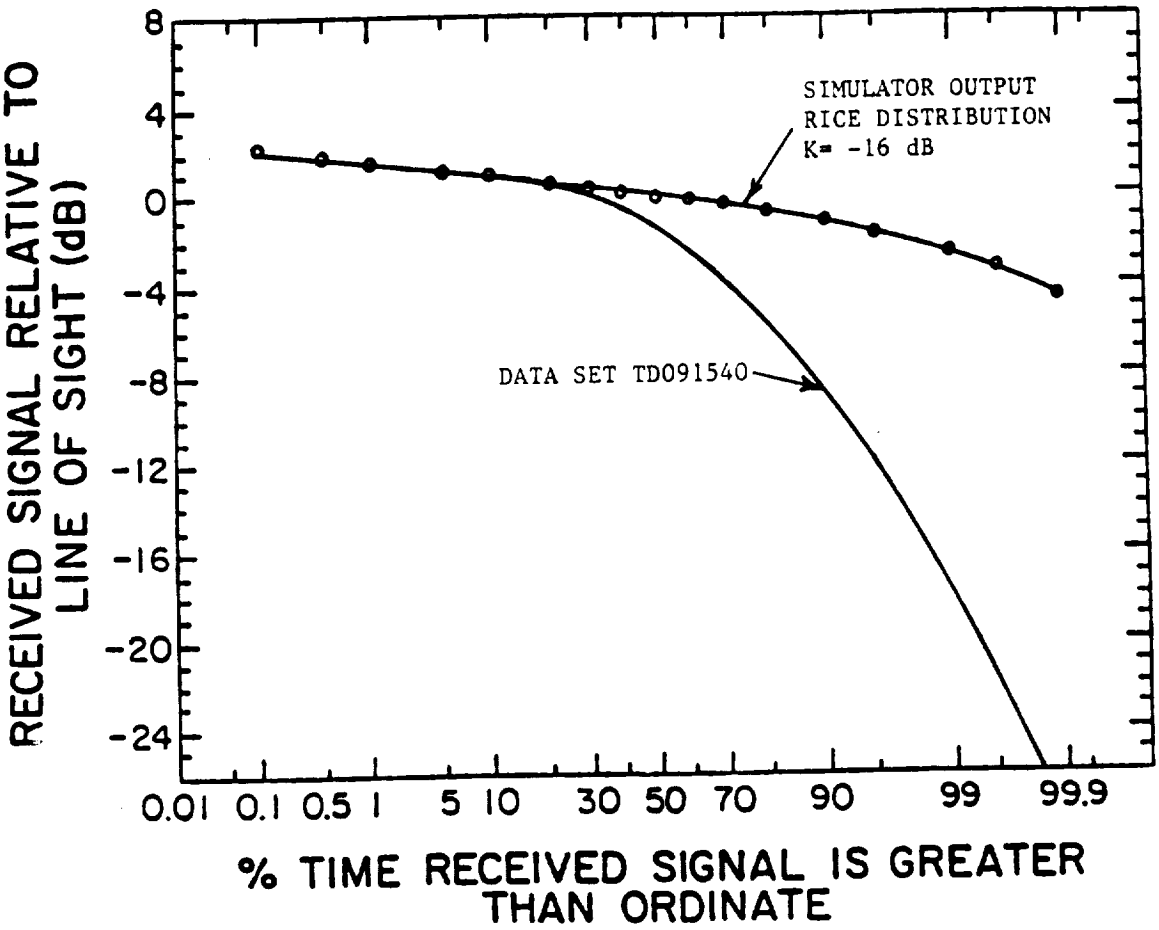

Figure C-2. Cumulative distribution plot of partially shadowed data set TD091540 and simulator output Rician distribution with input parameter K = -16 dB.

The first step in the matching process is to extract the VS distribution curve from the overall data set distribution. To do this, one must first realize that, in general, the portion of a total empirical LMSS distribution plot falling below about -8 dB is due entirely to vegetative shadowing, and that a VS distribution applies only to entirely vegetatively shadowed data. By knowing these two facts, one may remove a portion of the VS distribution curve from the overall distribution curve. The best way to illustrate how this is done is via an example. Figure C-3 shows the distribution we are trying to match to and the partial VS distribution that has been removed from it. The total data set contains 40,200 data points of which 47% or 18,894 points correspond to vegetatively shadowed data points. In the total distribution in Figure C-3, 99.77% of the total data points are above the -25 dB threshold. This corresponds to (1 - 0.9977)(40,200) = 92 data points equal to or falling below the -25 dB threshold. Now these data points are vegetatively shadowed data points so 92/18,894 = 0.0049 = 0.49% of the vegetatively shadowed data points are equal to or falling below a -25 dB threshold, or 99.51% of the vegetatively shadowed data points fall above a -25 dB threshold. Since we are talking about purely vegetatively shadowed data, the point at (99.5%, -25 dB) corresponds to a point on the VS distribution curve extracted from the overall data set. All the points for the VS distribution curve in Figure C-3 up to a threshold of about -8 dB are determined in this manner. This process must be stopped at about -8 dB because unshadowed data starts to corrupt the extraction of the shadowed data.

Once the partial distribution is extracted from the data, the simulator is set to generate about 10,000 purely shadowed data points and the parameters $\overline{K}$, μ_R, and σ_R are varied until the distribution of the simulator output matches that of the extracted distribution. The effects on the overall VS distribution due to varying the $\overline{K}$, μ_R, and σ_R simulator inputs is shown in figures C-4 through C-6. Varying the $\overline{K}$ and σ_R parameters tends to

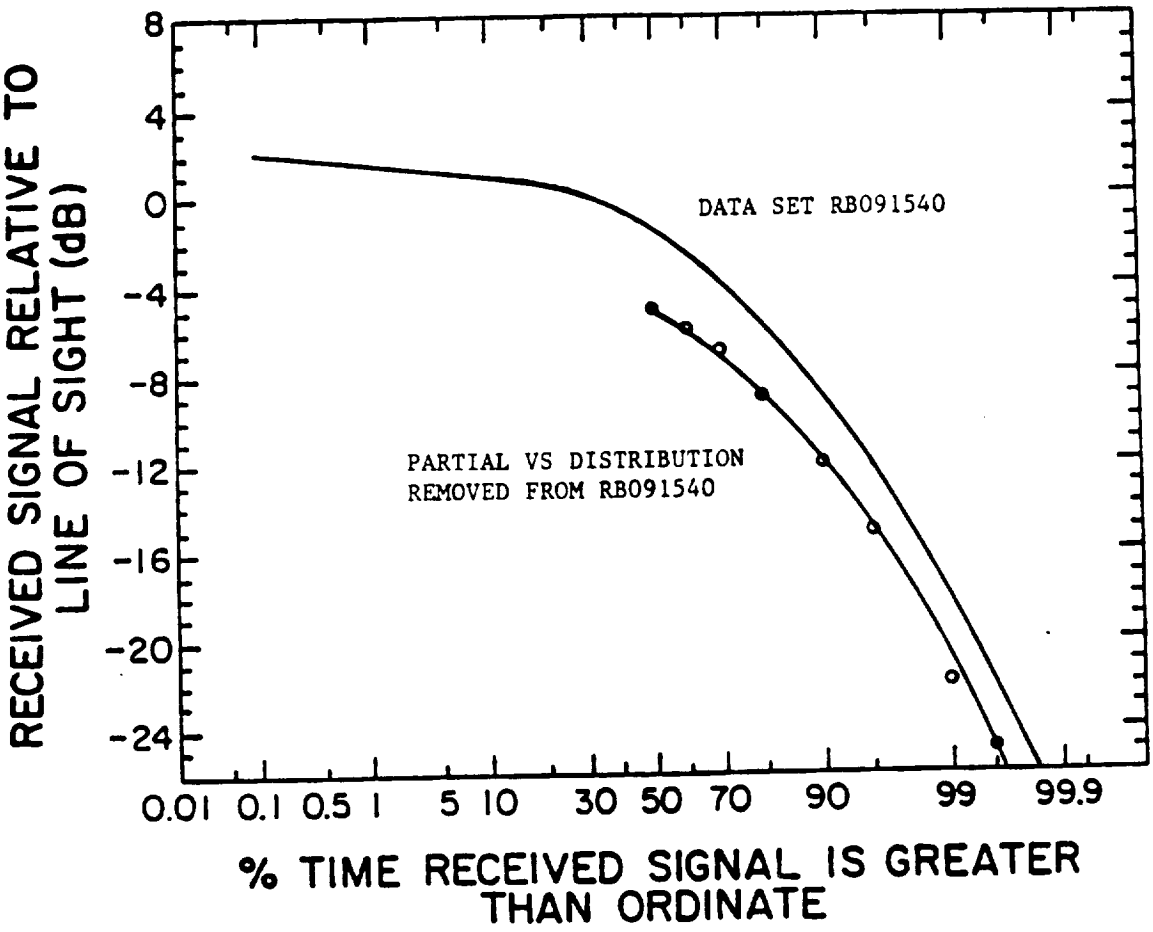

Figure C-3. Cumulative distribution plot of data set TD091540 and partial VS distribution extracted from it.

rotate the VS distribution about its mean value. Varying the μ_R parameter tends to shift the entire VS distribution curve up or down by the amount of μ_R. Because $\overline{K}$ and σ_R tend to have the same effect on the VS distribution (at least statistically), $\overline{K}$ is chosen to be about 2 to 4 dB greater than the K parameter determined in Section C.1. This range was chosen by examining the K and $\overline{K}$ parameters in the Vogel data.

The simulator output was found to match the partial distribution in Figure C-1 with parameters $\overline{K} = -12\,\text{dB}$, $\mu_R = -6.1\,\text{dB}$, $\sigma_R = 2.5\,\text{dB}$. The input parameter, K, was previously found to be -16 dB. The total number of points to generate is 40,200 and the percent shadowing is 47%. Figure C-7 compares the distribution of the simulator output with these input parameters to the distribution of the data set we are trying to match. Note the agreement is excellent.

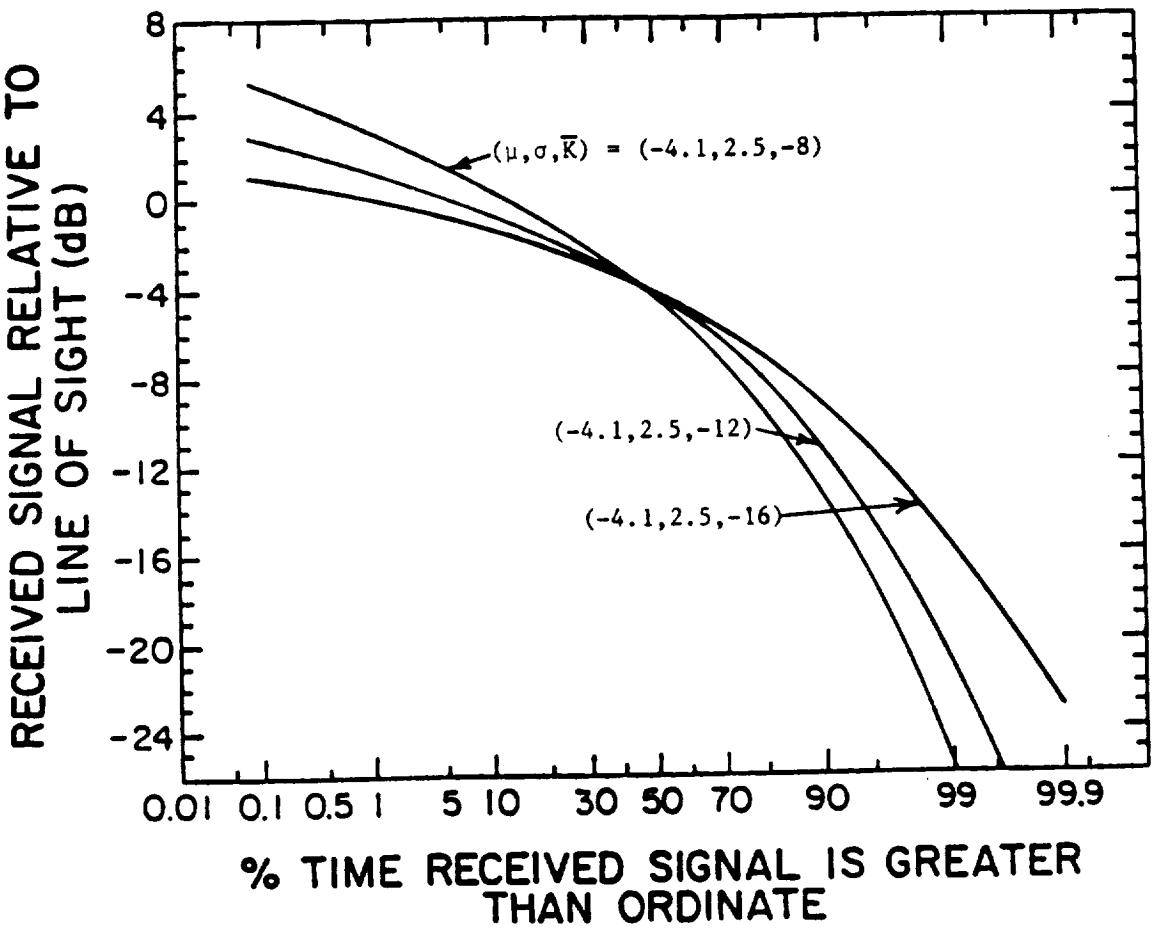

Figure C-4. Cumulative distribution plots of purely shadowed data output by the VT simulator showing the effect of varying the simulator input parameter $\bar{K}$.

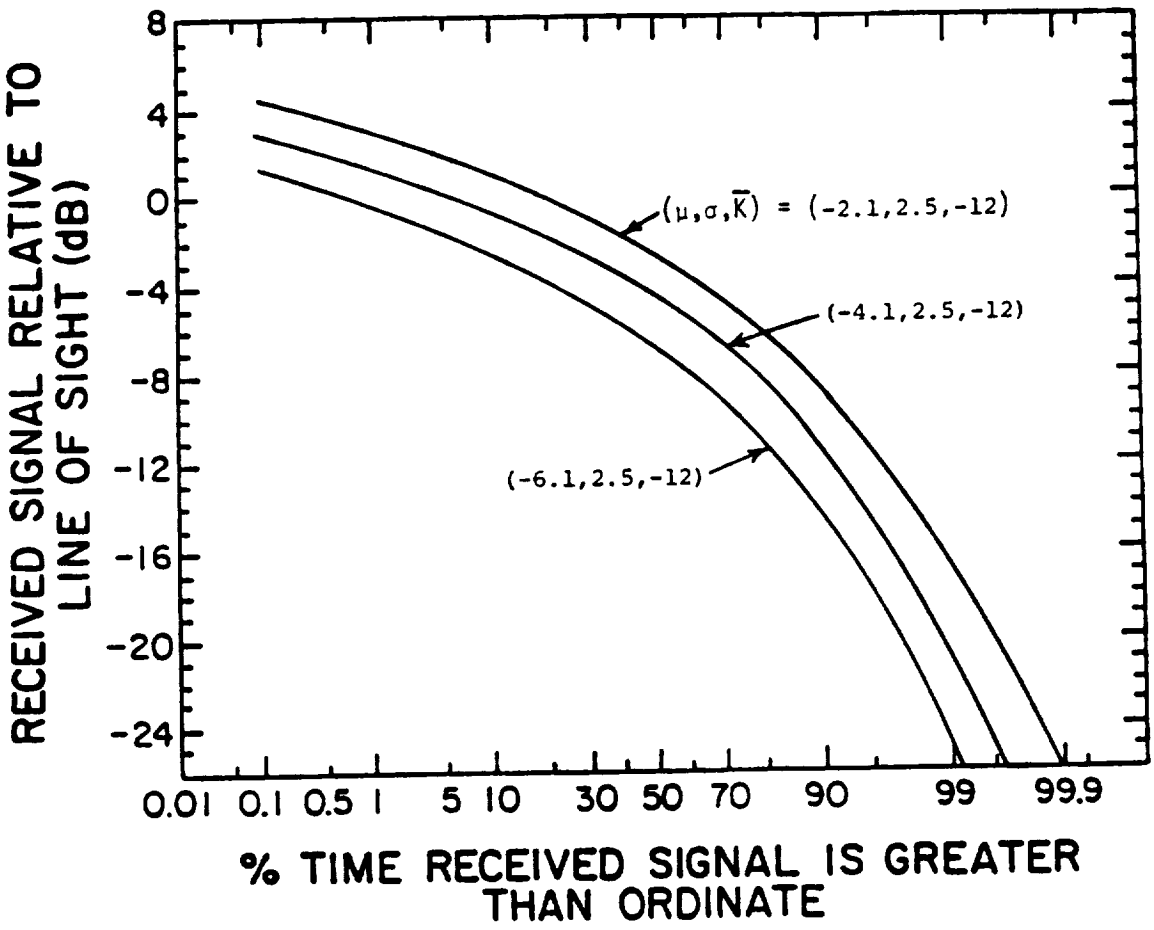

Figure C-5. Cumulative distribution plots of purely shadowed data output by the VT simulator showing the effect of varying the simulator input parameter μ.

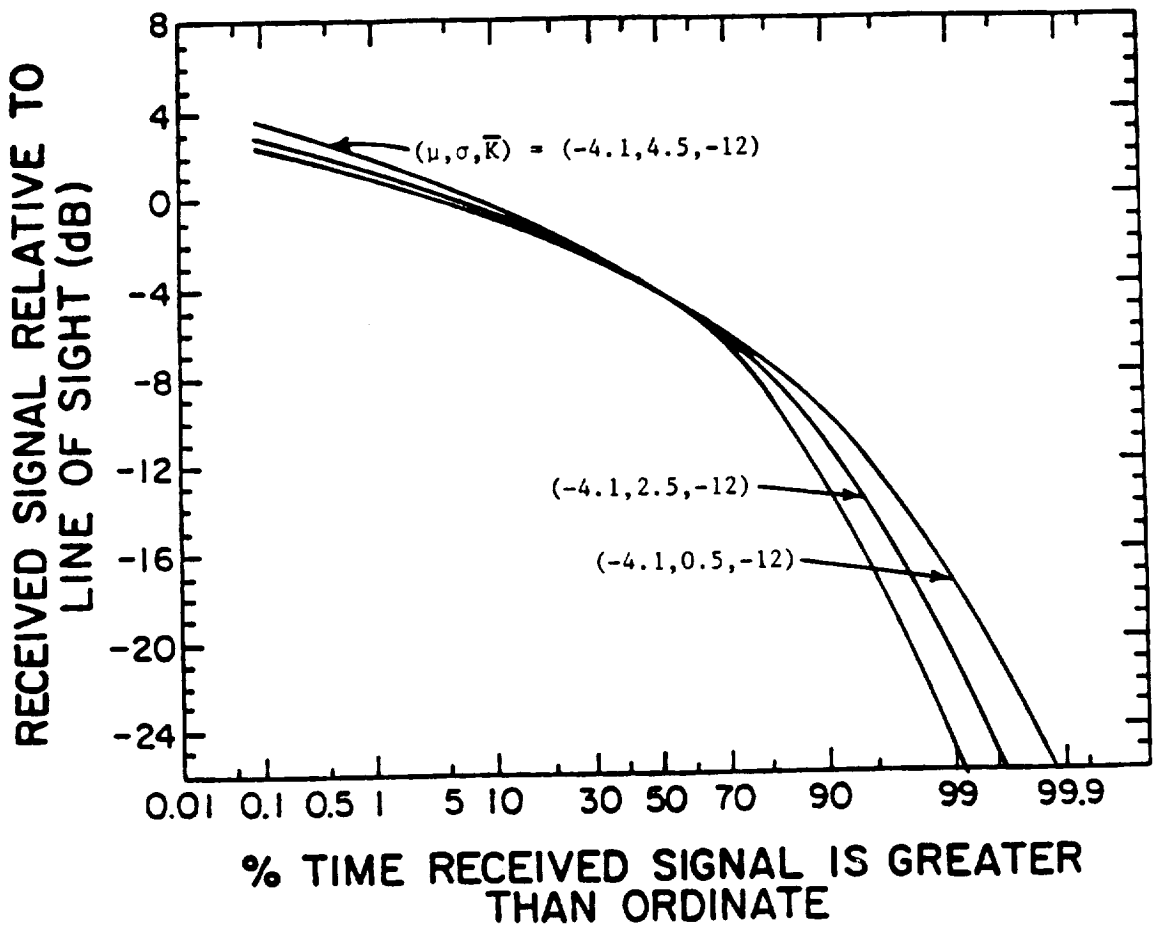

Figure C-6. Cumlative distribution plots of purely shadowed data output by the VT simulator showing the effect of varying the simulator input parameter σ.

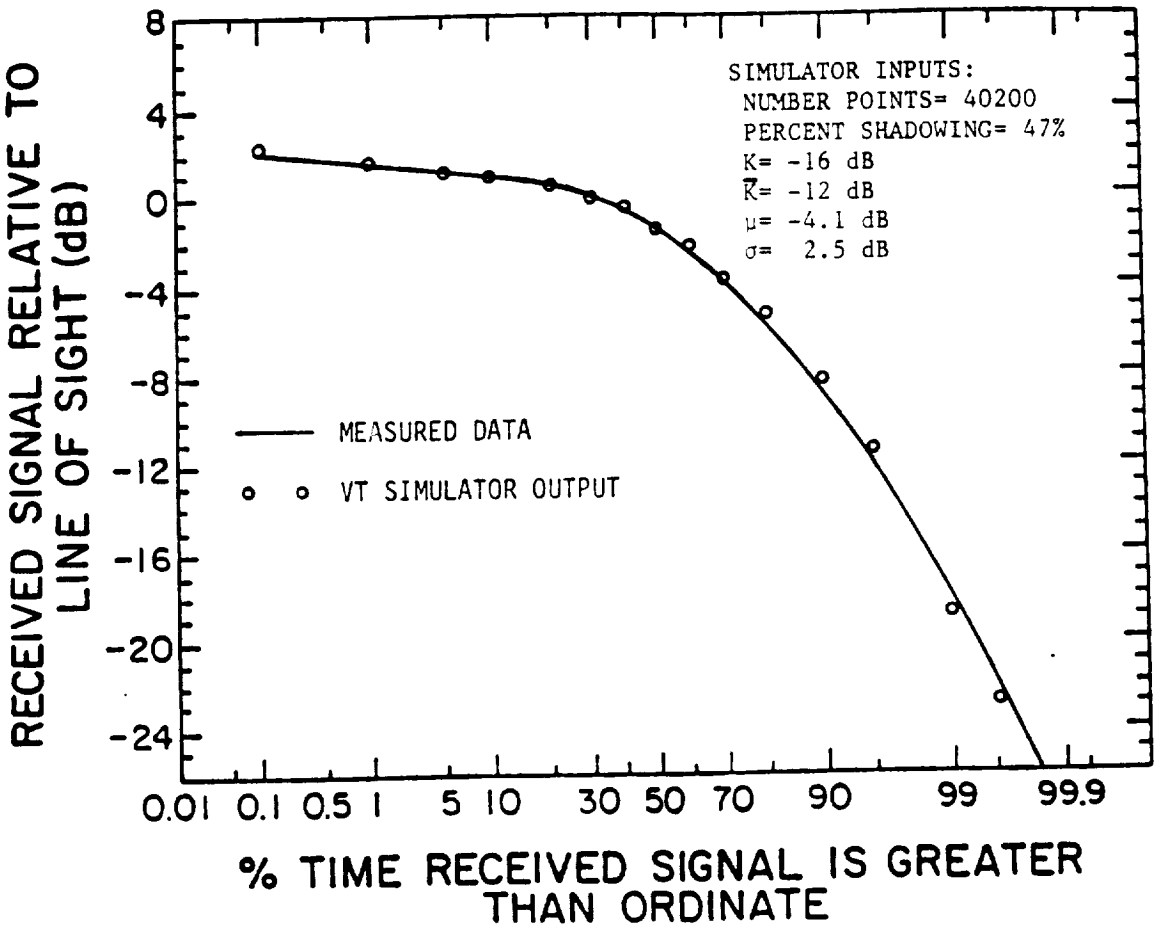

Figure C-7. Cumulative distribution plot of partially shadowed data set TD091540 and the VT simulator match to it.